FHWA-NJ-2023-001

ENERGY HARVESTING ON NEW JERSEY ROADWAYS
FINAL REPORT

January 2023

Submitted by

Hao Wang, Ph.D.
Associate Professor
Rutgers University

Lukai Guo, Ph.D.
Postdoc Research Associate
Rutgers University

Laura Soares
Graduate Research Assistant
Rutgers University

NJDOT Research Project Manager
Giri Venkiteela, Ph.D.

In cooperation with

New Jersey
Department of Transportation
Bureau of Research
And
U. S. Department of Transportation
Federal Highway Administration

DISCLAIMER STATEMENT

The contents of this report reflect the views of the authors who are responsible for the facts and the accuracy of the data presented herein. The contents do not necessarily reflect the official views or policies of the New Jersey Department of Transportation or the Federal Highway Administration. This report does not constitute a standard, specification, or regulation.

TECHNICAL REPORT DOCUMENTATION PAGE

1. Report No. FHWA NJ-2023-001	**2. Government Accession No.**	**3. Recipient's Catalog No.**
4. Title and Subtitle **FINAL REPORT** Energy Harvesting on New Jersey Roadways		**5. Report Date** January 2023 **6. Performing Organization Code**
7. Author(s) Hao Wang, Ph.D., Lukai Guo, Ph.D. and Laura Soares		**8. Performing Organization Report No.**
9. Performing Organization Name and Address Center for Advanced Infrastructure and Transportation Rutgers, The State University of New Jersey 100 Brett Road Piscataway, NJ 08854		**10. Work Unit No.** **11. Contract or Grant No.** NJDOT TO 361
12. Sponsoring Agency Name and Address Federal Highway Administration (SPR) 1200 New Jersey Avenue, SE Washington, DC 20590 New Jersey Department of Transportation (SPR) 1035 Parkway Avenue, P.O. Box 600 Trenton, NJ 08625.0600		**13. Type of Report and Period Covered** Final Report, June 2019 – November 2022 **14. Sponsoring Agency Code**

15. Supplementary Notes
Conducted in cooperation with the U.S. Department of Transportation, Federal Highway Administration.

16. Abstract
The project is to identify energy harvesting applications on roadways and bridges and conduct feasibility analysis and performance evaluation for large-scale and micro-scale energy generation. Solar energy harvesting can be achieved using different assets of roadway. The technical and economic feasibility of solar array in the right-of-way (ROW) was presented. Photovoltaic Noise Barriers (PVNBs) integrate solar panels with noise barriers to harvest solar energy while abating noise from the highway. The energy estimation models were first developed at project level and then used for state-level analysis, respectively, for top-mounted tilted, top-mounted bifacial, and shingles built-on designs of PVNB. On the other hand, piezoelectric energy harvesting can be achieved by compression or vibration modes. The new designs of vibration-based energy harvesters are proposed under multi-frequency bridge vibrations. A multiple degree-of-freedom (DOF) cantilever design concept was developed and tested in the laboratory. The optimized design was demonstrated and validated in full-scale tests for vibration-based energy harvesting. The research outcome provides recommendations for future implementation of energy harvesting in the roadway and bridge network of New Jersey for development of sustainable and smart transportation infrastructure.

17. Key Words Energy harvesting; Solar energy; Photovoltaic noise barrier (PVNB); piezoelectric material; bridge vibration; cantilever beam	**18. Distribution Statement** No restrictions.

19. Security Classif. (of this report)	**20. Security Classif. (of this page)**	**21. No. of Pages**	**22. Price**
Unclassified	Unclassified	111	

Form DOT F 1700.7 (8-72) Reproduction of completed page authorized

ACKNOWLEDGEMENTS

This project was sponsored by the New Jersey Department of Transportation (NJDOT) and the Federal Highway Administration. This project could not have been accomplished without the assistance of numerous individuals. The authors would like to express gratitude to Edward Liu and Pragna Shah with NJDOT, Dr. Ahmad Safari and Haochen Lyu with Rutgers University.

.

TABLE OF CONTENTS

LIST OF FIGURES **Page**

LIST OF TABLES **Page**

LIST OF ABBREVIATIONS AND SYMBOLS

NJDOT – New Jersey Department of Transportation
LED – light-emitting diode
PVNB – Photovoltaic Noise Barrier
DOF – degree-of-freedom
MFC – micro-fiber-composite
ROW – Right-of-way
ODOT – Oregon Department of Transportation
DOT – Department of Transportation
SHM – Structural Health Monitoring
GHG – greenhouse gas
PV – Photovoltaic
UHI – Urban Heat Island
TEG – Thermoelectric Generator
HAWT – Horizontal-axis Wind Turbine
VAWAT - Vertical-axis Wind Turbine
PE – Piezoelectric
AC – Alternate Current
MEMS – Micro-electro-mechanical System
RECs – Renewable Energy Credits
EEG – Renewable Energy Sources Act
SCP – Solar Collector Pavement
PGE -Portland General Electric
LLC – Limited Liability Company
ITC – Investment Tax Credits
BETC – Business Energy Tax Credits
SRECs – Solar Renewable Energy Credits
FDOT – Florida Department of Transportation
FHWA – Federal Highway Administration
APRR – Autoroutes Paris Rhin-Rhone
NSRDB – National Solar Radiation Database
NREL – National Renewable Energy Laboratory
POA – Plane-of-array
PPP – Public Private Partnership
SAM – System Advisor Model
PPA – Power Purchase Agreement
NPV – Net Present Value
GCR – Ground Cover Ratio
WIM – Weight-in-motion
PVDF – Polyvinylidene Fluoride
PAA – Poly Amino Acid
PSA – Piezoelectric Aggregates
AAD – Average Absolute Deviation
RF – Radio Frequency
WMS – Wireless Monitoring System

IoT – Internet of Things
HiSEC – Highway Sensing and Energy Conversion
EHPS - Energy Harvesting Pavement System
RPEH - Road-capable Piezoelectric Energy Harvester
ITS – Intelligent Transportation System
RFID – Radio Frequency Identification
EH – Energy Harvesting
MTS – Material Test System
FEM – Finite Element Model
FFT – Fast Fourier Transform
BEAST – Bridge Evaluation and Accelerated Structural Testing System
VMA – Voids in Mineral Aggregate

EXECUTIVE SUMMARY

Roadways and bridges are major civil infrastructures that play an important role in connecting communities, and moving people. Traditionally, roadway is regarded as the structure platform to carry traffic loading. Roadway surfaces and bridge decks are continuously exposed to vehicle loading and solar radiation, which induces mechanical vibration and thermal gradients in pavement layers. Mechanical energy can be converted into electricity via magnetic field for electromagnetic material or strain field for piezoelectric material. Solar energy can be harvested through photovoltaic cell, heat flux, or thermoelectric field. Therefore, the wasted energy in the roadway can be harvested and converted into usable energy that has different applications. Depending on the principle of each harvesting technology, the amount of energy output varies significantly. The large amount of renewable energy from solar radiation or wind can be directly used for electrical power and grid. On the other hand, the relatively small amount of energy can be used for traffic lighting, or powering sensors or communication devices.

Solar energy harvesting can be achieved using different assets of roadway. Photovoltaic Noise Barriers (PVNBs) are integrative structures that combine solar panels with noise barriers to harvest solar energy while abating noise from the highway. the design studies of PVNB are performed, respectively, for top-mounted tilted, top-mounted bifacial, and shingles built-on configurations. The energy estimation models were first developed at project level and then used for state-level analysis. The results show that the energy output potential of 56,164 MWh per year can be found in all NJ noise walls. Furthermore, a decision-making framework for site selection of PVNB was proposed along with the analysis of business models of PVNB as direct ownership or third-party ownership.

Piezoelectric energy harvesting can be achieved by compression or vibration modes. The new designs of vibration-based energy harvesters are proposed for applications under multi-frequency structure vibrations. A multiple degree-of-freedom (DOF) cantilever design concept was developed and tested in the laboratory for power generation. Under multiple frequency vibration scenarios, 3-DOF cantilever showed the higher possibility of matching resonant frequencies with vibration frequencies in a wide range. An optimization strategy is proposed for bridge applications. The specific procedures include bridge vibration acceleration measurement, simulation model development for estimating the resonant frequencies, regression model for optimization of mass combinations, and final installation on the full-scale bridge for validation. The feasibility of the proposed optimization strategy was demonstrated and validated in full-scale tests for vibration-based energy harvesting.

INTRODUCTION

Background and Motivation

The discovery of green energy resources that are renewable is one of the critical challenges facing the world for sustainable development. Petroleum, coal, hydraulic, natural gas, and nuclear energy are currently most common energy resources that are used for generation of power. Energy harvesting is a promising technique that can produce renewable and clean energy and improve sustainability of infrastructure. Energy harvesting technologies capture unused and wasted energy and convert it into a more usable form. Solar, wind, hydro, thermo, and kinetic energy are the common energy sources that can be used for energy harvesting in general. In recent years, researchers have begun to harvest electrical energy from the ambient environment using different techniques, such as piezoelectric, thermoelectric, electromagnetic, and photovoltaic energy harvesting.

The United States wants to reduce greenhouse gas emissions by 50-52% from 2005 to 2030 and reach 100% carbon-free electricity by 2035 [(1)]. Renewable energy sources, specifically solar power, are a solution to the federal government's environmental goals. Transportation agencies can benefit from renewable energy by utilizing various solar power technologies in roadway infrastructure. Traditional solar farms require a large amount of land, especially when targeting high energy production. Transportation agencies can install solar plants on their owned but unused land, such as the right-of-way (ROW). Oregon Department of Transportation (ODOT) become the first agency in the United States to do so in 2008. After ODOT's project, several other states including California, Florida, Ohio, and Massachusetts adopted the technology. However, it is desired to avoid creating a large land footprint by implementing solar integrated infrastructure on roofs, canopies, noise barriers, street lights, and traffic signs.

Photovoltaic noise barriers (PVNBs) use photovoltaic technology to produce renewable energy and simultaneously abate the noise generated from traffic. Photovoltaic modules can be retrofitted onto existing barriers directly on their surface or mounted on top [(2)]. The first PV Noise Barrier (PVNB) was installed in 1989 in Switzerland, and since then in several European nations including the Netherlands, Austria, France, and Germany [(3)]. This technology allows multiple uses of the same road and consumes a limited amount of land. However, few studies have been conducted to evaluate the design of PVNBs, especially how to install photovoltaic panels on the existing noise wall. The solar panels can be installed with different angles and positions, depending on the orientation of noise wall, to improve solar energy production.

PVNBs can add value and function to existing noise barriers apart from the renewable energy benefits. For example, they may provide aesthetic improvements created by novel transparent solar panels and require minimal maintenance. However, PVNBs are vulnerable to vandalism, can experience decreased efficiency incurred by shading effects and dust from the road, and can cause undue glare to drivers when the PV panels are 60 degrees from horizontal direction [(4)]. Furthermore, PVNBs may suffer a low adoption rate

because public agencies (such as DOTs) cannot directly benefit from tax-related financial incentives; however, to overcome this, public agencies can partner with the private sector to take advantage of those incentives. Therefore, more studies are needed.

On the other hand, energy harvesting could provide continuous power support for in-situ monitoring sensors placed on roadways and bridge decks. Traditional sensors used for monitoring in-situ condition of civil structures include accelerometer, displacement sensor, force sensor, resistance strain gauge, and optical fiber. Recently, wireless sensor network has been widely used for structural health monitoring (SHM). However, one of main limitations of wireless sensor is power supply for long-term application. Piezoelectric sensor with proper design of packaging can behave as smart materials for SHM. For example, highway bridges vibrate continuously due to moving vehicles and winds. The dynamic response of bridges causes strains in the electromagnetic or piezoelectric sensors attached to bridge members, which can be used to provide power supply for sensors.

Smart transportation infrastructure systems (roadway, bridges, etc.) are equipped with sensors for collecting traffic loading and structural health condition, which enables the communication between vehicles/structures and nearby control centers to ensure safety and mobility. As the total number of sensors keeps being added, the maintenance costs of sensors significantly increase. Moreover, the sensors can be malfunctioned if the power supply sources are interrupted. Such interruption can lead to discontinuous data collections with missing important data information. To ensure the continuity of data collection from sensors without interruption, one feasible solution is to develop off-grid energy harvesters to supply in-situ power for sensors.

Objective and Scope

The objective of this project is to identify potential energy harvesting technology for applications on roadways and bridges and conduct feasibility analysis and performance evaluation of the selected technologies for large-scale and micro-scale energy generation.

To achieve the research objective, the scope of work includes the following aspects:

- Comprehensive literature review on energy harvesting techniques and applications. First, the principles of different energy harvesting techniques are reviewed and compared, including photovoltaic, wind, geothermal, wind, piezoelectric, thermoelectric, electromagnetic, and electrostatic. Second, different methods of renewable energy harvesting on roadway are reviewed and summarized with real cases. Third, different applications of piezoelectric energy harvesting for smart transportation infrastructure are reviewed and summarized.

- Analysis of solar energy output at the right-of-way (ROW) of NJ roadway. The energy output at the selected site is first analyzed and then the state-level energy output is estimated using available ROW for solar array. The project-level

economic analysis is conducted assuming the business models of net metering and power purchase agreement.

- Analysis of solar energy output of photovoltaic noise barriers (PVNBs) and discussion of implementation issues. Three retrofitting designs of PVNB are compared and evaluated. Energy simulation is conducted to develop simplified models for state-level estimation in NJ. A framework of selecting the most appropriate site for PVNB is proposed considering economic, environmental, and social criteria.

- Development and evaluation of new designs of piezoelectric cantilevers for providing wide-band of resonant frequency to better match bridge vibration modes encountered in the field. The new 2-DOF and 3-DOF cantilever designs with multiple mass and piezoelectric components are fabricated and tested as compared to the traditional one-DOF cantilever to evaluate voltage outputs of cantilever designs under different vibration scenarios.

- Development of an optimization approach for piezoelectric energy harvester to maximize power outputs from bridge vibrations. The design optimization approach requires three critical parts: 1) multiple cantilever design options with adjustable masses in the field; 2) accurate simulation models for estimating energy harvesting performance; and 3) quantitative models for optimization of mass combinations. The optimized energy harvester designs were verified through comparing the energy outputs before and after design optimization.

The research outcome will provide recommendations for future implementation of energy harvesting in the New Jersey roadway and bridge network. The large-scale energy harvesting will help provide green energy, save natural resources, and reduce greenhouse gas (GHG) emission generated from traditional energy sources. The micro-scale energy harvesting will promote the development of sensors with in-situ power supply for smart transportation infrastructure.

ENERGY HARVESTING TECHNIQUES AND APPLICATIONS

Energy Harvesting Techniques

Photovoltaic (PV) Cell

Photovoltaic (PV) cell is used to convert solar radiation into electric power. The solar cell consists of a P-type semiconductor and an N-type semiconductor. When sunlight reaches the semiconductor materials of PV cell, free electrons are forced to flow in a certain direction. The negatively charged electrons move toward the N-type semiconductor; while the positively charged electrons move toward the P-type semiconductor. The working principle of PV cell is shown in Figure 1. The flow of moving electrons creates an electrical current when connected to electrical load [5].

The efficiency of PV is around 20-25% and it varies depending on the material used. The material can be silicon, thin-film or organic polymer. PV solar panels have wide applications in off-grid-small-household and rural electricity projects. The drawbacks from large-scale solar farms are the large land footprint required and there are toxic heavy metals (such as cadmium and lead) on its components.

Traditional PV solar panels requires low maintenance, and it is technological and commercial mature. Recently, concentrating PV is developed that uses optics, such as lenses to concentrate a large amount of sunlight onto a small area of solar photovoltaic materials to generate electricity in high efficiency [6].

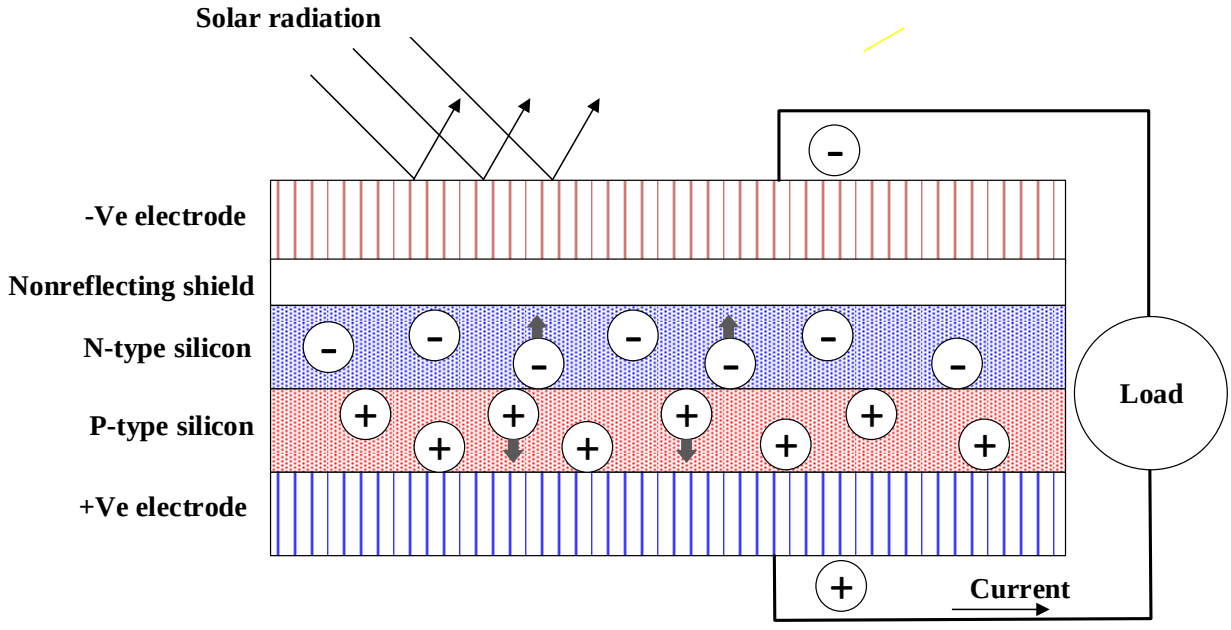

Figure 1. Working Principle of Photovoltaic Cell

Solar Collector System

A solar collector system consists of a network of pipes under road pavement with circulating fluid inside. As the pavement absorbs radiation from the sun and atmosphere, the pavement temperature increases, and heat is transferred to fluid inside the piping system due to temperature gradients. There are three basic heat-balance processes involved in pavement solar collector system: conduction, convection, and radiation, as shown in Figure 2. Conduction happens between pavement and the pipe walls. Energy convection occurs when there are temperature differences between the ambient air, pavement, pipe walls, and the fluid circulating in the pipes. Radiation via electromagnetic waves can occur without any material medium, including solar radiation transfer to pavement and thermal radiation between the ambient atmosphere and the pavement.

The heat captured by the piping system can be used in thermoelectric generators to generate electric energy or stored in energy reservoirs. During the winter, the stored heat can be used to melt snow on roads, produce electricity, and warm nearby buildings. Another benefit associated with pavement solar collector system is its ability to mitigate urban heat island (UHI) effects in metropolitan areas by reducing pavement temperature [7]. The cooling effect also helps to retard pavement deterioration and maintain pavement performance under high-temperature weather conditions.

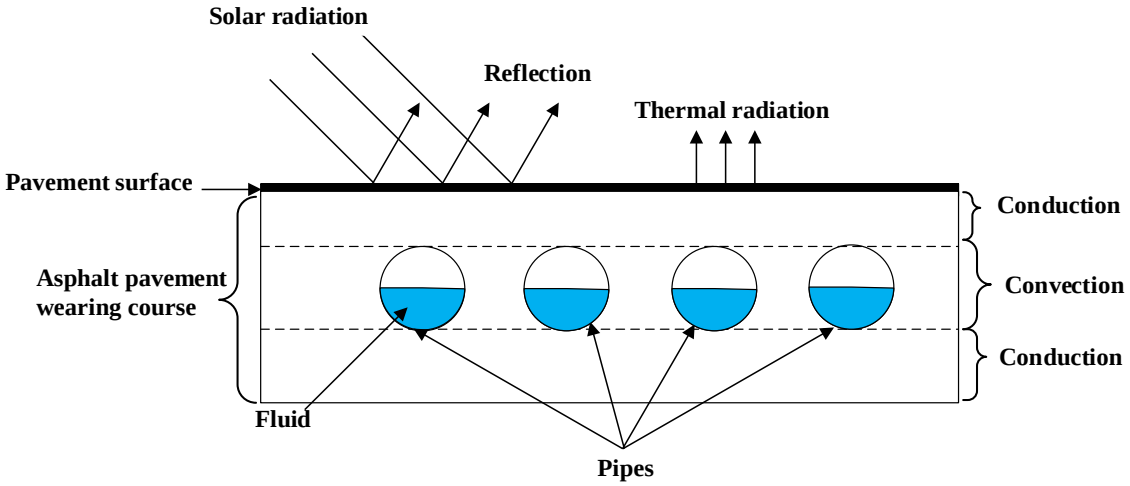

Figure 2. Working Principle of Solar Collectors in Pavement

Thermoelectric Generator (TEG)

Thermoelectric generator (TEG) harvests energy from thermal change of surrounding environment. TEG can utilize the temperature differences between pavement layers to generate electricity based on thermoelectrical principles. Discovered by T.J. Seebeck in 1821, the Seebeck effect has been widely used in most thermoelectric-generation technologies [8]. The Seebeck effect is defined as the generation of an electric field when there is a temperature gradient at two ends of a thermoelectric generator device (Goldsmid 2016). The temperature gradient of the conductor and the electric current generation are reversible. The TE module usually consists of two parallel N-type and P-type semiconductors with heat source and heat sink on each side, as shown in Figure 3.

According to the Seebeck effect, the high Seebeck coefficient, low thermal conductivity, and low electrical resistivity are required to optimize the conversion efficiency of thermoelectric generator. The low thermal conductivity and electrical resistivity ensure the minimum energy loss caused by heat conduction and Joule dissipation. Thermoelectric semiconductors are conventionally used to overcome the limitation of isotropic metals whose improvement is restricted by the Wiedemann-Franz law [8]. The major disadvantage of this technology is low efficiency, but using novel materials for TEG manufacturer could improve the efficiency.

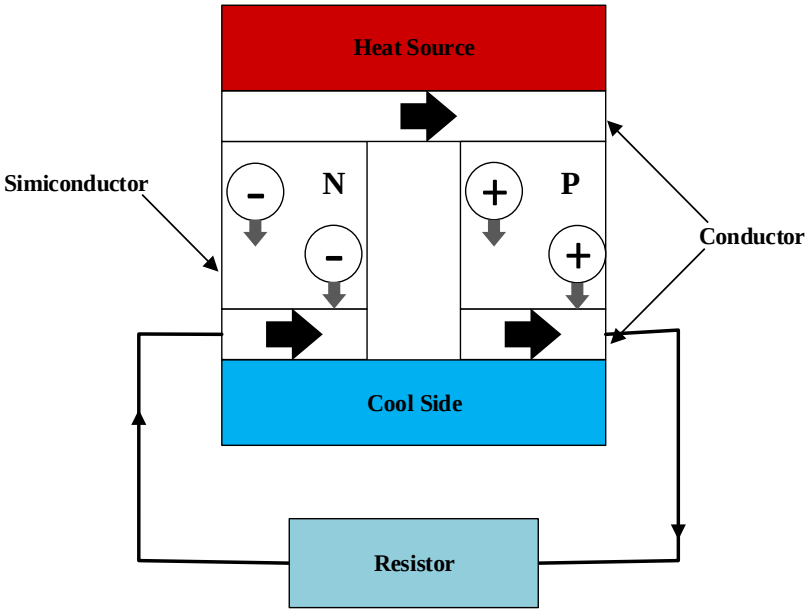

Figure 3. Working Principle of Thermoelectric Generator

Wind Energy Harvesting

A wind power system consists of a series of angled blades attached to a shaft. The wind creates rotation on the blades and, consequently, on the shaft through kinetic energy. Mechanical energy generated from the rotation moves the rotor inside a generator usually with the help of a gearbox and therefore electrical energy is produced. There are two types of wind turbines: the horizontal-axis wind turbine (HAWT) and vertical-axis wind turbine (VAWT) [9]. In HAWT, the rotor axis is parallel to the ground and in the direction of the wind, as shown in Figure 4. These turbines are usually equipped with self-starter and yaw system to turn the blades towards the wind. In the VAWT, the axis of rotation is perpendicular to the directions of wind and ground. These turbines are relatively simple and do not need any yaw system and a self-starting mechanism. Although the VAWT is less efficient (around 20%) than HAWT (around 60%), the VAWT is able to capture wind from different direction and in low speed [10].

The HAWT is difficult to transport, install, and maintain, and is relatively ineffective in urban situations. Although the VAWT is potential solution to urban and semi-urban areas, it has low efficiency and may require energy to start turning. However, the positive aspects of this turbine type are the lower noise, easy to maintain, lower construction and transportation cost and simple in design.

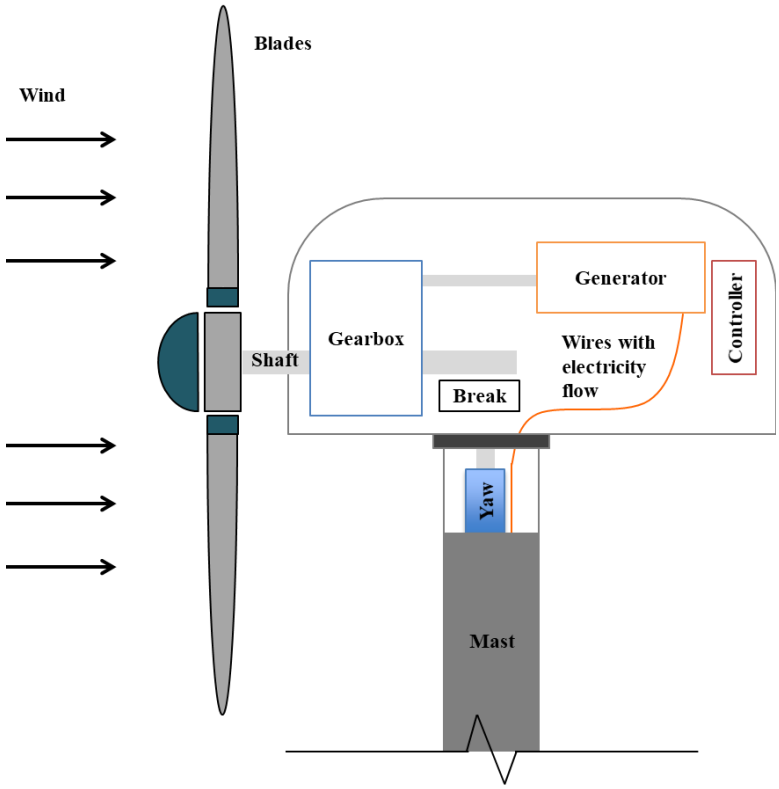

Figure 4. Working Principle of Wind Energy Harvesting (horizontal axis)

Geothermal Energy Harvesting

Geothermal energy is the heat energy coming from the deep inside the earth that is the energy naturally stored in the planet. Geothermal heat pumps and the underground thermal energy storage play important roles in the application of geothermal energy. Heat pumps are heat transfer devices that can enhance heat output of the fluid when receiving the relatively low-temperature geothermal heat input.

Figure 5 illustrates the main concept of geothermal energy under pavement surface using embedded pipes. The basic principle of the most common heat pumps is vapor compression with the use of compressor; the temperature of gas increases when it is compressed without the loss of heat. For underground thermal energy storage, the key is to minimize energy loss that is affected by storage time, temperature, volume, and thermal properties of storage medium [(11)].

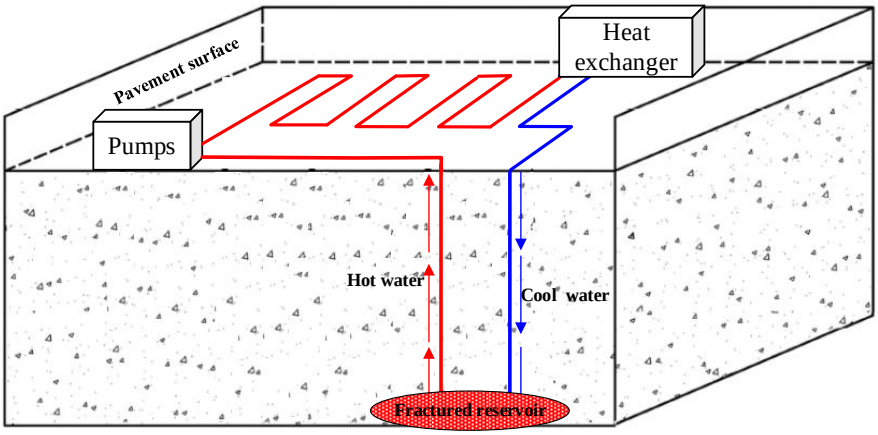

Figure 5. Working Principle of Geothermal Energy Harvesting

Piezoelectric (PE) Energy Harvesting

Piezoelectric materials generate electric charges when subjected to mechanical stresses or change geometric dimensions when an electric field is applied. The working principle of piezoelectric energy harvesting is shown in Figure 6. The voltage produced from piezoelectric material varies with time and results in an alternate current (AC) signal, which causes the direct and inverse piezoelectric effect, respectively [12].

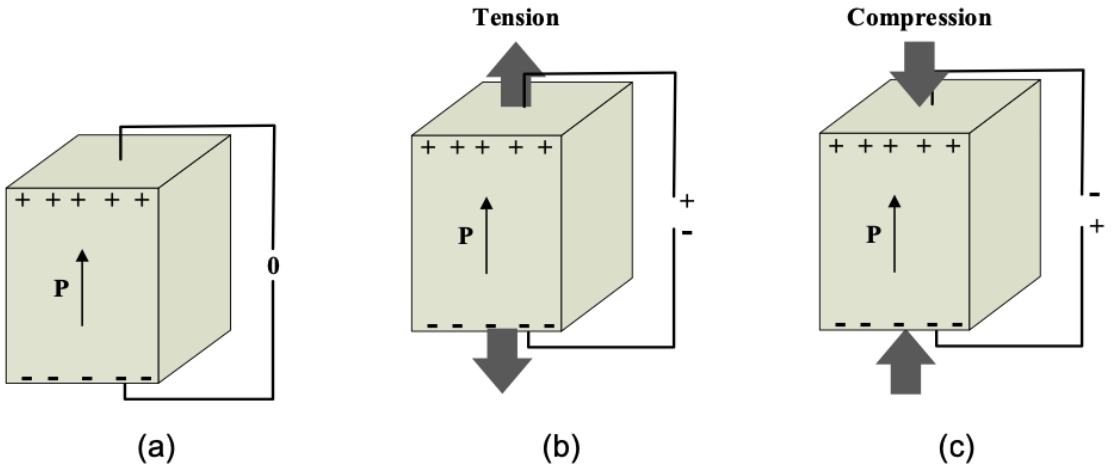

Figure 6. Working Principle of Piezoelectric Effect under (a) zero stress; (b) tension; and (c) compression

Piezoelectric materials can be classified into the following categories: single crystalline material (e.g., quartz), piezoceramics (e.g., lead zirconate titanate [PZT]); piezoelectric semiconductors (e.g., ZnO2), polymer (e.g., Polyvinylidene fluoride [PVDF]), piezoelectric composites, and glass ceramics (e.g., Li2Si2O5, Ba2TiSiO6). Although piezoelectric materials have different piezoelectric and mechanical properties, the most common ones are polymers and ceramics. Polymer materials are soft and flexible, while ceramics are

rigid. Polymer materials generate the lower energy than ceramics due to different dielectric and piezoelectric properties.

Many piezoelectric transducer designs have been proposed, such as the cymbal, multilayer, bridge, Moonie, thin layer unimorph driver and sensor (THUNDER), reduced and internally biased oxide wafer (RAINBOW), macro-fiber composite (MFC), and bimorph (Anton and Sodano 2007). The energy harvesting performance of piezoelectric transducer is affected by material, geometry design of transducer, and external loading.

Electromagnetic Energy Harvesting

Electromagnetic generator is the most common application based on Faraday's law for energy harvesting purpose through converting kinetic energy to electricity [13]. A relative transverse motion between an electric conductor (coil) and a magnetic field can produce electricity flowing through the conductor, as shown in Figure 7. The amount of electricity generated depends upon the strength of magnetic field, the velocity of relative movement, and the number of turns of coil.

Since the EM motor is a velocity-induced transducer, its application is preferred in the situations where vibration occurs in the structure. In roadway application, given the pavement vibration and the strength of magnetic field is limited in a large scale, utilizing electromagnetic effect to produce massive power from roadway is impractical. Electromagnetic effect is more commonly applied in a small scale on micro-electro-mechanical system (MEMS) for sensing purpose, especially on monitoring the bridge structural health [14]. Through the vibrational modes of bridge, electromagnetic generator is theoretically capable of producing sufficient electricity to maintain a wireless sensor hub for one or two reading daily.

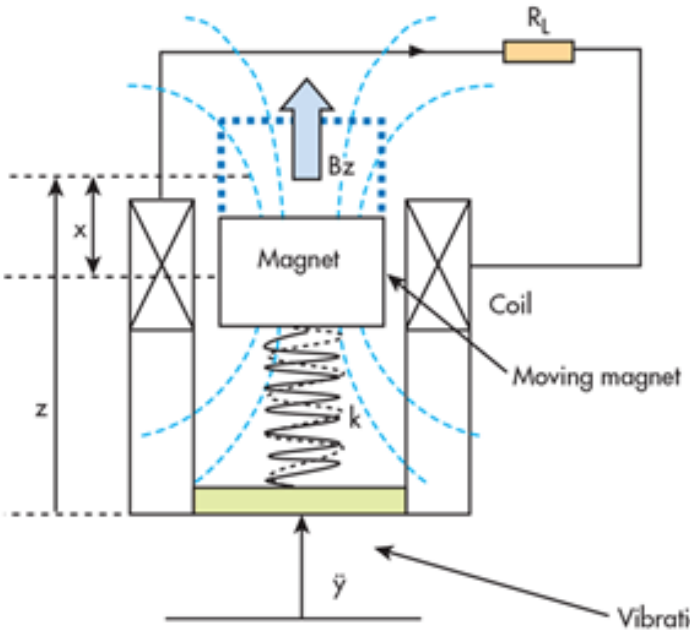

Figure 7. Working Principle of Electromagnetic Energy Harvesting

Electrostatic Energy Harvesting

Electrostatic converters are capacitive structures made of two plates separated by air, vacuum or any dielectric material [15]. In other words, the key point of electrostatic energy harvesting is to change the capacitance between plates. There are three major options under one vibrating electrode, as shown in Figure 8. All three options require two plates (one is fixed and another one can be either fixed or movable depending on the specific application) and one movable electrode (may combined with the movable plate).

- In-plane overlap, which changes the overlap area between plates by one vibrating electrode between them in parallel direction;
- In-plane gap closing, which changes the distance between plates by one vibrating electrode between them in vertical direction;
- Out-of-plane gap closing, which changes the distance between one fixed plate and one movable plate attached with one vibrating electrode.

Since the charge generated and stored by the capacitor is limited at initial stage (before vibration), the power output generated by a varied capacitance is weak. For the roadway application, the low vibration amplitude from pavement can further degrade the power output from electrostatic energy harvester.

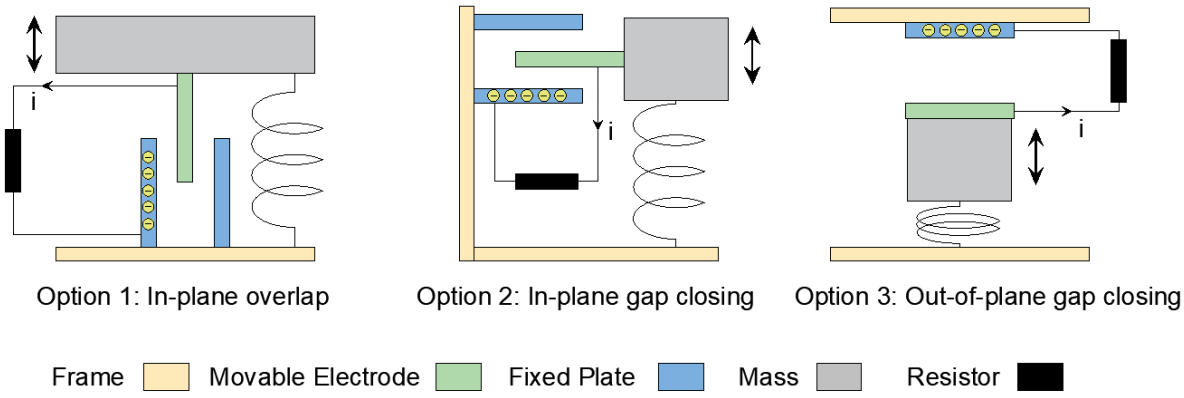

Figure 8. Working Principle of Electrostatic Energy Harvesting

Comparison of Energy Harvesting Techniques

Table 1 compares advantages and disadvantages of different energy harvesting technologies and their impact on roadway based on the literature review and the experience of research team. The impact on roadway considers the installation process on roadway, the disturbance to roadway maintenance and traffic safety, and the material and maintenance cost.

Table 1 - Comparison of Harvesting Technologies for Roadway Applications

Technology	**Disadvantage**	**Advantages**	**Impact on roadway**
Photovoltaic cell	High cost; Fragility to traffic loading; Small skid resistance	High energy output; UHI mitigation	High
Solar Collector	No electricity generated; Weather dependent	High energy output; Reduce pavement temperature	High
Thermoelectric	Low efficiency; High cost per unit	Wide applicability; Easily combined with other technologies	Low/Medium
Wind	Noise and aesthetic pollution; high cost; hazardous to traffic	High energy output	Medium
Geothermal	Need electricity or heat boilers for pumps	High energy output; Heating and cooling can be reserved	High
Piezoelectric	Transducer array and repeated loading for high energy output	Use for both energy harvesting and sensors	Low/Medium
Electromagnetic	Specific applications on bridges or speed bumps	Velocity-induced, Based on structure vibrations	Medium/High
Electrostatic	Need fast nechanic virbation	High voltage; low cost, compatitble with sensor	Low

RENEWABLE ENERGY HARVESTING ON ROADWAY

Solar Energy Harvesting on Roadway

Solar Array in the Right-of-Way

Solar power energy harvesting can be implemented along the highway, on rest areas, parking lots, adjacent buildings or on top of noise barriers. Ideally, the available solar technologies can be traditional (non-concentrating) and concentrating photovoltaics. However, concentrated PV requires large land occupancy, much larger than ROW, and has higher risk of glare putting drivers at risk. Therefore, most existing applications are non-concentrating photovoltaics.

Using solar power in the ROW not only increases the use of renewable energy but can also be profitable for transportation agencies. It decreases costs of purchasing energy and transportation agencies can receive money depending on the business model. The economic benefits can come from net metering when the energy produced is higher than the one used, from renting the ROW space for utility companies, and from selling the RECs (renewable energy credits) generated from the system.

Selecting the locations of the solar panels in highway ROW is very important to guarantee efficiency and safety of solar highway projects. The roadway should have the free space to implement the panels in a safe distance from the road and no future road expansion plan. The PV panels needs to have the right inclination to guarantee maximum efficiency and avoid glare.

Implementing solar power technology along the right-of-way (ROW) has been done since 1980 in Europe. However, it was only in 2008 that Oregon DOT implemented the first solar power in the highway ROW (right-of-way) in the United States. After that, a number of solar highway projects have been built by different state DOTs, such as Oregon, Colorado, Massachusetts, Ohio, Florida, and California. Figure 9 shows a picture of solar array at highway ROW (Oregon).

Figure 9. Solar Array at Highway ROW (Oregon)

Solar Noise Barrier

Solar Noise Barriers uses photovoltaic technology to produce renewable energy and simultaneously abate the noise generated from traffic. Photovoltaic modules can be integrated directly in the surface of the barrier, retrofitted or mounted onto the barriers [(2)]. The first PV Noise Barrier (PVNB) was installed in 1989 in Switzerland, and it has been undertaken in several European countries such as Netherlands, Austria, France and Germany [(16, 2, and 3).] This technology allows multiple uses of the same road and consumes a limited amount of land. The efficiency of the solar power is related to the photovoltaic material, radiance of the location and orientation of the noise barrier. The module can be standard polycrystalline solar panels, bifacial polycrystalline solar panels surrounded by toughened glass or thin-film solar cells encased in toughened glass [(17)]. Figure 10 shows a picture of photovoltaic noise barrier in Europe.

Figure 10. Photovoltaic Noise Barrier in Europe

Implementing solar power on noise barriers can be a solution to finance the cost of the barrier since the energy produced by the photovoltaic panels will bring financial benefits. Other benefits from PVNB are the value and function added to existing noise barrier, novel transparent solar panels could improve the aesthetic, wildlife protection, and minimal maintenance need. However, PVNB is vulnerable to vandalism, and can have shading effect and dust from the road which will decrease the efficiency of the solar system. There are glare complains when PV panels are 60 degrees from horizon [(16)].

Solar Noise Barriers are vastly used in Europe. In December 1989 the world's first Photovoltaic Noise Barrier (PVNB) was installed in Switzerland. The solar panels are top mounted in a 2-meter tall and 800-meter long noise barrier. The polycrystalline PV modules produce 108,000 kWh per year after deducting the electricity needed to power the monitoring system and inverters [(16)]. The first German PVNB was built in 1992, and after that several others were implementing across the country. Germany has subsided this project with the Renewable Energy Sources Act (EEG) and Energiewende policy. Although these incentives decreased over the years, the cost of photovoltaic technology went down which permitted for PVNB to maintain its feasibility.

Netherlands started retrofitting concrete noise barriers with PV panels in 1990 and one of the largest PVNB with 1.6 km long was built in 1998. The project still produces 176,000 kWh annually. In 2007, VicRoads, road and traffic authority in the state of Victoria in

Austria, began selling electricity from PVNB to local energy grid. The project has 500-meter-long and received AU$140,000 grant from Sustainability Victoria. There are 210 PV panels made of opaque amorphous silicon, which is considered to be a good material for noise barrier [16].

Solar Tree

Solar tree uses photovoltaic technology but in a unique and decorative design. This artistic aesthetic sculpture can enhance the efficiency of solar PV systems using a three-dimensional structure [18]. Due to its three-dimensional characteristic, when well designed, the different orientations and heights of the photovoltaic leaves can deliver more power than one PV panel with the same photovoltaic material area.

Solar tree is a good solution to raise awareness among citizens about renewable and sustainable energy, improve the public perception of solar photovoltaic technology by making it aesthetically pleasing, and reduce the land required to harness solar energy [18]. Although this is a good solution for solar power generation, solar trees have higher costs due to its design. In addition, shading effects can occur due the orientation of panels [18] and it can be hazards to birds, insects and eyesight [19].

Solar tree can be implemented in highway rest areas and parking lot among other locations. Another feature that a solar tree can have is to collect energy from wind when it has flexible stem rotating and by its shaking movement caused by the wind [20]. The Central Mechanical Engineering Research Institute in India [21] has created a few solar tree designs and its power can achieve 5 kW. In the US, the company Spotlight Solar, commercialize different models of solar trees with power range from 1.8 to 5.3 kW [22]. Figure 11 shows a picture of solar tree in highway rest area (Colorado).

Figure 11. Solar Tree in Highway Rest Area (Colorado)

Solar Canopy

Using solar canopy is a smart method to add multiple purposes on solar panels: primarily to generate renewable energy, but also to provide shelter and shadow. The use of solar

canopy in parking lots is expanding every year. However, solar canopy can also be used at gardens and on top of buildings. Solar canopy uses photovoltaic technology, and its efficiency is based on local radiance, orientation, and angle. This option of solar power can save land space since the space underneath is usable and it is also possible to develop an aesthetic pleasant structure design to fit its location.

Solar canopies are an elevated infrastructure design to accommodate a solar panel. Differently from solar roof where the tilt and orientation are fixed, solar canopies provide more flexibility to be installed in the best orientation and appropriate tilt for the location. However, for canopies installed in parking lots the angle is limited to 10° to avoid snow drifting, visual impact, and reduced shading for the car [23]. The lifetime of solar canopies is average 25 years and during this period it requires minimal or no maintenance. Electric vehicle charging station can be installed within the infrastructure to provide renewable electricity for electric vehicles avoiding losses from the grid.

The Solar Canopy in Michigan was implemented in 2012, and it is located at the interchange of I-96 and M-44 in Grand Rapids. The 385 solar panels are mounted above a carpool lot and have 100 kW capacity. The project was developed by the partnership between MDOT, the U.S. Department of Energy and the Michigan Energy Department. The cost of the whole project, $650,000, was funded by the federal grant from the Department of Energy. MDOT owns the project and the power is used to light the parking space and the interchange I-96 and M-44. The exceeding energy flows to the grid and MDOT receives credits through net metering. The solar canopy is generating approximately $13,500 each year via net metering credits. Figure 12 shows a picture of solar canopy in parking lot (Michigan).

Figure 12. Solar Canopy in Parking Lot (Michigan)

Solar Streetlight

Solar Streetlight technology uses solar panels installed in the light pole infrastructure to power the light. The energy produced by the photovoltaic panel during the day is storage in a battery and it is used at night for lighting the lamp. The technology requires low maintenance, reduces cost, and utilizes a renewable energy source, reducing

environmental impacts. The drawback of the technology are more susceptibility to theft due its components cost, snow and dust can reduce its efficiency, and batteries will need to be replaced during the streetlight lifetime, increasing its overall cost. Additionally, the energy harvested by the system may not be sufficient to maintain the lights on during the whole night. Specially during the winter when there is shorter days and longer nights. Moreover, solar power is not constant, a bad weather day could jeopardize the lighting, and therefore the safety in the street

Solar streetlight is a photovoltaic integrated infrastructure that combines a solar panel with a pole, lighting fixture, rechargeable battery, solar charger controller, and lighting sensor control. The system can be on-grid or off-grid, in which the solar energy is responsible for all the power used to light the lamp. The cost of grid-connected system is lower than off-grid system, because using the grid as a backup system decrease the size and costs of PV panels, batteries and inverters required. The costs of an off-grid street lighting systems are generally 2–4 times higher than that for grid-connected systems [(24)].

In 1988 a 15-solar streetlight was installed in the village of Sukatani in the province of West Java of Indonesia. Even though, the social perception of the PV streetlights was positive, the project had negative results. The negative results were associated with the lack of infrastructure for supply of the system components when broken, lack of financial support for batteries replacement for example, and the need for domestic lighting apart from outdoor lighting [(25)].

Solar Pavement

Pavements absorb a large amount of solar radiation and can reach 40 MJ/m2 per day [(26)]. Harvesting solar energy from pavement creates renewable energy and also helps to reduce pavement temperature in summer and mitigate the urban heat island effect. Solar Collector Pavement (SCP) is integrated into the pavement structure and can be configured to harvest either solar energy directly from pavement surface or thermal energy absorbed by the pavement.

Two types of solar pavement can be designed: thermal collector and electrical collector. In solar collector pavement, the heat absorbed by the pavement is transferred through a fluid flow and this energy may be stored as a low-grade heat reservoir. On the other hand, an electric collector pavement consists of PV panels made of tempered glass with high resistance to support passing weight and its main application is street signaling and light.

Solar collectors in pavement can be used for heating buildings, snow and ice melting. Although metallic pipes have high thermal conductivity, plastic pipes were typically used to avoid corrosion. Water and water-antifreeze mixtures (e.g., antifreeze glycols) are commonly used as heat exchanging fluids. The efficiency of solar collector is affected by geometrical and operational parameters, such as pipe spacing, depth, and fluid flow rate [(27)]. However, the piping system has several unavoidable limitations. First, pavement is weakened due to the placement of piping system inside it. Second, the leakage of pipe might happen under heavy load. Third, the piping system increases the difficulty of pavement rehabilitation.

Solar pavements with PV panels on the surface are usually 30% to 50% less efficient than traditional PV panels. This efficiency reduction is a result of flat-position installation; obstacles blocking the sun like trees, buildings, dirty and cars; and the efficiency reduction due to hot surface of pavement. Another drawback related to this technology is regarding safety since the transparent and glassy material on pavement can decrease skid resistance, which requires special treatment of glass.

In 2014, the company, SolaRoad, constructed a 70-m bike path with solar panels in Krommenie, Netherlands. Due to the success of the project, in 2016 the bike path was extended in 20 more meters. The pavement is consisted of a concrete bottom layer and a transparent tempered glass with a rough and transparent coating on top layer. The bike path generated 9,800 kWh in the first year [(28)]. It was found that the flat angle of solar panel is 30% less efficient compared to the electric power generated by the conventional rooftop PV panels [(29)].

In 2015, the company of Colas, in cooperation with the French National Solar Energy Institute, built a 1-km long solar road containing 2800 m^2 of PV panels in the region of Normandy on France (Figure 13). The technology is called Wattway that consists of a very thin film of polycrystalline silicon and is coated with a resin layer to increase resistance and friction. The solar cells were reported to be traffic resistant and skid resistant and thus can be used on all types of road infrastructure in the future. The power produced by the road was used to power the village lights. However, it was found that intense wear was caused by the traffic and the energy produced did not meet the expected [(30)].

In 2017, a solar highway with two lanes and the emergency lane was opened in Jinan, China. The 5,875 m^2 solar highway can produce 170 kWh annually per square meter that directly feeds the grid. The technology consists of three layers: insulation material on bottom layer, photovoltaic panel coated with a special silicon film on central layer, and transparent concrete on top layer. The highway suffered from severe damages after its inauguration. The investigation concluded that the objects that felt from moving vehicles were the main cause [(31)].

Figure 13. Solar Pavement - Wattway by Colas (France)

Comparison of Different Ways of PV on Roadway

The comparison of different applications of solar energy with PV panels are summarized in the following Table, including the efficiency, advantages, and disadvantages.

Table 2 - Comparison of Different Ways of PV on Roadway

Application	Efficiency	Advantages	Disadvantages
Solar Array in ROW	Equal to PV panels (9.5 – 22.4%)	- Use large available area - Add value to public ROW - Produce great amount of energy	- Visual impact - Vulnerable to vandalism - Roadside obstacle - Wildlife impact
Solar Noise Barriers	11% to 22%	- Add value and function to existing noise barrier - Novel transparent solar panels can improve aesthetic - Wildlife protection - Energy can help pay capital investment	-Vulnerable to vandalism - Shading effect - Glare complains when PV panels are 60 degrees from horizontal
Solar Tree	10 to 15% more than PV panels	- Visually pleasant (can be design to be aesthetic) - Can be used in small areas - Does not depend on road orientations - Can enhance efficiency of solar PV systems	- Shading effect due to random orientation of panels - Less efficient at zenith angles around 0° - Limited to low power applications with battery storage - Not suitable for grid connected systems due to inverter losses - Reflections can be harmful to human eye
Solar Canopy	Equal to PV panels (9.5 – 22.4%)	- Used as shelter and shadow - Use existing parking lot space and does not require extra space	- Produce small amount of energy - Restrict to parking lot orientation
Solar Pavement	30% to 50% less than PV panels	- Use of pavement surface and does not require extra space - Mitigate urban heat island effect	- Low efficiency - Existing projects produced less energy than expected - Panels can be covered by dust, dirt, snow and shadow - Performance drop due to high temperature - Thick glass to resist traffic weight decrease system efficiency

Experience from Previous Solar Highway Projects

Solar Highway Projects Implemented by Different DOTs

A number of solar array projects have been built by different state DOTs in U.S. using different business models, which are summarize as follows.

Oregon: Demonstration Project

The first US solar project in highway ROW was implemented in 2008, which is composed of 594 solar panels with 104 kW capacity. The system is located at the interchange of Interstate 5 and Interstate 205, and its power is used to light the interchange. The project is a public-private partnership between ODOT and Portland General Electric (PGE). PGE was responsible for financing, coordinating design, construction, operations, and maintenance. To take full advantage of tax incentives, PGE partnered with a financial institution (U.S. Bank) serving as a tax equity partner through a limited liability company (LLC). Those incentives include the federal Investment Tax Credits (ITC), accelerated depreciation, and Business Energy Tax Credits (BETC). The business agreement between partners includes a site leasing and PPA; the electricity produced is delivered to ODOT through net metering and used to light the interchange [32].

Oregon: Baldock Solar Station

The Baldock Solar Station is sited in a rest area on the south of Wilsonville on Interstate 5 and was placed into service on January 2012. It consists of 6,994 solar panels with 1.75 MW capacity. As the demonstration project, the Baldock is also a public-private partnership with PGE. The utility company again partnered with a financial institution to take full advantage of the tax incentives; however, instead of doing an LLC, the relationship was based on a sale-leaseback arrangement. This new agreement is less complicated and has less transitional costs. The benefits of this agreement include the federal Investment Tax Credits (ITC), accelerated depreciation, and Business Energy Tax Credits (BETC). Differently, from the previous Demonstration Project, Baldock business agreement was based on a site license fee paid to ODOT and ODOT also has the benefits of Renewable Energy Credits (RECs). The electricity is used to serve PGE customers, including ODOT.

Colorado: E-470 Toll Road Solar Project

The E-470 Road Solar Project is divided in 22 sites along a 17-mile stretch of the 47-mile orbital corridor around Denver. The 707.3 kW capacity solar project was installed in 2012 and its produced electricity is used to power road surveillance cameras, streetlights, variable message signs, toll collection equipment, toll plazas, and maintenance facilities along the corridor; and the E-470 Administrative Headquarters building. Adams Energy, now C2 Energy Capital, funded the entire project that costed $2.8 million. The developer retains all financial income derived from the project including the federal tax credits ($750,000) and Xcel Energy rebates ($180,000). The E-470 Public Highway Authority and Adams Energy have a 20-year PPA, but no lease agreement.

Colorado: Northwest Parkway

Built in 2011 in the northwestern portion of the Denver metropolitan area Northwest Parkway has 22 solar panels in seven locations and have 62 kW capacity. The generated

energy is used to powering under-deck bridge lights, roadside, and overhead signs, and tolled ramps via net metering with Xcel Energy. The solar developer Soltura Energy Capital funded the project that cost $350,00. The developer is also responsible for the maintenance. Although the project was driven by its social and environmental value, it benefits from the RECs, rebate, and PPA with the utility company. The PPA consists of a fixed rate of $0.052/kWh and an increase of 3.5% annually. The estimate save of the project for is $250,000 in 20 years.

Massachusetts: Highway Right-of-way Solar – Phase 1A

MassDOT implemented phase 1A of the solar project that intended to have more than 7MW. The phase 1A consists of eight bundled solar projects with 4.3 MW total capacity. MassDOT has a 20-year PPA and lease agreement with Amaresco. The public agency purchases power at a reduced rate, receives money for the airspace/land lease and from net metering credits. On the other hand, the developer retains all incentives from tax and SRECs (Solar Renewable Energy Credits). The tax incentives consist of the Federal Investment Tax Credits (30% total system costs can be directly subtracted from the system owner's income tax) and Modified Accelerated Cost Recovery System (tax base deduction centered on an accelerated property depreciation schedule). The state expects to generate at least $15 million in savings over the contract of 20 years for the whole project (Phase 1A and Phase 1B).

Ohio: Veteran's Glass City Skyway Solar

The Veteran's Glass City Skyway Solar Project, installed in 2011, was deployed to offset the electricity demand and operation cost associated with a 196-foot light-emitting diode lighted structure. The solar array has 1,164 solar panels and total capacity of 117.5 kW. The project was a result of a partnership between Ohio DOT and the University of Toledo. The University of Toledo operated and maintained the system during the research phase and then Ohio DOT assumed the ownership and responsibility. The highest revenue from the project is to sell SRECs (Solar Renewable Energy Credits). In 2011 the project generated 129 MWh, which could produce $29,000 to $42,000 in revenue. To finance the project Ohio DOT received a grant of $1.5 million from the Department of Energy and University of Toledo match with 259,132. The total cost of the project was $1,805,469.

Florida: Turkey Lake Service Plaza

Sited in the Turkey Lake Service Plaza at the mile marker 263 in Florida's Turnpike State Road 91, the solar project built in 2012 consists of 468 solar panels with 112 kW power capacity. Differently, from previously discussed projects, Florida state law does not allow PPA between public and private agencies. Without a private sector partner, the Florida Department of Transportation (FDOT) and Florida Turnpike Enterprise constructed and operated the solar project. The cost incentive of the project was a $127,920 rebate from Duke Energy, and the total project had a cost of $351,580. The payback period is calculated to be beyond 25 years.

Suggestions and Lessons Learned

Based on the guideline provided by FHWA and the experiences of various projects built by state DOTs, the suggestions and lessons for implementing solar highway projects were summarized below.

Overall

- Solar Projects take time and require a project champion (Baldock and Demonstration Project, Oregon)
- Create partnerships with external stakeholders (FHWA)
- Develop an internal interdisciplinary team to address the unique issues renewable energy projects in the ROW present (FHWA)
- Ensure there is contractual agreement flexibility in case road configuration changes in future (Northwest Parkway, Colorado)
- Challenge of mission alignment from some DOT staff to see connection between solar and transportation (Demonstration Project, Oregon)

Social

- Identify appropriate renewable energy technologies and potential sites through a statewide or regional feasibility study (FHWA)
- Review long-range transportation plans to identify potential siting conflicts or to develop guidelines for how renewable energy and alternative fuel facility projects might be included in statewide transportation planning (FHWA)
- Large number of solar panels along highway ROW may be perceived as visual impact.
- It is important to work closely with local municipalities (Northwest Parkway - Colorado and Baldock and Demonstration Project - Oregon)

Financial

- Electric utilities may not be interested in solar projects due to their lack of business and environmental interest (Turkey Lake Service Plaza, Florida)
- Procurement took more time and cost were higher than anticipated (Turkey Lake Service Plaza, Florida)
- Try to lock in fixed energy cost rate for six years and then fixed annual rate increase for the remainder of the agreement (E-470 Tollway Solar Project – Colorado)
- Look for utility and government rebates (E-470 Tollway Solar Project – Colorado)
- The utility was reluctant to approve the project for net metering, MDOT had to reduce the project which costed additional $25,000 to $30,000 (Solar Canopy, Michigan)

Laws and Regulations

- VTrans was not able to take advantage of financial incentives that were only available to taxable entities such as developers (Fair Heaven Welcome Center, Vermont)
- Revise state UAPs (Utility Accommodation Plans) to include renewable energy (FWHA)
- Identify state statutory or regulatory constraints that preclude resource development and devise resolutions that would instead foster such development (FHWA)

Geothermal Energy Harvesting on Roadway

Geothermal energy harvesting uses the energy from heat derived within the sub-surface of the earth. Geothermal energy harvesting uses the energy from heat derived within the sub-surface of the earth, which has been used for decades as a clean, renewable, and cost-effective source of energy.

Although energy can be generated for different applications, the most usual application on roadway is for heating purposes. Geothermal energy does not depend on the weather or time of the day, and it is a cost-effective solution for snow melting or deicing [(33)]. The process consists of a pipe system in which heat is extracted from underground soil and carried in a circulating fluid. The heated fluid cycles back to the surface, where the tubes are embedded in the pavement, melting the ice and then flows back to underground soil, this system is repeated continuously. The fused fluid can be ground water from warm aquifer pumped to the surface and then refilled [(34)].

The installed heating capacity is determined by the climate conditions and the system purpose: snow melting at a specific snowfall rate, de-icing, keeping clear of ice, etc. For example, snow melting requires higher heating capacity than ice-formation prevention. The system design is composed by the heat source; the supply temperature with or without heat pump; the depth of the heating tubes in the pavement; the lengths of tubes; and distance between them [(35)].

Although there are different ways of using geothermal energy to generate electricity, the most common way for roadway applications is using the heat for deicing. Several example projects have been built and summarized below.

<u>Japan: Sidewalk heating in Aomori City</u>
Aomori City in Japan is considered one of the snowiest cities among the world with populations of 300 thousand or more. An annual snowfall can exceed 10 m. In this scenario, in 2012, two sidewalks heating system using geothermal were installed, as shown in Figure 14. The total covered area is 659 m^2: one sidewalk covered 334 m^2 and the other one 325 m^2. Each unit employed four borehole heat exchangers (each 150 m long) and one electric heat pump with electrical capacity of 22.5 kW. The total heat output of a unit was roughly 35 MWh. The operating costs of this sidewalk heating system were given with 6 Euros/m^2/year for the electricity consumption only and the operation time in the first two years was 500 hours annually [(36)].

Figure 14. Sidewalk heating in Aomori City, Japan – condition on the snow-melting section in December 2002

Switzerland: Access Way Heating

The project consists of 25-m^2 pavement composed of a geothermal system for snow melting on an access road to a private parking area near Zurich. The total heat output was 9 kW and total operation time in winter was 600 hours. Geothermal heat source consists of one borehole heat exchanger with a depth of 260 m. The total costs for drilling and installing the borehole heat exchanger, piping and heating installation in the pavement, and the control system and the commissioning was 855 Euro/m^2. The electricity needed per year is around 350 kWh [(35)].

France: Novatherm

French company, Eurovia, developed a project in Merignac using geothermal technology to clear ice and snow on road surface. They designed two projects, one with vertical heat exchangers that proved to be more efficient, however, more expensive since its drilling were up to 40 m (120 ft). The horizontal heat exchanger had satisfactory result of de-icing in a rate of 1 cm per hour. Both projects required heat pumps of 30 Watts, and had 4 watts of thermal energy generated for every watt of electrical energy consumed [(37)].

U.S. (New Jersey): Bridge Deck

In 1969, heat pipes were used for deicing a bridge deck in Trenton, New Jersey The system used ethylene glycol-water mixture as the circulating fluid. It had pipes embedded 2 inches below the pavement surface and a horizontal grid buried 3 to 13 feet below the pavement on 2- foot levels. The system snow melting rate is between 1/4 and 1/2 inches per hour in a regular condition where the air temperature ranged between 20 and 35 degrees Fahrenheit. Comparing to an electric heating system that produce around 68 Btu/h/ft^2, the geothermal system is more efficient and requires only 2% of the electrical power required for the electric system [(33)].

U.S. (Texas): US 287 in Amarillo

In the late 1980s, conventional geothermal wells were used to heat concrete decks on the north and south-bound of the two-lane bridges on US 287 in Amarillo over N. 15th

Avenue in Texas (Figure 15 [38]). Each bridge had a heated area of 8600 ft^2 and the purpose of the project is ice prevention with a heat flux of 12 W/ft^2 [33]. Each structure used 50 geothermal wells that were located between the bridges and on the east side of each bridge. Each 4-inch diameter geothermal well was 176-feet deep, did not reach ground water, and contained two pipe loops. The costs of construction and operation were $1,200,000 and $7,500, respectively [33].

Figure 15. Amarillo, TX geothermal heating system construction: heating hoses in place ready for concrete pour

Wind Energy Harvesting on Roadway

Wind harvesting energy converts kinetic energy from the wind to mechanical energy and then electrical energy. Uneven solar heating of land and sea surface produces winds and the wind is strong and steady in some locations, which is attractive to harvest wind energy. There are a few new technologies being studied like airborne wind energy, wind turbine with tip rotors, and multi-rotor wind turbine. However, the two mature and most used types of turbines are: horizontal axis turbine and vertical axis turbine. After solar energy, wind is the alternative source more used by the transportation sector according to a survey performed by Grasman et al. (2011) [39].

Highways provide a considerable wind resource for harvesting energy due to its traffic. However, the turbulent wind is generated due to traffic instead of steady wind, which is more suitable for vertical axis turbine. Some other concerns related to the implementation of wind turbines along highways are noise, aesthetics and, specially, safety. Since the turbines must be placed in a high traffic area, which have high wind volume, several safety provisions must be considered in the project. Some of these safety measures are highway guards surrounding the rotating turbine blades and warning labels [40].

<u>Horizontal Axis Wind Turbine</u>

In horizontal axis wind turbine (HAWT), the turbines extract kinetic energy from wind, convert to mechanical energy at the rotor axis and then convert mechanical energy into

electrical energy using an electric generator [41]. The rotor axis is parallel to the ground and in the direction of the wind. These turbines are usually equipped with self-starter and yaw system to turn the blades towards the wind [10]. Its components are foundation, tower, nacelle, rotor blades, hub, and transformer. The number of blades can vary; however, three blades are usually the most efficient. The tower can be made of steel truss latticework or tubular pole, the last one is aesthetic preferable.

The blades of HAWT are positioned to the side of the gravity center of the turbine, which increase the system stability. It has ability to wing warp, which gives the turbine blades the best angle of attack. This type of turbine also has the ability to pitch the rotor blades in a storm to minimize damage [42]. Tall tower allows access to stronger wind in the sites with wind shear and allows the placement on uneven land or in offshore locations. Most HAWT are self-starting and its efficiency can reach 59.3% [43].

Usually HAWT are built far from an urban area due to several concerns: 1) turbines might cause noise and aesthetic pollution; 2) turbine blades could damage local wildlife [41]; 3) it affects radar in proximity, it is relatively ineffective in urban situations; and 4) there are other public safety concerns [10]. Construction of HAWT has a lot of difficulties such as difficulty operating in near ground winds, difficult to transport (20% of equipment costs), and difficult to install (require tall cranes and skilled operators). Besides, this technology is hard to perform maintenance and decrease in efficiency on wind farms due to wake effect [44].

Vertical Axis Wind Turbine

Vertical Axis Wind Turbine (VAWT) provides potential solutions for wind energy harvesting when the wind flow is complex. This technology differs from the previous one by the axis of rotation, which is perpendicular to the directions of wind and ground. These turbines are relatively simple and do not need any yaw system and a self-starting mechanism [10]. The Darrieus turbine is the most common VAWT, it has higher performance and a symmetric profile blades [45].

VAWT can work with lower and turbulent wind, which makes this technology a promising solution in urban and semi-urban areas. Other advantages are: low environmental impact, produce energy from any direction wind, simple in design, quieter than HAWT, easy to maintain, lower construction and transportation costs, and it is most effective at mesas, hilltops, ridgelines, and passes. However, VAWT have low efficiency [10], around 19% [46]. Its blades constantly spin back into the wind causing drag and low starting torque that may require energy to start turning. VAWTs are able to fulfill specific energy generation requirements that HAWTs cannot fulfill. Although HAWT achieves higher efficiencies, this performance only happens when there is high quality energy wind, which is constant and strong [47].

Missouri DOT developed two 1.2 kW vertical-axis wind turbine at The Conway Welcome Center on route I-44. The turbines were installed in different travel direction and it powers the light over the information counters. The facility provides 85 car parking spaces, and

75 trucks and recreational vehicle parking space. Together with the wind turbines, automatic sink and toilets to conserve water are green initiatives [39].

French motorway operator Autoroutes Paris Rhin-Rhône (APRR) tested a 1.5 kW vertical-axis wind turbine from Cita Production in the road A6 between Paris and Lyon. The wind power generated by passing trucks is designed to supply roadside devices such as road signs, cameras, traffic monitoring sensors, and weather stations, where connection to the electricity grid would be too expensive [48].

ANALYSIS OF SOLAR ENERGY AT ROW OF NJ ROADWAY

Project-Level Solar Energy Analysis

Solar Energy Analysis Method

PVWatts estimates the electricity production of a grid-connected photovoltaic system, in which the user inputs the system size, module type, system losses, array type, tilt angle, and azimuth. The azimuth angle is 0° when the panels face north and 180° when facing south. The data files used in the application include the National Solar Radiation Database (NSRDB) 1961 – 1990 data (TMY2) and the 1991-2010 update (TMY3). PVWatts assumes an albedo of 0.2 for all hours of the day for TMY2 and uses the hourly value provided in TMY3 [49].

The PVWatt has several sub-models embedded on its application to estimate the solar energy production. The application uses Perez model with slight modifications. The Perez model uses the anisotropy of the sky's diffuse irradiance to predict irradiance on a tilted surface. The model algorithm for the Diffuse Irradiance (D_c) on a tilted surface of slope (S) is given in Equation 1-3 [50].

$$D_c = D_h \left[(1 - F_1) \left(\frac{1+\cos\beta}{2} \right) + F_1 \frac{a}{b} + F_2 \sin\beta \right] \quad (1)$$

$$a = Max[0, \cos\theta] \quad (2)$$

$$b = Max[\cos 85^\circ, \cos Z] \quad (3)$$

where, D_h is the horizontal diffuse irradiance; F_1 and F_2 are the circumsolar and horizontal reduced brightness coefficients, respectively; a and b are terms that account for the respective angles of incidence of circumsolar radiation on the tilted and horizontal surfaces; and θ and Z are the solar incidence and angles on the tilted surface and the horizontal, respectively.

The angle of incidence is found using Equation 4 [51].

$$AOI = cos^{-1}[\sin\theta_{sun} \cos(\gamma - \gamma_{sun}) \sin\beta + \cos\theta_{sun} \cos\beta] \quad (4)$$

where, AOI is the angle of incidence, β is the tilt angle, γ is the surface azimuth, γ_{sun} is the sun azimuth, and θ_{sun} is the solar zenith.

The plane-of-array (POA) which measures the incident irradiance on the module is calculated using Perez 1990 algorithm shown in Equation 5 [49].

$$I_{poa} = I_b + I_{d,sky} + I_{d,ground} \quad (5)$$

where, I_b is the beam normal input multiplied by the cosine of the angle of incidence, $I_{d,sky}$ is total sky diffuse on the surface, and $I_{d,ground}$ is the ground reflected irradiance.

Solar Energy Analysis Result

The case study analyzes the implementation of a solar array on the highway right-of-way of US-1 in North Brunswick, NJ, as shown in Figure 16. The design parameters are calculated, and an economic analysis is performed for two business models, net metering if the project is single owned and PPA if the project is third-part owned.

Figure 16. Solar ROW on US1 - North Brunswick, NJ

The project assumed a security distance of 60 feet from the edge of the road, same value used for ODOT in the Demonstration Project [32]. The panels are orientated facing south, orientation that provides the most energy absorption. The design parameters calculated to optimize the energy production is the panel tilt and the distance between rows. The optimal panel tilt can be found by fitting a polynomial equation of energy output by tilt data. The data is obtained using PVWatts [52], a web-application developed by the National Renewable Energy Laboratory (NREL).

The optimal tilt for the solar array was determined by founding polynomial equation using the results from PVWatt for a 4 kWdc size system in the studied location facing south. Figure 17 shows the graph and the polynomial equation for the annual energy output based on the tilt. The highest energy output is achieved when the tilt is 37 degrees.

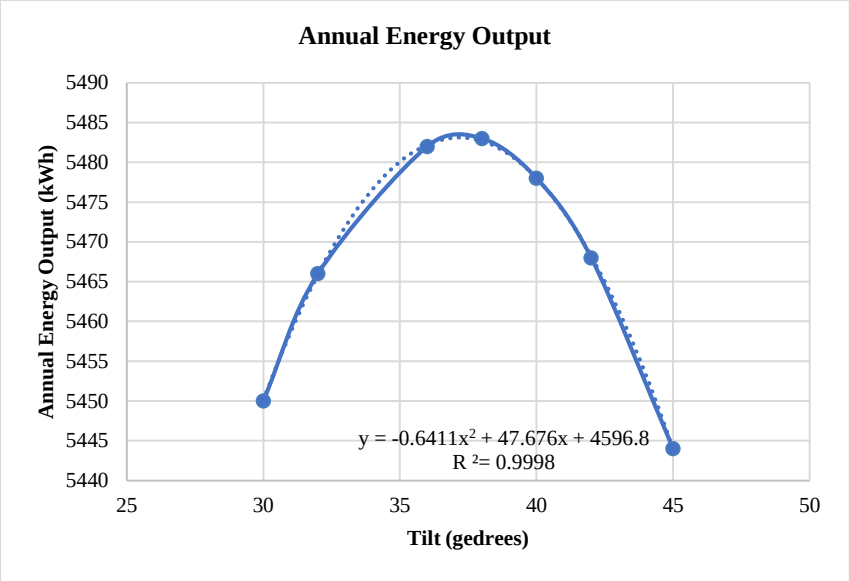

Figure 17. Annual Energy Output (kWh) of a 4kWdc system facing south on ROW in North Brunswick, NJ

The inter-row spacing is calculated with basic trigonometry, as shown in Figure 18 [53]. Determining the inter-row spacing can be very challenging. When the distance is too small each row casts a shadow on the row behind decreasing the system efficiency; however, calculating the distance to avoid any shadow from the anterior row will require much more space reducing the number of panels installed. Then, the total energy output may be too small to justify the panels' implementation.

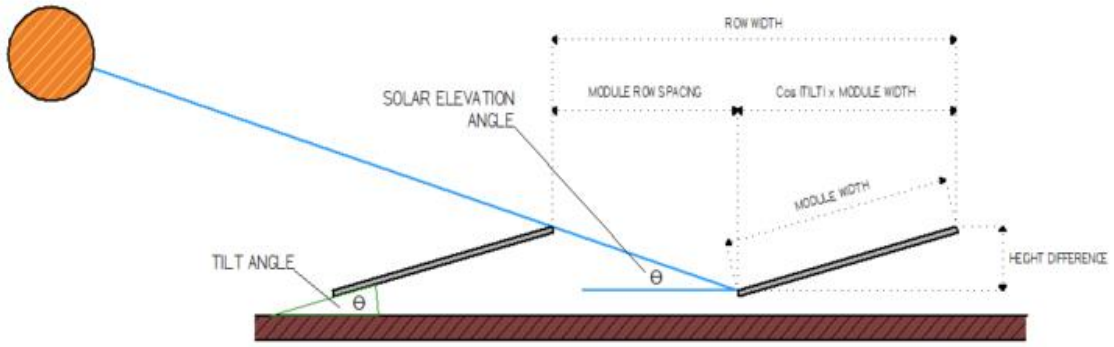

Figure 18. Module Spacing Scheme

For this case study the inter-row spacing was calculated to avoid module shading cause by another module at noon on winter solstice, the day that the sun has the smallest elevation angle. Figure 19 is the sun chart for North Brunswick, NJ was obtained on the University of Oregon Solar Radiation Monitoring website [54] for December 21, 2019. The sun elevation angle at noon is around 26 degrees.

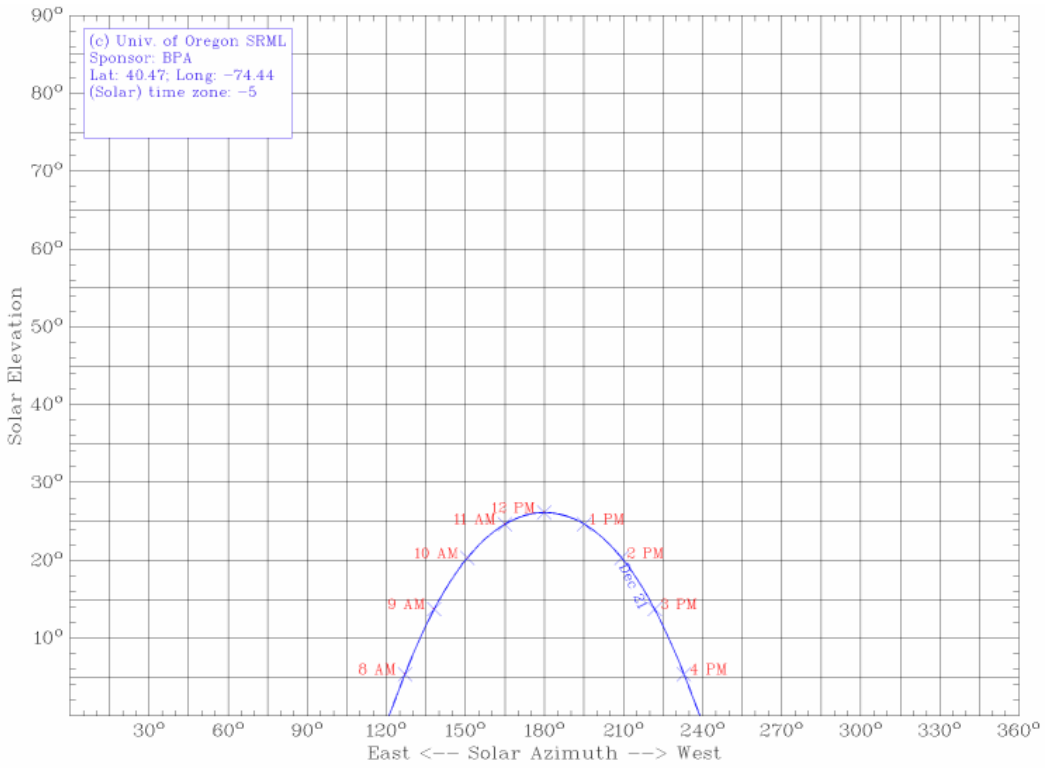

Figure 19. Sun chart from North Brunswick, NJ obtained at University of Oregon Solar Radiation Monitoring Laboratory website

The solar module used for the calculations is the SPR-P19-310 from Sunpower and its dimensions are 0.998 m x 1.690 m. They are assumed to be installed on a landscape position to minimize shading on the following row. The modeling distance spacing calculated with the aforementioned parameters is 1.25 meters. The annual energy output was calculated using HelioScope, a web-based software developed by Folsom [55]. The design used the parameters calculated above, including the specific solar panel SPR-P19-310 from Sunpower. The design accommodates 117 modules, total of 36.3 kW power, and two inverters of 24 kW power each. The system annual production is 51.7 MWh.

Project-Level Economic Analysis

Business Models of Solar Highway Projects

Public agencies, like DOTs, cannot take advantages of the tax-related financial incentives available for investments in renewable energy systems. To implement a feasible renewable energy project in that scenario, public agencies partner with the private sector to take advantages of all taxes incentives. This partnership is called 3P (public-private partnership), and in this case, the project is third-party owned. If the public agency did not partner with a private agency and built, operate, and maintain the renewable energy facility, it is called Direct Ownership. Renewable energy project can use financial benefits depends on the type of business. For third-party ownership, it is possible to benefit from Federal Investment Tax Credits, some state tax credits, rebate, and renewable energy

credits (RECs). In the case of direct ownership, the benefits can come from rebates, RECs, federal grants, and research funds [32].

Public-private partnerships can be very beneficial to DOTs, besides taking advantages of the taxes initiatives; the private sector partner is also responsible for the upfront capital cost, as well as the operation and maintenance responsibilities [32]. For the project to be profitable to the public agency as well as to the private company in case of third-party ownership, there are different business agreements: net metering, lease, and PPA. When the agency owns the facility, the business agreement used is net metering.

Net Metering

Net metering is a bill credit provided by the utility company for electricity generated by a grid-tied system in surplus of a customer's on-site consumption [32]. In other words, the customer-generator of solar energy would become a small electricity generator being compensated by the excess amount of energy that is not used in the facility [54]. Forty-one states and Washington D.C. have rules that require electric utilities to provide net metering [32]; however, every state has different rules. New Mexico, for example, does not have net metering fee rule. In this case the utility company may impose high charges making it less profitable for the DOT [54]. In New Jersey, at the end of an annualized period, the customer-generator of renewable energy receives full retail credit on their utility bill for each exceeded kWh [57].

Airspace/Land Lease

To build a renewable energy facility at the right-of-way, it needs to meet the Utility Accommodation criteria. First, the facility needs to meet the definition of "utility," which is satisfied by a renewable facility that produces energy. Last, the facility needs to meet the public service criteria specified in the definition. Usually, this last one is met when the facility provides service to the general public or when it is dedicated to own use of a transportation agency. Besides those criteria, the facility must be conforming to the policies and standards from the Utility Accommodation Plan, which is an agreement between the transportation agency and the FHWA [32].

In case the facility cannot be fitted under a state's Utility Accommodation Plan, there is the possibility of the site under an air space lease. The air space lease is usually permitted when the project does not conflict with the operation, maintenance, and safety of the highway facility. All air space lease agreement needs to be approved by FHWA [32]. Under airspace lease, the transportation agency must charge a fair lease rate at market value; however, the agency may seek FHWA’s approval to charge below-market lease rates in case the facility is in the public interest for social, environmental and economic purposes [32]. Any resulted revenue from leasing must be used for transportation purpose [54].

Power Purchase Agreement

Power Purchase Agreement is a long-term contract that commits the solar developer to finance, build, operate, and maintain the solar system. On the other hand, the transportation agency purchases the electricity produced. The energy price is fixed, usually lower than current utility rates, and sometimes includes an annual price escalator

[32, 54]. The private sector partner benefits from the guaranteed electricity sales, captured tax and financial incentives. This business agreement is not authorized in all US territory. In Florida, for example, is not permitted for a public agency to be involved in a PPA, in that case, the facility is owned by the FDOT like the Turkey Lake Service Plaza Solar Project [58].

Economic Analysis Method and Parameters

The economic analysis of a solar array is performed by using the System Advisor Model (SAM) developed by NREL [59]. The web-based tool can be used to evaluate the performance and economic feasibility of solar projects for different financial models. The tool calculates the energy output of the solar system by inserting the project parameters. The output generated includes the initial investment cost, payback time and lifetime cashflow. The residential and commercial model have the renewable energy system on the customer side of the electric utility meter (behind the meter), and power from the system is used to reduce the customer's electricity bill. Power purchase agreement (PPA) projects have the system connected to the grid at an interconnection point, and the project earns revenue through electricity sales. The project may be owned and operated by a single owner or by a partnership involving a PPA or leaseback arrangement. On the third-part ownership the system is installed on the customer's (host) property and owned by a separate entity (developer). The host is compensated for power generated by the system through either a PPA or lease agreement.

The cash flow is used to describe the economic evaluation of a company or project. The suitable cash flow for the analysis could be after-tax cash flows, before-tax cash flows, incremental cash flows, among other types. The cash flow registers the operating, investing, and financing activities of a company or project. The inflation rate is used to input the current dollar in a cash flow required in the year the cost is incurred. The current dollar cash flows will change over time depending on the inflation. The cash flow can be converted from constant dollars (F_n) to current dollars (F_m) in a period of m-n years by the Equation 6, where e is the constant inflation rate.

$$F_n = F_m/(1+e)^{m-n} \tag{6}$$

The discount rate used in financial analysis represents the time value that an investor waits for a return on an investment, and it reflects the interests that the money could get from being invested. The discount rates are often used to account for the risk inherent in an investment. Using the nominal discount rate to calculate the present value of a future payment, the inflation is already included in it, to exclude inflation the real discount rate should be used. In other worlds, the nominal discount rates and current dollars include inflationary effects, while real discount rates and constant dollar exclude this phenomenon. To calculate the nominal discount rate (d_n) from the real discount rate (d_r) and inflation (e), the Equation 7 can be used.

$$d_n = [(1+d_r)(1+e)] - 1 \tag{7}$$

The case study analyzes the project as single-owned, or third part owned. When the project is owned by the DOT, the benefits from tax incentives cannot be considered. The

main economic parameters used by SAM to calculate cash flow and payback time are summarized in Table 3.

Table 3 - Financial Parameters

Parameter	Value	Source
Federal income tax rate	21%*	Tax Policy Center – Urban Institute & Brooking Institute [60]
State income tax rate	9%*	NJ Treasury, Division of Taxation [60]
Real discount rate	1.37%	Average of the last 10 years – OMB Circular A94 [60]
Inflation Rate	1.1%	CPI, Northeast region in November 2020 – U.S. Bureau of Labor Statistics [63]
Loan rate	6%	>5.99% Funds; >3.99 Lendingtree, >3.49% Credible and Monevo
State sales tax	0%*	PV energy sales tax exemption [64]
Federal ITC – Investment Tax Credit	26%**	Solar Energy Industries Association [65]
Production based incentive	SREC $221/1,000kWh (+1.1%) 10 years	New Jersey's Clean Energy Program [66] and NJSREC [67]
Electricity increase	1.1%	Following inflation rate
Net salvage value	0%	SAM default [59]

* For Single Owner projects the federal and state taxes are 0%
**26% of the cost of the system is deductible from taxes until 2022, after that the value drops to 22%

The energy generated by this project can either be used by street lighting in the same location or to feed the grid and to reduce the electricity bill cost of the state DOT. The Department of Transportation cannot sell energy, different models could be implemented like a PPA, or if it is owned by the DOT the energy should be used by the agency and not sold. The energy required from the project was calculated assuming that the system was installed to net the consumption of a mile of street lighting. The electricity consumption is calculated for 30W lamps, and one streetlight every 30 meters for a mile, total of 54 lamps. Table 4 summarize the energy consumption per season, assuming each season lasts 4 months.

Table 4 - Streetlight Energy Consumption per Season

Season	Daily streetlight operation (hours)	Total Energy Consumption (MWh)
Spring	10	19.4
Summer	8	15.6
Fall	10	19.4
Winter	14	27.2

During the summer the days are long and therefore the number of hours that the streetlight will be on is small. The opposite occurs during the winter, short daylight requiring more hours of streetlight operation than that for the other seasons. The total annual consumption required for the study case is 81.65 MWh.

Economic Analysis Results

Single Owner – Net Metering

The module cost is estimated to be $0.32/Wdc and the inverter $0.07/Wdc. The balance of system, installation labor and installer margin, and overhead are assumed to be $1.02/Wdc. The indirect cost considered is $0.11/Wdc for permitting and environmental studied, which totalize an initial investment of $56.7k. The financial benefits occur in the reduction of the electricity bill, as shows in Figure 20. The electricity rate used in the analysis is 8.48 cents/kWh. Figure 20 shows the cost of the electric bill with the system and without the system. The reduction of the electric bill using solar energy is 63.3% in the first year and the reduction increases on the following years.

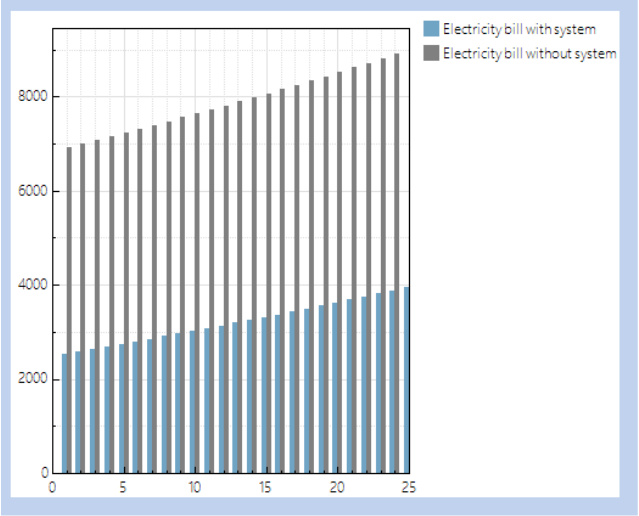

Figure 20. Electric bill with and without the system - Single Owner

Figure 21 shows the after-tax cash flow of the system during the 25 years lifetime. This analysis does not include a battery cost. It assumes that during the day the energy feed the grid and during the night, when the streetlights are being used the electricity is obtained from the grid, and DOT has a discount in their bill for the energy produced, also called net metering.

The after-tax cash flow shows that until year 10 the project has a great return due to the RECs selling. From year 11 on, the profit comes from a cheaper electricity production compared to buy the electricity. Until year 15 the system is being paid through out a loan, although in the first 10 years the RECs overcome the principal and interest, from year 11 until year 15 the cash flow is negative. After the loan is paid the cash flow is positive again. The payback time of the project is 4.0 years with a Net Present Value (NPV) of $94.3k, proving that the project is very profitable.

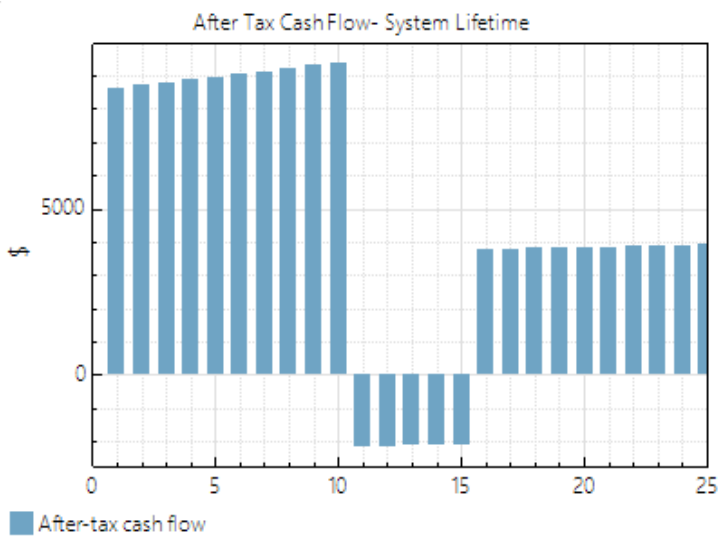

Figure 21. After Tax Cash Flow System Lifetime

Third Part Owner – PPA

In this section the analysis assumes that the system is owned and operated by a private company. The energy is used by the DOT and the system is also implemented in the DOT property. The private company benefit from selling the electricity to the DOT by a pre-fixed cost called PPA agreement, and the DOT benefits from paying less for the electricity than the regular rate that it pays to the utility company. For this scenario, the private company pays income taxes, however it also benefits from tax credits. In NJ photovoltaic projects have sales tax exemption, so even though is a private company, there is no sales tax in the project.

Four scenarios varying the electricity price of the PPA, and the rebate was analyzed. The scenarios and respective results are summarized in Table 5, and the after-tax cash flow from the host and developer is found on Table 6. The graphs show the after tax cash flow ($) in the vertical axis through time (years) in the horizontal axis.

Table 5 - Third Party Results Summary

Scenarios	PPA (cents/kW)	Rebate (% of System Cost)	Host NPV ($)	Developer NPV ($)
Scenario 1	8.48	-	5,411	67,960
Scenario 2	7.63 (-10%)	-	13,516	62,134
Scenario 3	5.94 (-30%)	-	29,629	50,549
Scenario 4	4.24 (-50%)	10%	45,839	46,901

Table 6 - Host and Developer After tax cash flow for Third Party Ownership

Scenarios	Host (NJDOT)	Developer (Third Party)
Scenario 1	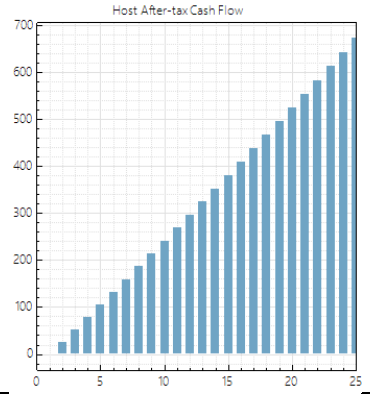	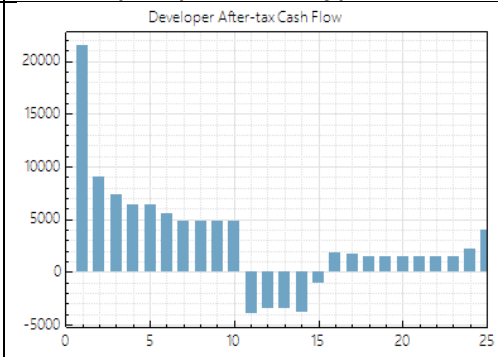
Scenario 2	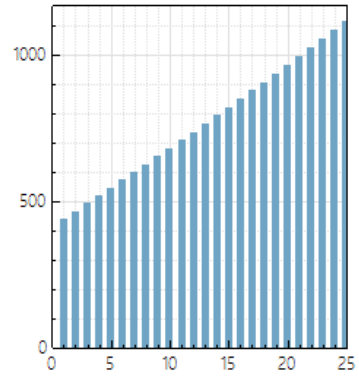	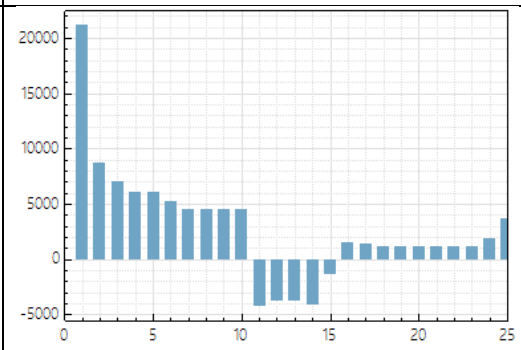
Scenario 3	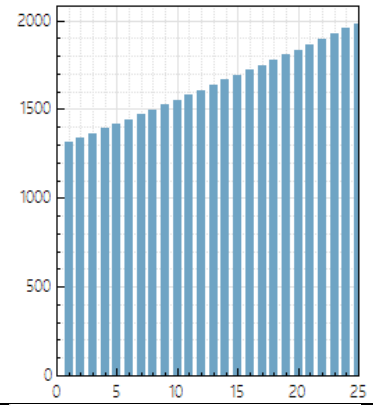	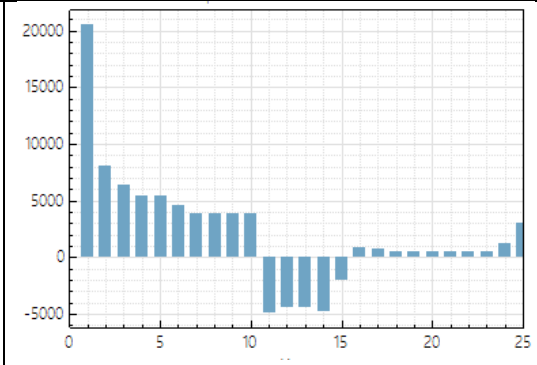
Scenario 4	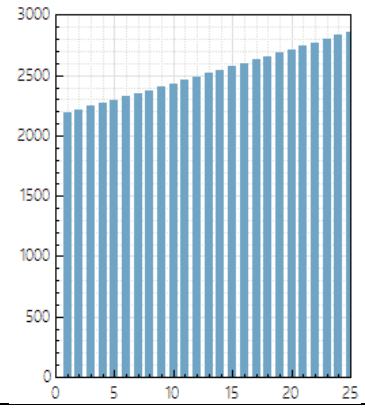	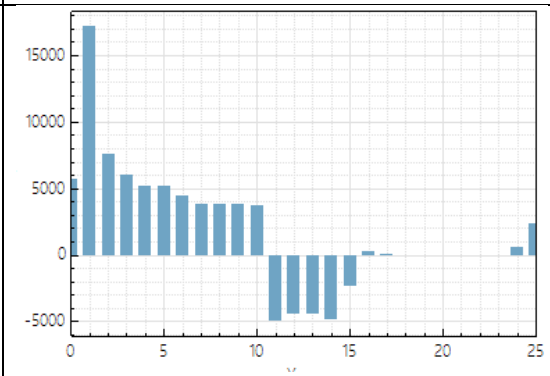

The results show that the project is profitable for the host and developer in all four scenarios. The Scenario 1 is very profitable for the host; however, the NPV for the developer is small and probably not enough to justify the investment. On the other hand, the Scenario 4 is similarly profitable for the host and the developer.

The analysis showed that the profitability is the highest when the system is owned by the agency itself. Although public agencies cannot beneficiate from tax incentives, the NJDOT do not have to pay for income taxes, different from a third-party developer. Moreover, the energy generated by the system is used freely when the system is owned by the NJDOT. Although the monetary benefits are smaller than when the project owner is the transportation agency, the business is still profitable, and all the responsibility associated with the system is from the third-party developer. Besides the responsibility related to operating and maintaining, in this model the initial investment is from the developer. The NJDOT has no initial cost, or any cost, and still beneficiate from a lower electricity rate at the same time promotes a renewable and clean energy.

State-Level Solar Energy Analysis

New Jersey has 164,000 miles of roads with rights-of-way. Some ROWs are too small or inadequate for solar power implementation; however, NJ is mostly plane and can have a great potential of solar energy production on the ROW. This section used shape files on ArcGIS software combining layers to estimate the available are for solar system implementation on the state's ROW. To define the available area some assumptions were defined and included in the NJ map. The ROWs considered in this project are the ones by major roads. The map used for the analysis, shown in Figure 22, has the center line of the major roads in the state. The road width was assumed to be 86 feet which include lanes, shoulders, and median between lanes.

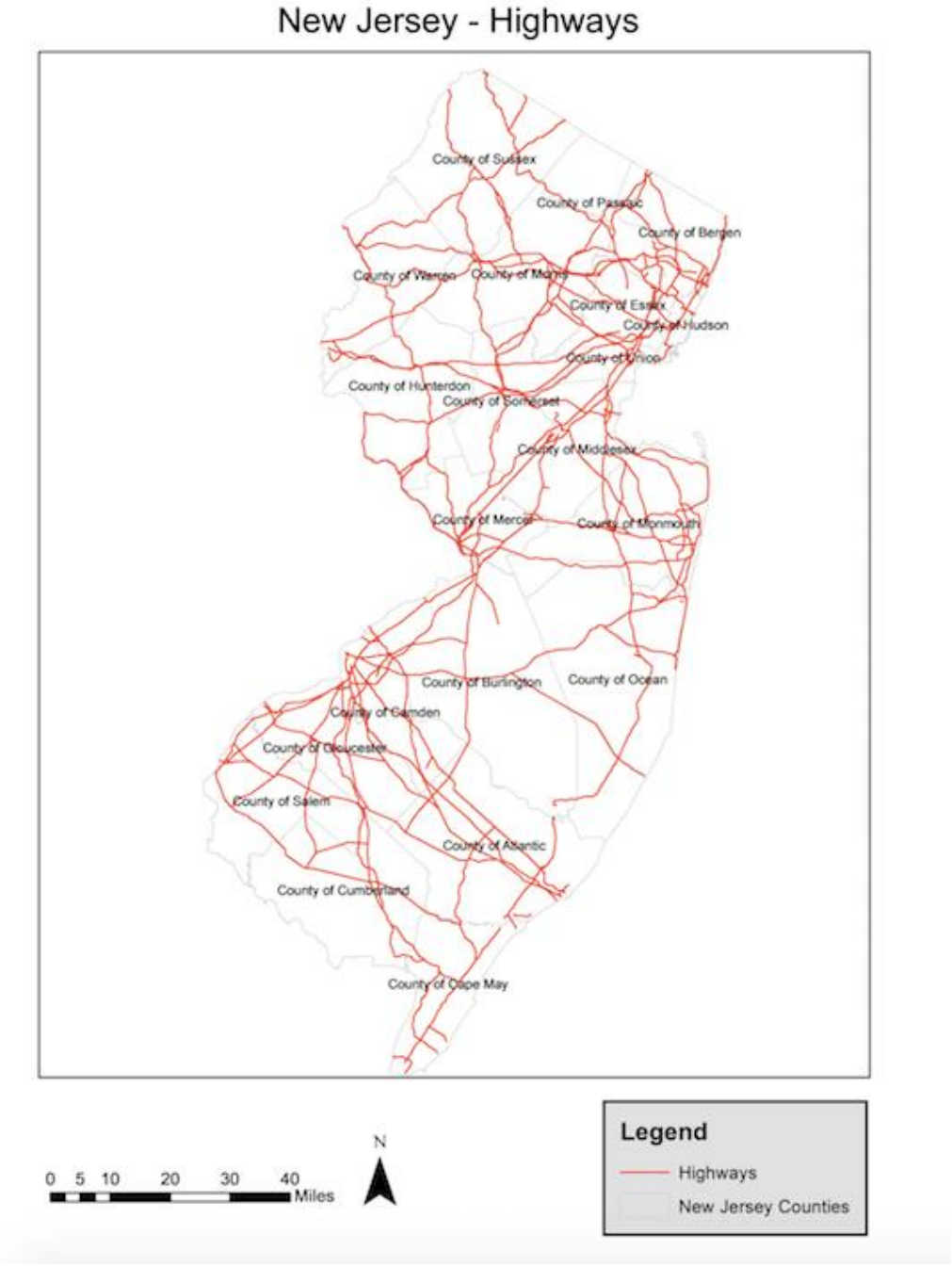

Figure 22. New Jersey Highways Map

For safety reasons the study assumed that the solar array is installed 60 feet from the edge of the road, this value is the same used in the Demonstration Project developed by ODOT [32]. A buffer of 103 feet from the center line was applied on all roads, representing the road width and the clearance area of 60 feet, as shown in Figure 23(a). Figure 23 shows a zoom in area of the map to clearly represent the layers used. The layers would not be visible in the state-level map; however, the area results are for the whole state.

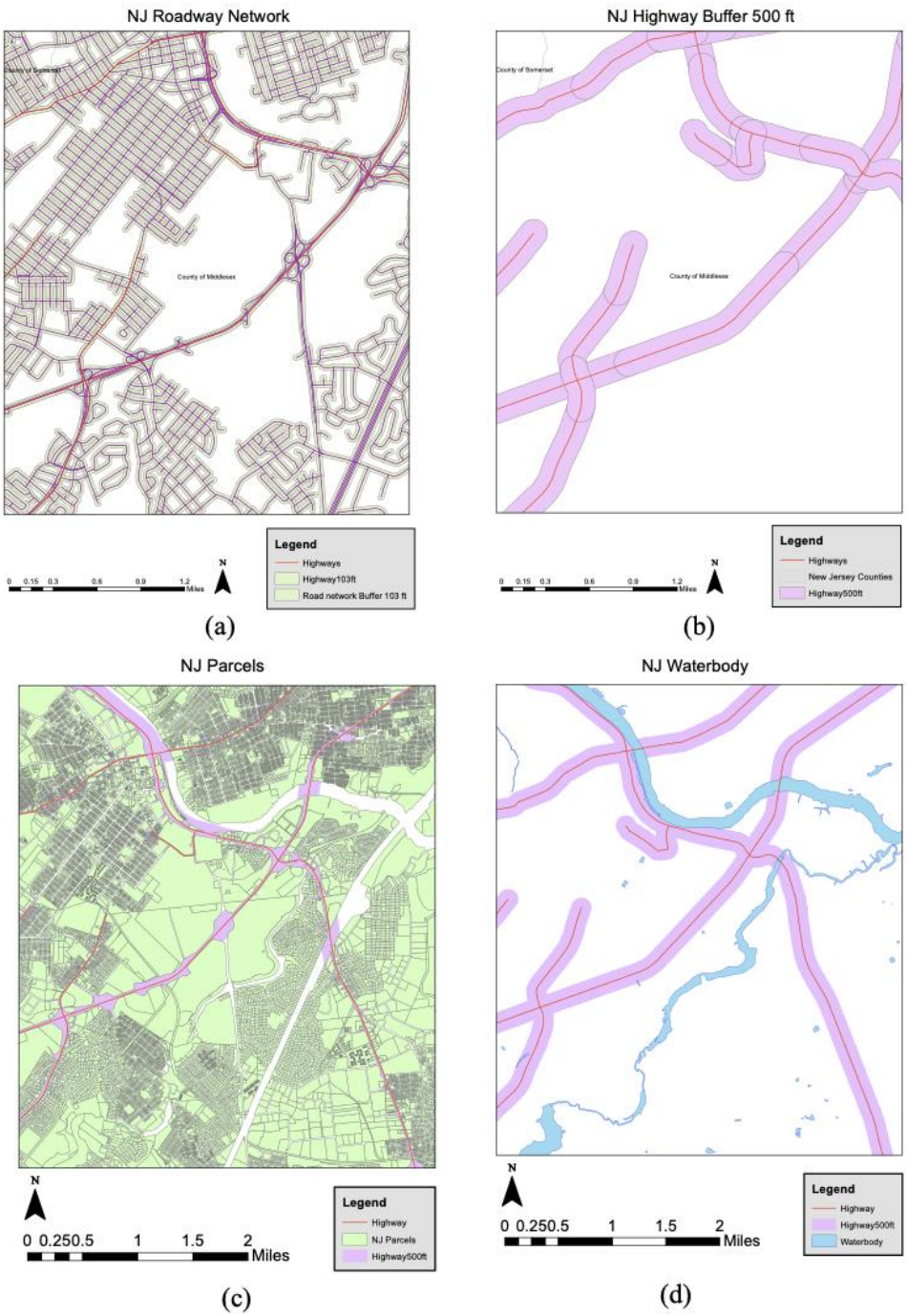

Figure 23. New Jersey Highway map with layers (a) road width and safety clearance, (b) area of study for solar power implementation, (c) parcels, (d) waterbodies

The solar system was assumed to be installed maximum of 500 feet from the major highways center line. Therefore, a buffer of 500 feet was applied and presented in Figure 23(b). The state's properties map was not available. To define the ROW areas a map with partials was used to be cropped from the previous buffer created. The partials map shows the private owned lots, ergo, the areas not included in the map is state owned. Figure 23(c) shows the partials in green, the visible pink areas resulted from the buffer is

assumed to be the ROW. The solar system needs to be installed in a dry terrain; hence, the waterbody areas need to be excluded from the analysis. Figure 23(d) shows the waterbody map on the highway center line and 500 feet buffer map layers. The waterbody layer was also cropped from the buffer resulting in the available area for solar power system implementation on the ROW, as shown in Figure 24.

Figure 24. Available area for Solar Arrays on NJ Highway ROW

Figure 24 presents a zoomed in area of the NJ highway map with the available area for PV system implementation in green. The total area available in NJ in 40.62 km^2. This study presents a rough estimation of the state-level solar potential. Factor such as terrain, vegetation, slope, signs, and visibility blockage were not considered in the analysis. The energy output estimation was calculated using the PVWatts web-based tool developed by NREL. All panels were assumed to be facing south with tilt angle of 36°. The ground cover ratio (GCR) represents the proportion of area that are covered by solar panels. In this estimation the GCR is assumed to be 0.4 and efficiency of the system is assumed to be 19%. The NJ ROW solar capacity estimation was found to be 3.1 MW which can produce 4,270,596 MWh annually.

ANALYSIS OF PHOTOVOALTIC NOISE BARRIERS IN NJ ROADWAY

Design Configurations of Retrofitted PVNB

There are four design configurations for PVNB by retrofitting existing noise barriers: top-mounted tilted, top-mounted bifacial, shingles built-on, and vertical built-on. The illustrations of PVNB configurations are shown in Figure 1. In the top-mounted tilted configuration, the solar panel is installed on top of the barrier with an angle designed to maximize the solar absorption. Top-mounted bifacial PVNBs have their panels installed on the top of the barriers at an angle parallel to the face of the barrier, allowing the panels to harvest energy on both sides. In the shingles built-on configurations, rows of angled panels are installed along the face of the barrier. Lastly, a fourth configuration called vertical built-on is found in the literature and can be considered a simplified design of the shingles built-on, where the panels are installed at a 0° angle from the barrier.

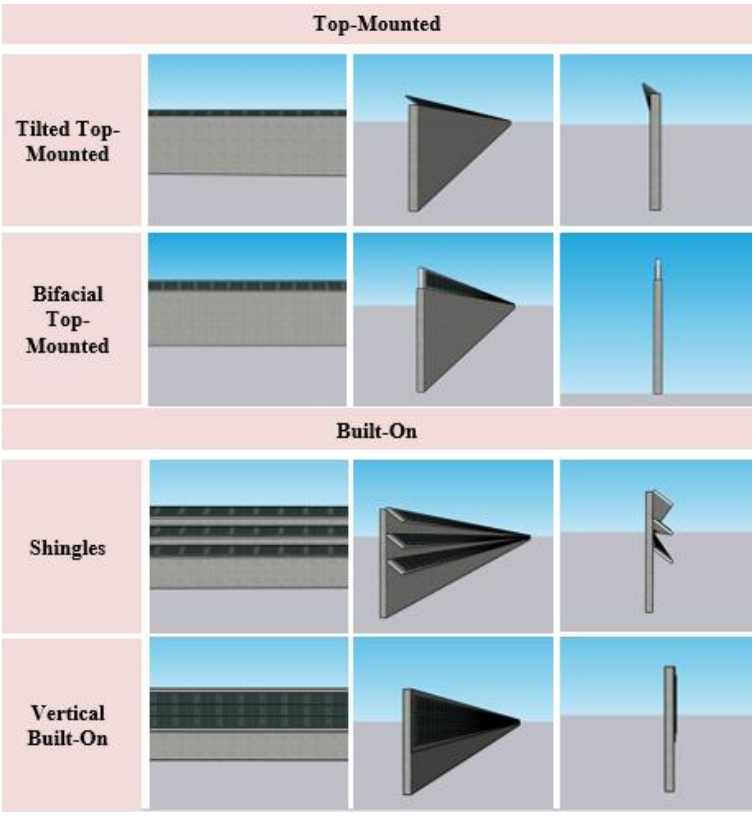

Figure 25. Retrofitting PVNB with four design configurations

Although the top-mounted titled and bifacial designs do not utilize the large surface area of the barrier face, these designs may have the higher energy absorbed per panel. Top-mounted tilted produces the largest energy output when facing south and top-mounted bifacial produces the largest energy output when facing east-west. The shingles built-on design takes advantage of the large surface area of the barrier, increasing the number of panels installed per length unit when compared to the top-mounted configurations. The tilted angle of the panels also increases the energy absorption for the configuration;

however, the panels create self-shading on the lower rows, thereby increasing energy loss. Lastly, the vertical built-on configuration has large area of photovoltaic material, but the vertical position is not optimized to absorb the solar energy, which results in a small energy harvested per panel. Table 7 presents the advantages and disadvantages of each PVNB configuration. The vertical built-on is not considered in further analysis since the shingles built-on configuration presents similar design concept but generates more energy than vertical panels.

Table 7 - PVNB configurations advantages and disadvantages

PVNB Configuration	**Advantages**	**Disadvantages**
Top-mounted tilted	Angled optimized to absorb the most energy	Small photovoltaic area
Top-mounted bifacial	Absorb energy from both faces	When facing north-south, the north face absorbs very little energy (for Northern hemisphere)
Vertical built-on	Does not alter the noise barrier design	The vertical panels position absorbs lower energy than if tilted; Bad aerodynamic for panel cooling
Shingles built-on	Angled panels can increase energy absorption	Losses due to self-shading; Safety related to solar panels projected towards the highway

Estimation of Energy Performance of PVNB

Analysis Methodology

The energy output of PVNB was analyzed using Sketchup, a 3D design software, using the Skelion plug-in. The Skelion plug-in allows the inclusion of photovoltaic solar panels in the design. The software allows for self-shading loss to be accounted for in the simulations, which is essential for the shingles built-on design. Skelion uses PVWatts for solar energy production estimation, a web-based application developed by the National Renewable Energy Laboratory (NREL). The energy production is estimated using the Perez 1990 algorithm to calculate the plane-of-array (POA) beam, sky diffusion, and ground-reflected diffusion irradiance components [69, 70]. PVWatts sub-models also include the thermal model by Fluentes, the hourly calculation of the sun position, and the angle of incidence [71]. The data obtained from the simulations are plotted and fitted into a model for each configuration. The models are used to calculate the estimated energy output by inputting the barrier orientation. Each retrofitting configuration has a slightly different methodology for modeling the system energy output as a function of the barrier orientation. The energy estimation models were developed for each design configuration, as detailed below.

Top-Mounted Tilted PVNB

For the top-mounted tilted configuration, the optimal tilt angle should be calculated first. The optimal tilt angle depends on the orientation of PVNB, so a range of PVNB orientations were considered. The annual energy output for an array of angle values and a given orientation was found using PVWatts, the output of which was fit as a second-degree polynomial function of the angle. The global maximum of this function provided the optimal tilt angle for the given orientation. For simplification, this process was performed in orientations for every 20°, and the results were used for plus/minus 10° intervals. The panels were always assumed to be facing southern face of the studied barrier; therefore, the studied orientation (or azimuth) varies from 90° to 270°.

After the optimal angles were determined, the authors used Sketchup to design PVNBs for each orientation and calculate the total energy output. This simulation resulted in an equation where the annual energy output per meter is a function of the orientation. The equation was then used on a dataset with more than 300 noise barrier segments to estimate total annual energy output based on barrier length and orientation. As expected, and shown in Figure 26, the orientation that produces the highest energy is 180° (south-facing).

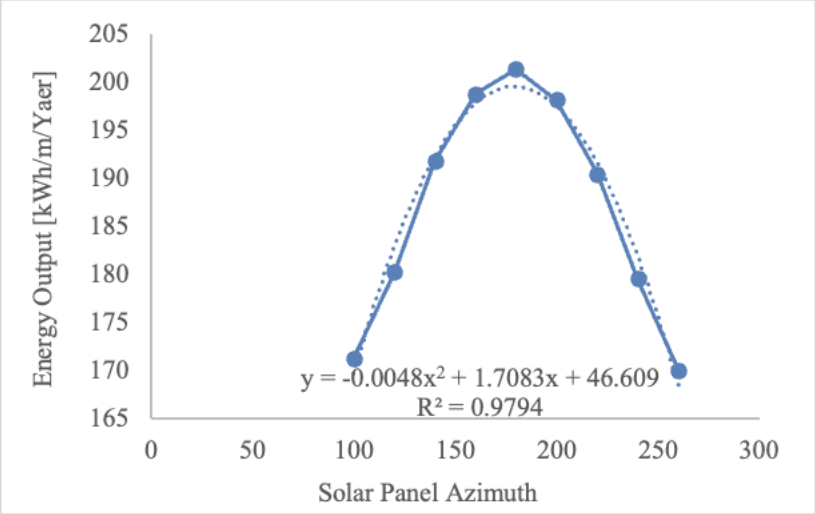

Figure 26. Energy Outputs with solar panel azimuths for top-mounted tilted PVNB

Top-mounted Bifacial PVNB

The top-mounted bifacial configuration does not require an optimum tilt calculation since the panels are installed parallel to the face of the barriers. The simulations were conducted using Sketchup resulting in a set of data pairing the orientation with the energy output. A second-degree polynomial equation (shown in Figure 27) was fitted with R-squared values greater than 0.9. The total annual energy output was then calculated following the same process as the previous configuration.

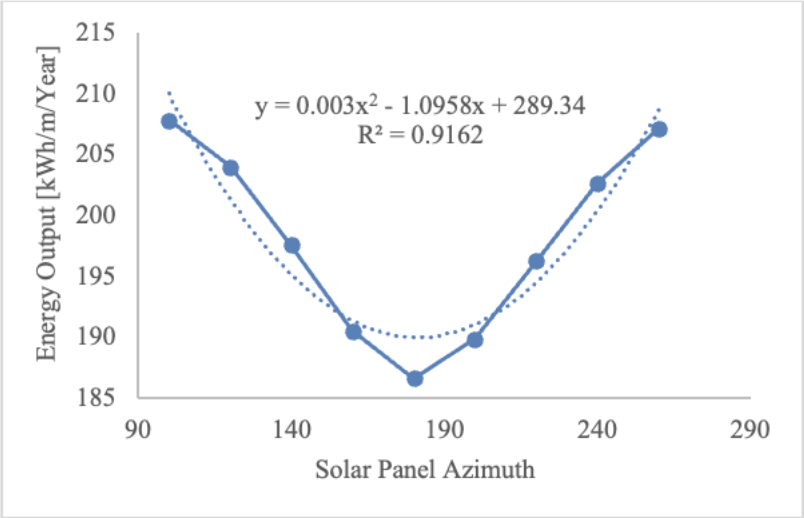

Figure 27. Energy Outputs with solar panel azimuths for top-mounted bifacial PVNB

Shingles Built-on PVNB

To simulate the total energy output of a shingles built-on system, one must first determine the angle and size of the solar panels and the inter-row distance between them; however, shingles configuration design can be very complex. The panel size, angle, and inter-row distance can vary to minimize self-shading. For simplification, this study assumed the same solar panel size, inter-row spacing of 1 meter, and angle tilt of 45 degrees.

The simulation for different orientations was performed using Sketchup with the Skelion plug-in, which considers the self-shading from the shingles. Figure 28 presents the fitted equation for (a) 3-shingles and (b) 4-shingles configurations. The data can be better fit using third or fourth-degree polynomial equation; however, the second-degree polynomial fitted equation has a satisfactory R^2 higher than 0.95.

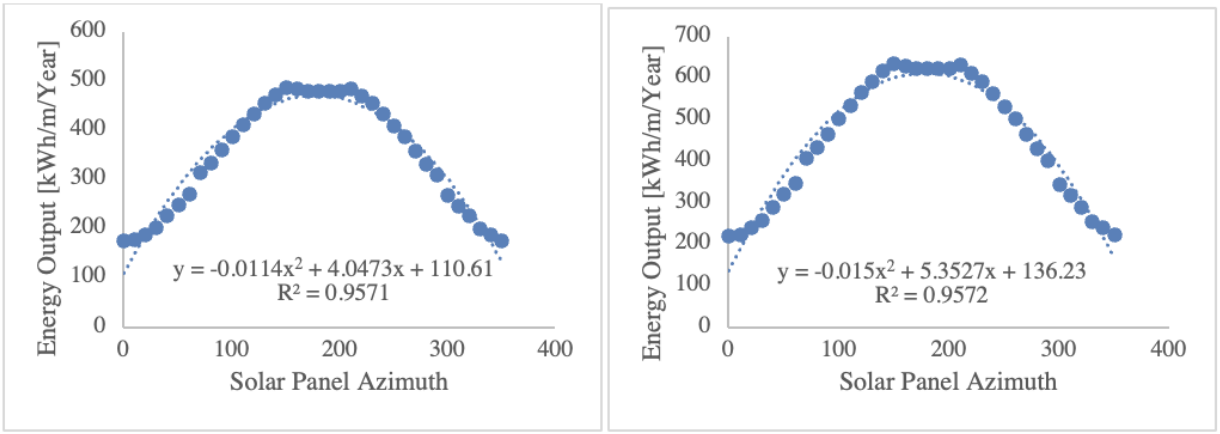

Figure 28. Energy Outputs with solar panel azimuths for shingles built-on PVNB: (a) 3-shingles, and (b) 4-shingles

Verification of Energy Estimation Models

Two case studies were analyzed to verify the developed regression models for energy output estimation. The case studies are noise barriers from Springfield, NJ, and Parsippany, NJ, which were selected because the barriers have rather extreme orientations, mostly facing east-west and north-south, respectively. The Springfield case study was a noise barrier with 175.5° azimuth (facing south) along I-78. The barrier is 493 meters-long and approximately 5.2 meters high (17 feet). The Parsippany barrier, along I-278, has a 116.1° azimuth (facing southeast) and is 1,068 meters long and approximately 5.5 meters high (18 feet).

Table 8 shows the results for the annual energy outputs versus their fitted values. For the top-mounted tilted, the percentage difference in outputs versus their fitted values are 0.1% and 6.0% for two case studies. These are acceptable levels of difference. Top-mounted bifacial also presented good results, the percentage difference between the outputs and fitted values from two case studies are 1.5% and 1.8. For the shingles built-on configuration, the differences in results for the Springfield and Parsippany 3-shingles and 4-shingles cases are 5.4%, 0.6%, and 1.1%, respectively. This confirms the model provides a good estimate of the energy output.

Table 8 - Verification of estimated and simulated energy outputs

PVNB configuration	Case 1: Springfield, NJ		Case 2: Parsippany, NJ	
	Simulated (kWh/m/Year)	Model (kWh/m/Year)	Simulated (kWh/m/Year)	Model (kWh/m/Year)
Top-mounted Tilted	198	199	180	170
Top-mounted Bifacial	187	189	199	202
3-shingles Built-on	496	470	429	427
4-shingles Built-on	NA	NA	549	555

Another verification was performed to validate the assumption of using 45° angle for the PVNB configuration with shingles built-on. The Springfield and Parsippany case studies were used again due to their orientations. Several simulations for each case study were performed varying the angle of the shingles aiming to find the combination of angles that harvest the most energy. Shingles with a small angle are close to a vertical position, absorbing less sunlight. However, this causes little shade on the following shingle row. Shingles with a large angle, close to a horizontal position, tend to absorb more sunlight, especially during summer months, but the flatter position creates shade on the following shingle, increasing the system losses.

Figure 29 shows the simulation models for the built-on shingles with the highest energy output, where Figure 29(a) is for 3-shingles in Springfield, NJ, Figure 29 (b) is for 3-shingles in Parsippany, NJ, and Figure 29 (c) is for 4-shingles in Parsippany, NJ. The

simulated annual energy output is 275.6 MWh, 477.6 MWh, and 617.9 MWh. The model results with 45° angle are 0.3%, 4.0%, and 5.1% smaller than the configuration with the highest energy output, proving that the 45° angles for the shingles are a good approximation and a great solution for simplifying state-level analysis.

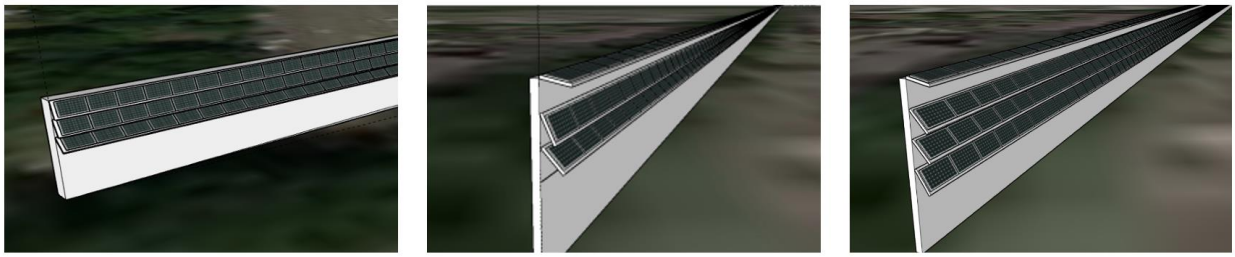

Figure 29. Built-on shingle design with the highest energy outputs: (a) 3-shingle at Springfield, NJ, (b) 3-shingles, and (c) 4-shingle at Parsipanny, NJ

State-level Energy Estimation Results

After verifying the estimation models and assumptions for energy outputs, state-level energy estimation was performed for retrofitting PVNB on existing noise barriers in New Jersey. Currently, there are 72 noise barriers in New Jersey totaled 10,268,832 square feet along 106.3 miles. The average height of noise barrier is 17 ft. Although a barrier of 13 ft is high enough to accommodate four shingles of solar panels, which represents 83% of the barriers in New Jersey. The vertical clearance of 5ft from ground to panel was considered, which avoids damage on the solar system in case of vehicle crash and prevents the parts of solar system falling on the crashed vehicles. These noise barriers are divided into 345 noise barriers segments based on their exact locations as provided by NJDOT. The beginning and ending latitude and longitude of each barrier segment were used to find average orientation and length of each segment. This information was used as the inputs for the developed regression models and the energy estimation results are presented in Table 9.

Table 9 - State-level energy estimation in NJ with different PVNB configurations

PVNB Configuration	Energy Output (MWh/Year)
Top-mounted Tilted	27,196
Top-Mounted Bifacial	21,246
Built-on 3-shingles	48,934
Built-on 4-shingles	56,164

The results are presented by each PVNB configuration; however, in the case of actual solar implementation, the most realistic scenario would be a mix of the designs. he configuration that produces the highest energy output is the shingles built-on, followed by top-mounted tilted and top-mounted bifacial. The estimated energy could provide electricity for 2,390 to 6,310 houses, assuming average energy consumption of 8.9 MWh per household per year [(78)]. It can also save the electricity bills for 809 to 1,672 miles of

streetlight, assuming that streetlights are installed every 20 meters on both sides of roadway and have 50-W light bulb working on average 11.5 hours per day.

Potential Implementation of PVNB

Site Selection Framework

PVNB implementation can result in economic, environmental, and social benefits; however, selecting the locations for PVNBs along highways is crucial in guaranteeing the efficiency and safety of solar highway projects. For instance, the roadway should have the free space to implement the panels at a safe distance from the road and no future road expansion plan that will encroach on that space. Additionally, PV panels need to have sunlight available at the proper inclination and orientation to guarantee maximum efficiency while avoiding glare. The decision making framework to select the appropriate site is proposed in Figure 30 to consider various factors should be considered, which this paper discusses in its decision-making framework for PVNB projects.

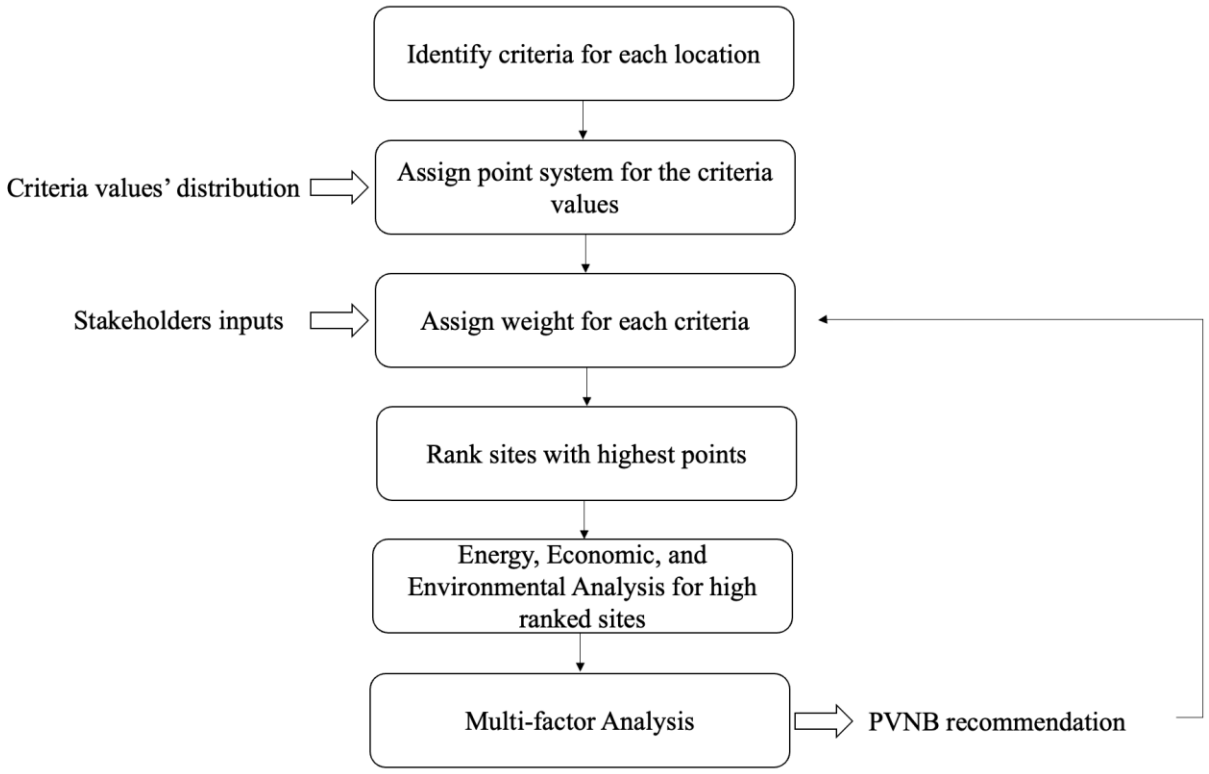

Figure 30. PVNB decision-making framework

The first step in the decision-making framework is to identify the criteria for the project and classify them into economic, environmental, and social categories. A number of selection criteria at each category is summarized in Table 10. Then, a ranking or point-based method should be assigned based for each criterion. The weight for each criterion, which will then be multiplied by the points from the points-based method, can be defined by the project stakeholders. At the end of this process, the ranking of potential sites is

presented. The sites with the highest rank should be analyzed for specific design configuration to maximize energy generation and as well as economic and environmental benefits of renewable energy. The metrics, or factors, can then be normalized and applied in multi-factor analysis. Finally, the most appropriate site is recommended for the implementation of PVNB.

Table 10 - Potential site selection criteria

Economic	**Environmental**	**Social**
• Solar Irradiation • Barrier direction • Distance to power grid • Accessibility for maintenance	• Solar Irradiance • Barrier direction • Region electricity source	• Highway traffic • Electricity rate • Electricity availability • Distance from barrier to highway shoulder

The first criterion of the economic category is solar irradiation. The main economic gain of a solar system is from electricity, either from sales or cost savings. The barrier direction has a similar impact than that for solar irradiation. Except for the top-mounted bifacial configuration, all other configurations produce more energy when facing south. Therefore, south-facing barriers generates more electricity increasing economic gains. For top-mounted bifacial, a barrier facing east-west is preferable. The distance from the barrier to the power grid will impact the initial investment. The greater the distance, the greater the cost for the electrical connections. The last criterion is the accessibility for maintenance. When the location is not easily accessible, an investment must be considered to either build access or create a closer lane for operation.

The solar irradiance and barrier direction also have impact on environmental and economic category. The higher the energy produced, the higher the environmental benefits. The environmental benefits can be measured by the amount of greenhouse gas emissions (GHGs) avoided by using the solar system subtracting the ones from manufacturing and installing panels, as compared to generating electricity from the regional electricity source. Therefore, when the system is installed in a location with high solar irradiation and on a noise barrier with an optimal orientation, the energy produced is higher. Additionally, a region where the electricity plant uses the fuel types that emits high GHGs, like natural gas and heavy oil, will also benefit more from the solar system than the regions with clean electricity sources. On the economic side, the implementation of PVNB can have beneficial social impact when the region lacks electricity or has high electricity cost due to electricity transport costs.

Highway traffic volume has two impacts on the social category. First, the solar system can cause an adverse reaction in the public; therefore, choosing a location with lower traffic volume may be beneficial. The second aspect is related to accidents; the solar system presence can increase the severity of a collision due to components that may fall and electrical connections. The distance from the barrier to the highway shoulder also impacts the driver's security. The farther the PVNB is from the highway, the better the driver's safety perception and the less likely the chances of a collision reaching the system.

The aforementioned criteria can be quantified using a point-based ranking method. An example is shown in
Table 11, in which points are assigned for each identified criterion. After assigning points for each criterion, weight can be added to translate the priority of different agencies. The decision-making method using weighted criteria should be elaborated with different stakeholders, in which each stakeholder assigns their weights for the criteria, and an average of the weights can be used for the final analysis. This method will identify potential barriers that will promote economic, environmental, and social benefits.

Table 11 - Example of points-based method for barrier evaluation

Category	**Criteria**	**Points**		
		5	**3**	**1**
Economic and Environmental	Solar Irradiation (kWh/m^2)	>4.5	4.5-4.25	<4.25
Economic and Environmental	Barrier Direction	S	SE and SW	N, NE, and NW
Economic	Distance to Power Grid	<0.5 km	0.5 – 1 km	>1km
Economic	Accessibility	Yes – easily accessible	Yes – difficult access	No
Environmental	Electricity source	Natural gas and fossil fuel	Coal	Renewable
Social	Highway traffic (vehicles/day)	<5,000	5,000 – 20,000	>20,000
Social	Electricity rate (cents/ kWh)	1^{st} quartile	3^{th} and 4^{th} quartile	4^{th} quartile
Social	Electricity available	No	-	Yes
Social	Distance from shoulder (m)	>2	0.5 - 2	0.5

Selection of Business Models

The implementation of PVNB can be profitable for state DOTs. The economic benefits vary depending on the business models, such as net metering, renting the space to utility companies, and selling the Renewable Energy Credits (RECs) generated from the system.

Renewable energy projects can utilize various financial benefits depending on the type of business arrangement. For instance, 3P projects can reap the benefits of Federal Investment Tax Credits, state tax credits, rebates, and RECs. Under a direct ownership model, the benefits can come from rebates, RECs, federal grants, and research funds. In the case of 3P projects, there are different business agreements which make the project profitable for both the public and private agency: net metering, leasing, and Power Purchase Agreement (PPA). When the agency owns the facility, the business agreement

used is net metering. Net metering is a bill credit provided by the utility company for electricity generated by a grid-tied system in surplus of a customer's on-site consumption [72]. Under airspace lease, the transportation agency must charge a fair market value lease rate; however, the agency may seek FHWA approval to charge below market lease rates in case the facility is in the public interest for a social, environmental, and economic purpose. Any resulting revenue from leasing must be used for transportation purposes. A PPA is a long-term contract that commits the solar developer to finance, build, operate, and maintain the solar system. On the other hand, the transportation agency purchases the electricity produced for a pre-agreed rate [73].

Solar farms along the right-of-way (ROW) have been successfully implemented by several state DOTs, such as Oregon, Colorado, Massachusetts, Ohio, Florida, and California. Table 12 presents the year, the number of panels, power capacity, energy destination, and business model of different solar highway projects in the United States. The first highway solar project built in Oregon in 2008 has 104 kW capacity. Due to the success of the project, four years later the ODOT implemented its second project with seventeen times more power following the same business model of 3P ownership. In the same year, two more solar projects were implemented, one in Colorado (also under 3P ownership) and one in Florida following a direct ownership business model. Colorado also had a project built in 2012, but with much smaller capacity. Florida has a legal barrier that prevents PPA agreements; any party selling power in Florida must adhere to the same rules as large utility companies [74]. Ohio also has a direct ownership project with power capacity of 117.5 kW.

Table 12 - Existing solar farms on Right-of-Way and business models

State	Year	No. of Panels	Power Capacity (kW)	Energy Destination	Business Model
Oregon	2008	594	104	Light interchange	Third-part Ownership
Oregon	2012	6,994	1,750	Serves Portland General Electric (PGE)	Third-part Ownership
Colorado	2011	22	62	Under-deck bridge lights, roadside and overhead signs, and tolled ramps	Third-part Ownership
Ohio	2011	1,164	117.5	N/A	Direct Ownership
Colorado	2012	N/A	707	Road surveillance cameras, streetlights, variable message signs, toll plazas, and maintenance facilities	Third-part Ownership
Florida	2012	468	112	N/A	Direct Ownership

The economic return of PVNBs can be concern for project implementation. It is important to avoid costly, over-engineered systems and ineffective designs due to the lack of PV system quality standards and guidelines [75]. Previous analyses have shown that the electricity benefit of PVNBs alone cannot fully pay for the barriers themselves; however, by reducing the net present value when compared to the noise barrier without solar system, and when considering ecological benefits, the project can be even profitable [80].

Impact of Solar PV on Roadway

It is important that the solar PV in the highway right-of-way (ROW) should be deployed in a way that does not affect the operation and maintenance of roadway and does not cause safety risk of road users and maintenance crew. The potential impacts of solar PV and their countermeasure solutions were summarized based on previous solar highway projects.

Glint and Glare

Glint (increase in brightness) and glare (reflectivity) can be an issue to traffic safety. According to FWHA report on Alternative Uses of ROW from 2012, glint and glare did not present any issues for the Ohio DOT Demonstration Project. Solar panels are design to absorb and not reflect light energy. Based on ODOT's report on Solar Highway Program, solar panels typically have an albedo of 30%, compared to surface materials such as dry sand at 45%, needle-leaf coniferous trees at 20%, grass-type vegetation at 25%, and broadleaf deciduous trees at 10% [32, 54]. There is one situation which glare can occur that is when the panels are placed in high elevation. The panels will reflect direct light from the incident angle; therefore, glare analysis must be performed in the sites in high elevation [54].

Electromagnetic Field

The electromagnetic field is associated with electrical potential, voltage, and currents. The inverter, which is a device that takes the electricity from the solar panels and turns it into alternating current (AC) and puts it out on the electrical grid. The inverter generates radio frequency radiation. The wires connected to the inverter act as antennas, so the radiation may be picked up hundreds of feet away from the inverter [76]. There are no federal regulations governing the exposure to electromagnetic fields [77]. However, the electromagnetic field exposures measured near photovoltaic panels are extremely small, even lower than that from many household appliances [32].

Aesthetic

According to the FWHA Report on the Alternative Uses of Highway Right-of-Way, the renewable energy projects should blend in with the highway and the surrounding natural environment and maintain a continuity of visual form without distracting interruptions. The federal policy 23 CFR Section 645.205 (a) claim that it is in the public interest for utility facilities to be accommodated in the ROW of federal highways as long as such use and occupancy of the ROW does not adversely affect highway or traffic safety or its aesthetic quality. To accomplish this requirement, the state DOT should work with architects and considered having a local art commission. For example, both the Demonstration Project (Oregon) and Northwest Parkway Tollway (Colorado) worked close to the municipality and the community to mitigate the concerns about aesthetic.

Safety and Security

Installing solar arrays raise some safety and security concerns due to the potential for traffic accidents and vandalism. To ensure safety, a few measures must be taken. First, one of the biggest criteria for site selection is the site access for construction, operation and maintenance. Analysis like whether acceleration and deceleration lanes will be necessary, whether there will be restrictions to a site based on peak hour traffic, season, or other factors [32]. Secondly, it should be defined the distance between the highway and the solar power infrastructure. Caltrans required a 52- foot setback. The solar panels in Carver, Massachusetts were set back approximately 60 feet from the roadway, the same distance as ODOT's Demonstration Project.

Another major problem that can cause accidents is driver distraction. To mitigate distractions and increase driver's awareness it is needed to place signage along the road to warn the traveling public about an upcoming solar array. The solar array structure is a roadside obstacle and can be harmful in case of vehicle collision. To decrease the damage, barrier should be implemented when proven that the impact on the barrier is less severe than the impact on the solar array structure. The developer of solar array needs to work closely to the DOT Safety Engineers to select the best barrier option. To avoid vandalism, a fence is usually placed to protect the renewable power installation. DOTs should be careful to not affect the aesthetic with the fence.

Snow Drift and Deposition

Photovoltaic array may affect the existing snow drifting, and depositional increasing of ice and snow that build up on the roadway. Avoid placing the PV array system in areas susceptible to a high snow drift, or the system should be installed on the leeward side of the roadway. Adding a clause in the contract that providers must also perform certain ground maintenance duties at the installation site, including snow blow and removal.

Roadway Maintenance and Operation

The site location process must include the understanding of roadway maintenance operation firstly so the photovoltaic infrastructure does not disturb its maintenance. Secondly, the developer need provide the maintenance that the surrounding area from the site needs. For example, the developer should be responsible for mowing within and just outside of the security fencing. Developer should coordinate within DOT ROW and Maintenance representatives to perform mowing activities. The solar array also cannot disturb snow removal, rainstorm management, leaf pickup, dead animal removal and pavement repairs.

Implementation Challenges

The implementation of PVNB faces some challenges include reducing the risk of traffic accidents, efficiency loss due to soiling, noise absorption, and social impacts.

The risk of traffic accidents increases when PVNBs are present. The electric components are susceptible to fire and falling panels can increase the accident severity. Locating the safest place to accommodate the electric components is essential, and the panels' attachment infrastructure should be designed and calculated to resist high impacts. The

panels must be constrained to the structure; suitable retention devices should be added inside the glass and designed to withstand any stone impact from passing vehicles [75]. Glare is another potential cause of accidents and should be analyzed for high elevation sites, where the panels reflect direct light from the incident angle [73]. Although there are a few cases where glare is an issue, solar panels are designed to absorb and not reflect sunlight. Solar panels have similar solar reflection rate to that of roadside vegetation. Based on the Oregon DOT report on the Solar Highway Program, solar panels typically have an albedo of 30%, compared to roadside surface materials such as dry sand at 45%, grass-like vegetation at 25%, and broadleaf deciduous trees at 10% [73, 78]. Another critical problem is snowdrift from panels. Areas susceptible to large snowdrifts should either be avoided, or the panels should be installed on the leeward side of the roadway.

Energy loss due to soiling is one of the major issues that decreases the efficiency of PVNBs. The soiling loss depends on geographic region, local environmental, level of development (rural, suburban, and urban), tilt angle, and rainfall. The loss rate is specific for each location and varies throughout the year. Kimber et al. (2006) [79] studied the effect of soiling in California, where rainfall was limited during an annual, months-long dry season. The study concluded that for each day without rainfall, the energy losses incurred by soiling increased on average by 0.2%, which represents annual loss rate between 1.5% and 6.2%.

The primary function of a noise barrier is to abate the sound from traffic, yet the inclusion of photovoltaic material by itself does not aid this purpose. The analysis performed here assumed an existing noise wall with no requirement for more noise absorption. When noise absorption is required, the most appropriate configuration can be shingles built-on [80]. It is beneficial to use glassy material in the photovoltaic system to reflects noise combined with sound absorption materials in the non-PV areas [4]. Vallati et al. (2015) [81] performed an acoustic and energetic study with five different PVNB configurations, including top-mounted with 60° tilting angle, vertical built-on, and three other configurations (T-shaped, and two curve-shaped). The results showed that the T-shaped, and the top-mounted tilted presented the best acoustic results.

Other environmental issues include impact of solar system on natural environment, such as the effect of glare on birds. Social issues must also be considered for project implementation. Community support is essential for the project acceptance and avoiding vandalism. Publicizing the electricity destination and disclosing the benefits of the solar system for the region is crucial for public approval.

PIEZOELECTRIC ENERGY HARVESTING FOR SMART INFRASTRUCTURE

Monitoring Vehicle and Pedestrian Traffic

The working principle behind piezoelectric sensor for monitoring vehicles can be either compression-based or vibration-based. For compression-based category, it relies on an instantaneous impact from vehicles rolling over the sensors to produce a pulse from piezoelectric elements. For vibration-based category, it relies on the pavement vibration generated by the passing vehicles to produce a wave signal from a system containing a mass and piezoelectric elements.

For compression-based piezoelectric sensor, the most typical one is the piezoelectric weight-in-motion (WIM) sensors which are directly embedded under the pavement along the wheel path. The design of piezoelectric WIM sensor can be as simple as shown in Figure 31(a): piezoelectric elements are embedded into a cement plate and connected with a cable to capture instantaneous pulses under traffics. Based on the results from previous study, it is confirmed that the WIM sensor built by cement-based piezoelectric composite patch have high anti-jamming ability, fast response, high accuracy, promising durability, and simple installation and maintenance [82]. Besides the measurement of vehicle weight, piezoelectric sensors can also detect traffic flow condition and measure vehicle speed [82].

For vibration-based piezoelectric sensor, the most common application is the piezoelectric accelerometer set on the roadside to capture pavement vibration caused by traffic. As shown in Figure 31(b), piezoelectric accelerometer mainly includes a seismic mass and piezoelectric disks. Once the pavement is vibrated by the passing vehicles, the mass inside the accelerometer will be vibrated and further impact the piezoelectric elements under the mass. Those piezoelectric elements will produce weak signals due to the limitation of pavement vibration. Those weak signals will then be amplified by the preamplifier inside the accelerometer for further signal process and analysis [83, 84].

Figure 31. (a) cement-based piezoelectric composite sensor [65]; (b) piezoelectric accelerometer [68]

Instead of using devices with bulk piezoelectric elements to monitor traffics, another option is to utilize micro-electro-mechanical system (MEMS) techniques to built smaller

sensors with less energy consumptions and higher accuracy. Ye et al. (2017) [86] developed an acceleration sensing node through assembling a micro-electro-mechanical system (MEMS) with a low energy consumption hardware design inside a monomer casting nylon box, as shown in Figure 32(a).

Each component used in this system was low powered: the CPU required 2.937 μW in run mode and 29.7 μW in low-power run mode; the MEMS sensor costed less than 2 mW power supply; the ADC needed 12.5 mW to reach a sampling rate of 100 ksps. This design also saved energy costs from without using an adapter and a data acquisition device. Based on the field test results on this sensing system, it was confirmed that this sensing system was able to measure the vehicle weight and speed with low errors of 1.11 % and 1.32 %, respectively. However, the battery set in this system still can only supply limit electricity to this system under a duration much less than 2~3 years.

To further improve this system, Ye et al. (2019) [87] developed another battery-free monitoring sensor, which was smaller but required external electricity supply from a cable, as shown in Figure 32 (b). They also updated the entire system by adding a series of front-end devices and back-end devices. Besides the sensors, the front-end devices also contained the triggers, camera, and gateway, while romote server and browser were added as a group of back-end devices. The whole system can be powered by solar panels or batteries.

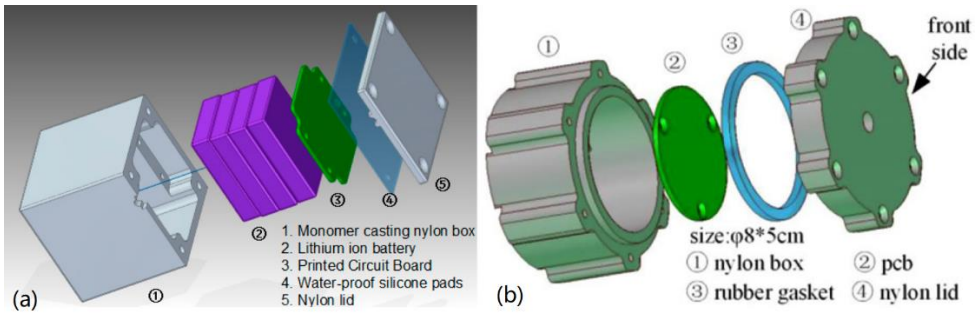

Figure 32. Traffic monitoring sensor design (a) with internal battery; (b) without internal battery

The piezoelectric sensor can be also used for detecting pedestrian or bicycle in the crosswalk or community roads. The sensors for detecting pedestrians can be any piezoelectric elements (e.g., film, plate) covering the most likely pedestrian movement area, while the sensors for detecting bicycles are usually cables laid across the roadway, as shown in Figure 33. Considering the low pressures but high frequencies of pedestrian or bicycle movements, the material selections for those piezoelectric sensors are usually piezoelectric polymers, such as polyvinylidene fluoride (PVDF) or poly (amino acid) (PAA), which are flexible with high sensitivity and durability.

Figure 33. (a) piezoelectric mat for detecting pedestrian; (b) piezoelectric cable for detecting bicycles

Monitoring Pavement Cracks

Piezoelectric transducers for structural monitoring purpose usually require a cooperation between two transducers. One piezoelectric sensor (as an emitter) is excited by electricity to produce a multiple-peak pulse at one end based on the reverse piezoelectric effect. The pulse is then transmitted through the structure and received by another piezoelectric sensor (as a receiver) at another end. After that piezoelectric sensor is excited by the pulse, a signal can be generated based on piezoelectric effect. Any cracks occur inside the structure will change the transmitted pulse, and thus the signal generated by the receiver [88]. The signal change will then be used to detect crack initiation and development.

For the detailed design of the emitter and receiver, it can be varied based on the specific structure under monitoring. If the structure is metallic, dual thin piezoelectric films [89] or plates [90] are sufficient to produce and receive detectable signals across the structure. The shape of thin piezoelectric films, either rectangular or circular, can be customized based on the specific in-service structure to efficiently monitor its structural health [89]. One processing system is usually required to interface with the dual piezoelectric elements [89] for outputting a specific pre-programmed diagnostic waveform (e.g., 5-peak sine wave) and analyzing the back signal. Such processing system can be portable, as shown in Figure 34(a). The sensing unit can also be wirelessly active. For example, a wireless active sensing unit (11×10×4.5 cm) was designed and assembled that contains four functional modules, including a computational core, a sensing interface, an actuation interface, and a wireless communication channel [90]. The computational core can command piezoelectric pads through a wireless communication channel to excite the surface of plate at one end and to record the response of the plate at another end. Those input-output response data were further used to fully characterize the linear behavior of the plate. With developing time-series system identification models based on those input-output data, the occurrence and severity of structural damage in the plate were identified and quantified.

For pavement structure with asphalt or cement concrete, thin piezoelectric films cannot produce the pulse with sufficient energy to cross the structure. Piezoelectric disks are usually needed to generate stronger pulses or waves across the harder and larger structures. Moreover, the wave attenuation across the pavement structure can be more complicate compared to that across the metallic structure. Those uncertain and complex factors make such applications on pavement structure still under the research stage.

Karaiskos et al. (2015) [91] proposed an idea to set a pair of low-cost and aggregate-size piezoelectric transducers at different locations of concrete structure, as shown in Figure 34(b). When there is an increased porosity or damage accumulation inside concrete structure, the pulse from transmitter to receiver will be arrived with a longer transit time or even not arrived. Both piezoelectric transducers are allowed to be attached on the surface of concrete structure if the indirect transmission path is used for structural monitoring.

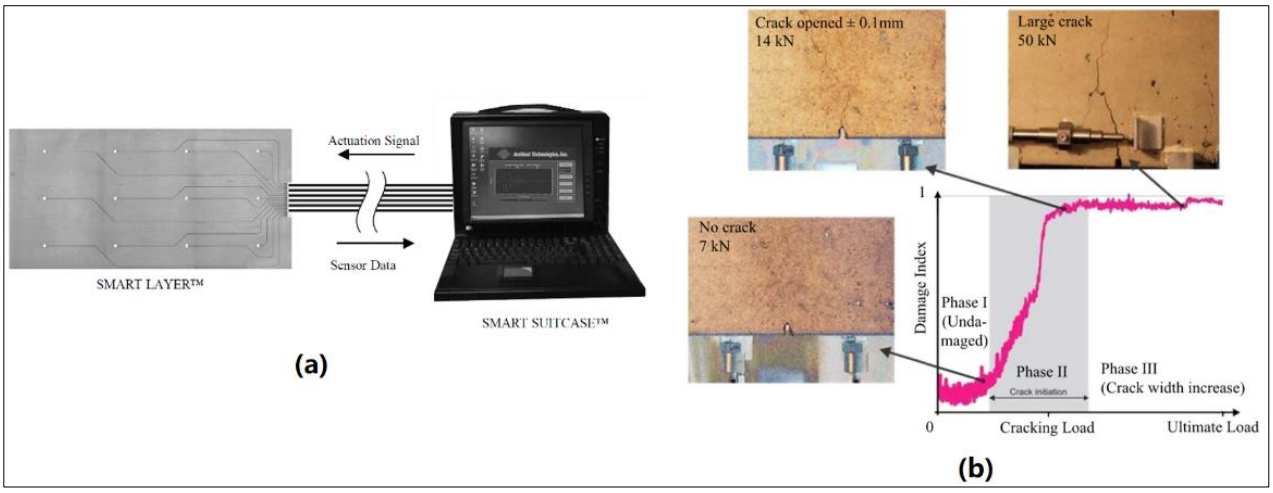

Figure 34. (a) commercialized thin piezoelectric films with a processing system to monitor metallic structure; b) thick piezoelectric disks to monitor cracks inside concrete structure in laboratory

Ji et al. (2019) [88] used a two-piezoelectric sensors system in asphalt pavement to intelligently monitor the concealed cracks inside the pavement. Based on the laboratory tests on asphalt mixture sample with embedded piezoelectric aggregates (PSA), the average absolute deviation (AAD) (between the receiving signal amplitudes after crack occurrence and in the healthy state) was found as the key indicator to quantify the growth of crack width, although the coefficient of acoustic wave attenuation was affected by the loading frequency, asphalt mixture composition, propagation distance, and environmental conditions.

Lajnef et al. (2013) [92] developed a self-powered strain sensing system for pavement structural health monitoring purpose under a FHWA-funded project (FHWA-HRT-12-072). The system consisted of an H-shaped strain gauge for monitoring strain events inside the roadway, an antenna surrounding the gauge for transmitting the data to radio frequency (RF) reader, an array of floating gate computational circuits for computing and storing the sensing variables, and a piezoelectric transducer for supplying electricity to all sensor

electronics. Compared to other cable-free sensor designs, this system design used an inductive coupling technique to transmit extra power (200 mW) from reader coil (set in vehicle) to sensor coil (set inside pavement) to meet the significant power requirement for data transmission. In other words, this system had two power sources: one was from the piezoelectric transducer, mainly for powering the sensors; another one was from the external RF reader, mainly for data transmission, as shown in Figure 35.

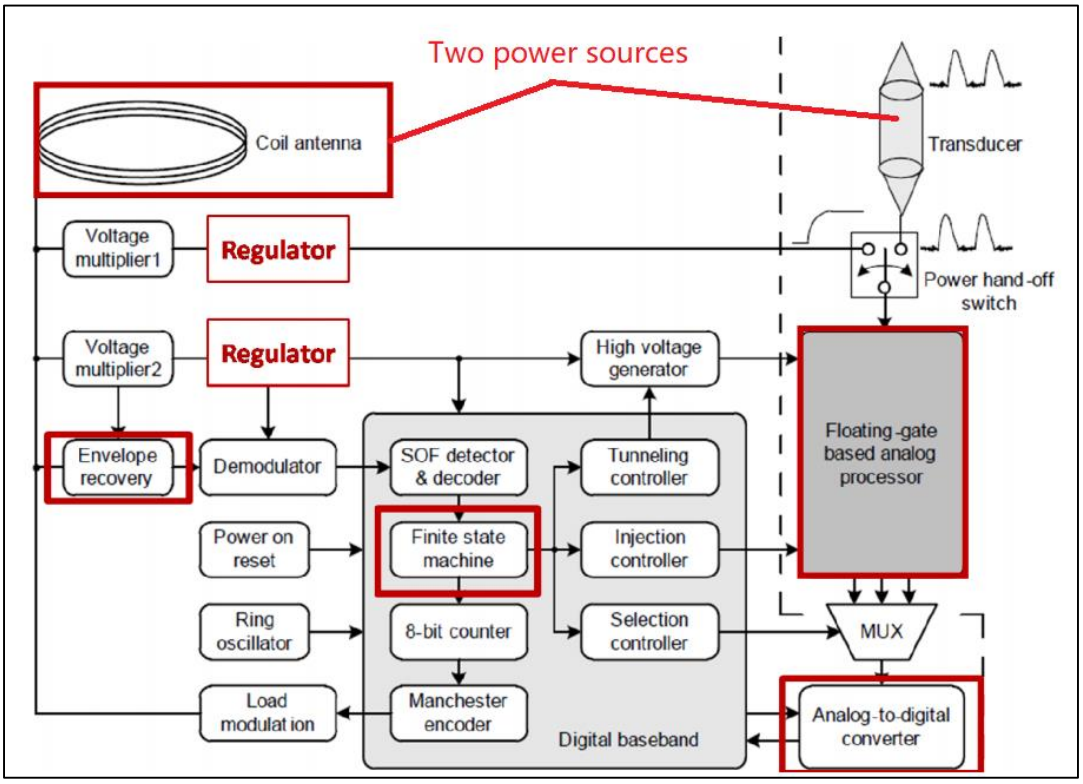

Figure 35. System architecture of the sensor for pavement condition monitoring [75]

A follow-up study conducted by Alavi et al. (2016) [93] developed a spherical packaging to protect each of these wireless sensors, as shown in Figure 36(a). Three packaged sensors were placed inside hot-mix asphalt beam specimens and the voltage change caused by the progression of cracking damage (from bottom to up) was observed. It was found that the rate of strain variation did reflect the relative damage (previous and present) over time points. That study verified the feasibility of using piezo effect to locate the crack and measure its severity via the cumulative time distribution and standard deviation of load and frequency, as shown in Figure 36 (b).

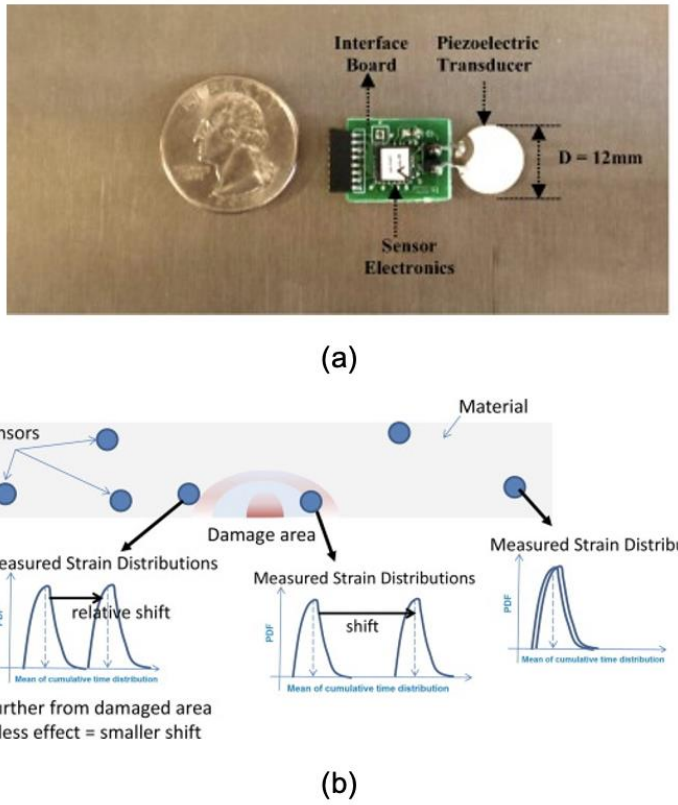

Figure 36. (a) Prototype of self-powered wireless sensors; and (b) the PDF shifts due to damage progression [75]

Bridge Structure Health Monitoring

Bridge structure requires more frequent and comprehensive health monitoring compared to other parts of highway system, due to the rapid aging process in bridges, a significant traffic level increase, and the severe consequences of bridge collapse. One economical and efficient option to continuously monitor the bridge condition is to set a wireless monitoring system (WMS) in the bridge. The WMS has several advantages over a conventional wired monitoring system, including a low cost, an easy installation and maintenance, and no negative impact on existing highway infrastructure [94]. However, one big challenge from the WMS is to power it without using any battery or any remote electric resource, considering the high cost of periodic battery replacement and the extra labor costs of cable installations [95]. Since the WMS is often installed in locations with low light intensities, solar power may not be the prior solution in certain application. Instead, the kinetic energy from bridge vibration can be a more ideal option for powering the WMS in the bridge based on piezoelectric effect.

Most designs of piezoelectric energy harvester set on the bridge from previous studies are consistently as simple as one conventional piezoelectric cantilever by far [96, 97, 98, 99, and 100], as shown in Figure 37. Instead of developing detailed piezoelectric energy

harvester designs, considering the more complicate structure of bridge than the structure of roadway on ground, the major research objective from previous studies had more focus on searching optimal installation locations on the bridge for producing maximum power output from the energy harvester.

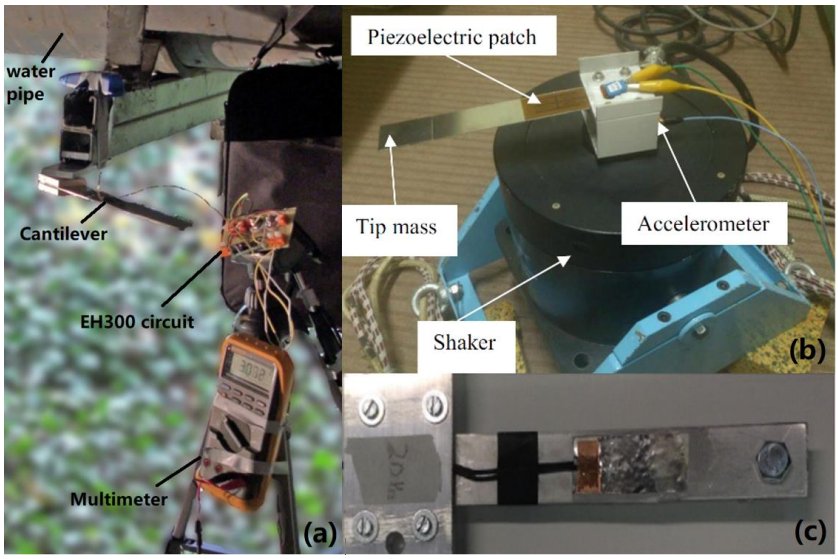

Figure 37. Piezoelectric cantilever set in the bridge: (a) field tests [97]; (b) laboratory tests [98]; and (c) system design [99]

Peigney and Siegert (2013) [97] measured the accelerations of several locations (three points on girders and one point on a pipe) on a pre-stressed concrete highway bridge to select the best location for setting the energy harvester. They found that the highest level of vibration did occur on the water pipe, whose acceleration did reach up to 0.3 m/s^2. Such acceleration level was ten times the acceleration on the girder at mid-span. Then, they bonded two bimorph piezoelectric patches to both surfaces of a steel plate to make a piezoelectric cantilever. After set the cantilever on the water pipe, as shown in Figure 37 (a), they obtained mean power of 0.03 mW from the cantilever. To utilize certain low power output for operating the WMS, an EH300 circuit was connected between cantilever and WMS. The EH300 circuit did contain a storage capacitor to accumulate the energy from cantilever and a switch to release the electricity from the capacitor when the voltage was enough to run the WMS in a short term. As a result, the capacitor was charged in 210 seconds and a controlled voltage of 1.8~3.6 V was able to be reached for powering WMS with a low duty cycle.

Hu et al. (2013) [101] integrated a bridge structural health monitoring (SHM) system, consisting of distributed nodes with a base station. Each node contained an S-mote board, an acceleration sensor board, and/or a strain sensor board, as shown in Figure 38. The S-mote board included a microcontroller unit providing a computational core, a radio-frequency (RF) module for wireless communication, a power management unit supplying power to other modules, and two low-power sensors measuring temperature and humidity. An acceleration sensor board (having Silicon Designs 1221L accelerometer) or a strain sensor board (having piezoelectric sensors, semiconductor strain gauges, and foil strain

gauges) was connected with the S-mote board via sensor expansion pins. The microcontroller required minimum power of 330 µA in active mode and 0.2 µA in off-mode under a voltage of 2.2 V. The current required for sampling acceleration and strain data was 13.4 mA and 14.1 mA, respectively. The major power consumption from this system was from data transmission and reception by RF module, around 71.5 mA under 7.2 V supply voltage in total. To save the energy consumption from this system, instead of sampling the data all day long, a duty-cycle approach was performed to shorten the active sampling for only 1 hour/day. As a result, the service life of this system can be extended from 7 days to 168 days based on the power from two 3.6V lithium batteries.

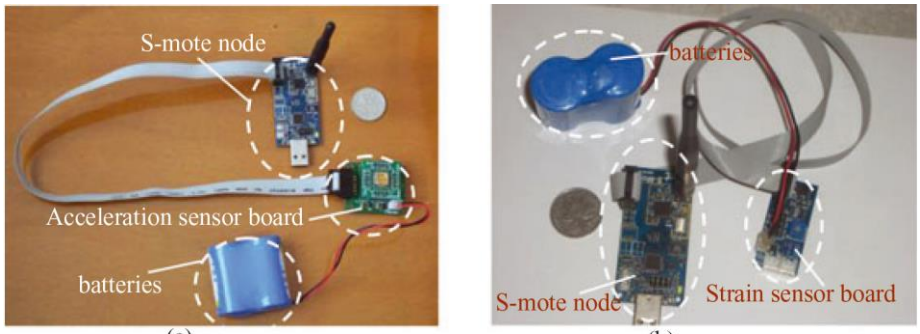

Figure 38. S-mote node with a) acceleration sensor board; b) strain sensor board [101]

Zhang et al. (2014) [102] estimated the power output from a piezoelectric cantilever-based harvester set on bridges using numerical simulation. Various properties of the bridge under different traffic conditions were discussed in the simulation, mainly including different span lengths and roadway conditions. As results, the power output decreased as the span length was increased or the roadway condition was improved. Meanwhile, the energy harvester set on the middle of the girder did produce higher power output than the one set on ¼ or ¾ girder. Under a dominant frequency ranging from 2.6 Hz to 6.5 Hz, the average output power from a cantilever set at the middle of a 16.76 m-span position can reach to 2 mW if there is only one passing vehicle and the roadway condition is very poor. Once continuous passing vehicles work on the bridge, the average power output from the cantilever can be further increased to 3.5 mW under the same bridge condition and installation location. Such level of power output was enough to supply electricity to wireless sensors in the bridge.

Considering that the power output from an energy harvester can be different when the bridge is damaged or not, Cahill et al. (2016) [99] tried to directly monitor the bridge structural health according to the variation of power output from the energy harvester. The results from their numerical simulations and laboratory experiments verified the feasibility of using the amount of harvested energy to detect damaged conditions in the bridge, especially through damages which can significantly change the bending stiffness of the bridge. Since the major purpose of the power output from the cantilever was to directly monitor the bridge structural health, instead of using ceramic PZT patches, the cantilever was built by a 52 µm PVDF film attaching on an aluminum beam. The maximum energy output from this PVDF-cantilever did reach up to 7.5 µJ when its resonance frequency was equal to the natural frequency of the bridge at 12.8 Hz.

Wang et al. (2016) [103] assembled a piezoelectric cantilever beam, an acquisition card through gateway and cloud platform, and an acquisition card by local read with a computer, to build a wireless vibration sensor system. After capturing the consistent vibration information collected by the wireless collection card and the vibration generated by cantilever beam, the accuracy of wireless vibration sensor is evaluated to monitor the bridge through the gateway and cloud platform, in case that the bridge excessively vibrates. The final goal of building the wireless vibration sensor system is to develop bridge health monitoring system based on Internet of Things (IoT).

Powering LED lights at Considerable Power

One of the most common applications from roadway piezoelectric energy harvesters is to power LED lights in some critical locations (e.g., crosswalk area, intersection). Since the minimum voltage output required to flash a LED light is at least 2 V and the current required to ensure the sufficient light intensity from the LED light is around 20 mA, the power output from the piezoelectric energy harvester shall be at a level of 40 mW to keep the LED light turning on in normal or at a lower level to keep the LED light flashing.

For piezoelectric disk or plate design, both field and laboratory tests have shown the feasibility of flashing LED light by piezoelectric energy harvesters. Xiong (2014) [104] assembled piezoelectric disks into a protective package and embedded the entire package at one weight station, as shown in Figure 39 (a). In the field test, an instant power output of 116 mW, equivalent to an average power output of 3.1 mW, was produced per truck. As shown in Figure 39 (b), the power output can flash the LED lights on the stop sign. Wang et al. (2018) [105] stacked piezoelectric disks and set them with carrier substrate. An extra a rigid shell and protection pads were added to improve the device's structural strength, waterproofing, high-temperature insulation, and corrosion resistance The maximum power from that device did reach up to 50.4 mW, which was sufficient to flash LED lights.

Roshani et al. (2016) [106] developed highway sensing and energy conversion (HiSEC) modules using various configurations and different numbers of PZT rod elements. The configurations of boxes containing various shapes of PZT elements were considered. The feasibility of the harvester design was tested in the laboratory to measure electrical energy. The results showed that HiSEC modules can be used in powering LED traffic lights and wireless sensors. Guo and Lu (2017) [107] introduced energy harvesting pavement system (EHPS) using two conductive asphalt layers and one piezoelectric material layer. The piezoelectric material layer is composed of a number of piezoelectric rods embeded in asphalt mixture. Under a high frequency (30 Hz) external vibration, the maximum electric power from the proposed EHPS can be approximately 300 mW based on laboratory testing results.

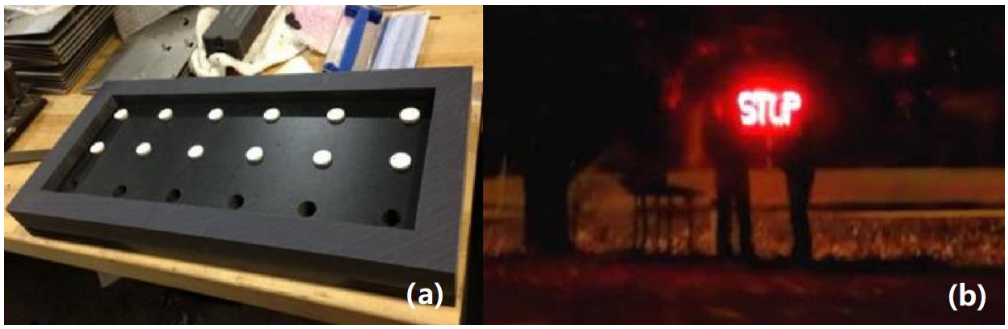

Figure 39. (a) piezoelectric energy harvester with piezoelectric disks; (b) field demonstration [104]

For piezoelectric cymbal or bridge-shaped design, one traditional design was to use a cymbal structure to convert vertical compression to horizontal tension, as shown in Figure 40(a). Based on the results from previous study by Zhao et al. (2010) [108], such piezoelectric transducer in a cymbal design did produce up to 1.2 mW under a 0.7 MPa load at 20 Hz. To further improve the power output from such bridge design, Jasim et al. (2018) [109] assembled 64 bridge transducers in one 17.8 × 17.8 × 7.6 cm energy harvester. As shown in Figure 40(b), the energy harvester contained four layers and each layer had 4 × 4 transducers. The size of each bridge transducer was 32 × 32 × 2 mm. Instead of basic homogenous PZT disks, the PZT strip used in each bridge transducer was built by seven 3.71-mm-width PZT 5X segments connected by 1-mm-width electrodes, as shown in Figure 40(c). As results from laboratory tests, this energy harvester did produce 26.6 to 30.1 mW under a loading stress of 0.7 MPa at 5 Hz, which turned to be sufficient to flash LED lights.

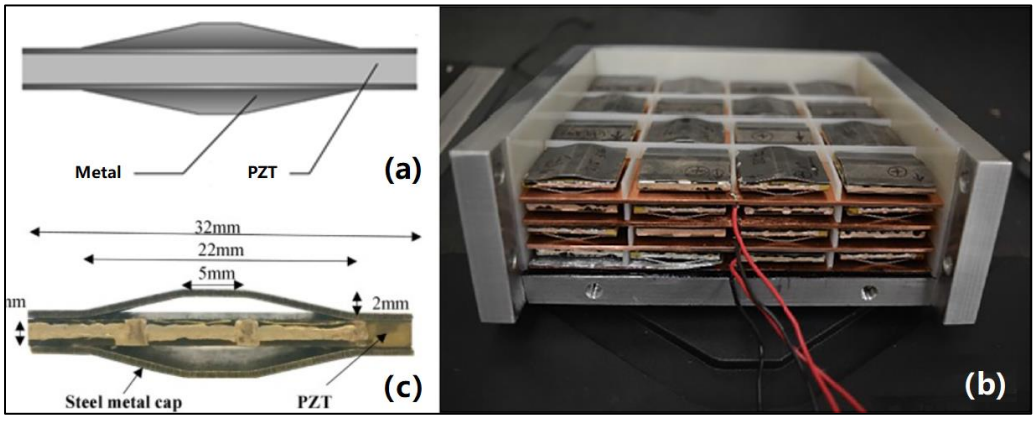

Figure 40. (a) typical piezoelectric cymbal design; (b) energy harvester with transducer arrays; c) bridge-shaped piezoelectric transducer [109]

Liu and Wang (2019) [110] developed one radially layered cymbal piezoelectric energy harvester which worked under road traffic, as shown in Figure 41. This energy harvester mainly consisted of two metal cymbal caps and two axially piezoelectric rings. The other spaces in this energy harvester were filled by metal components (e.g., metal rings, metal disks). Compared to conventional cymbal transducer designs having high resonance frequencies (over 200 Hz), such design has a resonance frequency much closer to the

pavement vibration frequency, around 20 Hz. As a result, this radially layered cymbal piezoelectric energy harvester did produce a power of 0.92 mW under a load of 500 N at a frequency of 20 Hz.

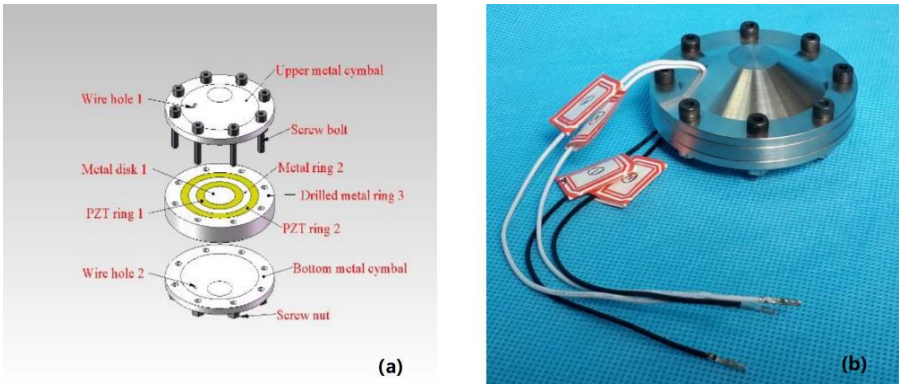

Figure 41. The radially layered cymbal piezoelectric energy harvester: (a) schematic and (b) prototype [110]

For piezoelectric beam design, the major purpose is to more efficiently deform the piezoelectric element through bending. Hwang et al. (2019) [111] proposed the design of a 50 cm × 20 cm road-capable piezoelectric energy harvester (RPEH) containing 80 piezoelectric generators inside. Each piezoelectric generator was built by a two-end fixed piezoelectric beam and pressed by an active bar in the middle to generate electricity through bending, as shown in Figure 42(a). The piezoelectric material selected in this device was PZT-PZNN ceramic. This RPEH was set on the surface of pavement, as shown in Figure 42(b). In the field test, it produced a maximum voltage output of 46.52 V and a maximum power output of 4.3 W under a medium-sized vehicle at 90 km/h. Such level of power output can be used to run a temperature sensor and transmit the measurement data in wireless. This device was also demonstrated at a highway rest area. It produced up to 2.08 W power output under a vehicle at speed of 30 km/h. The power produced from this RPEH can be used to illuminate LED indicators to improve the safety of pedestrians within the rest area [112], as shown in Figure 42(c). Another way of bending the piezoelectric harvester was relying on a bridge-type displacement amplification method, which was built by a joint structure with a moving plate.

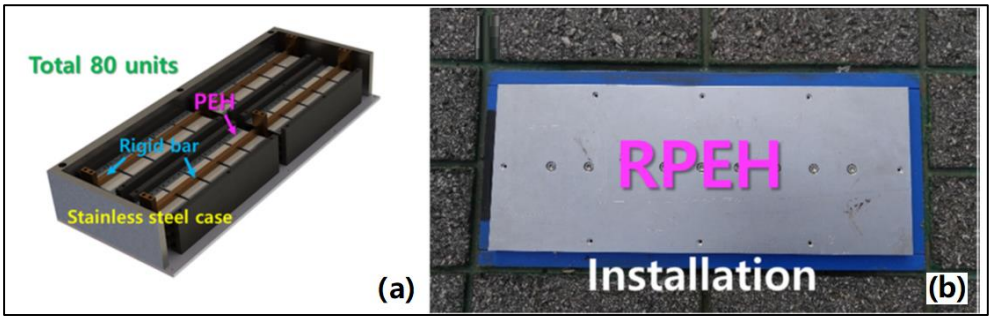

Figure 42. (a) prototype of RPEH; (b) RPEH installation on road surface; and (c) RPEH working at night [111, 112]

Besides using rigid and brittle ceramic piezoelectric materials, Jung et al. (2017) [114] built a flexible energy harvester using polyvinylidene fluoride (PVDF) polymer on the purpose of reaching stable performance and improving durability under repeated traffic loading. Each unit harvester was built via stacking nickel-based conductive fabric tapes, PVDF thin film, and polyimide substrate. All of these energy harvesters were connected with each other in parallel and placed in the vertical direction with a curvature having 50-300 mm radii, as displayed in Figure 43(a). As a result, the maximum instantaneous power output of 200 mW was produced across an external resistance of 40 kΩ under the speed of 8 km/h and weight of 2.45 kN. Shin et al. (2018) [113] developed another flexible energy harvester via adding a displacement amplification module to increase the bend of unit harvester while requiring a small vertical deformation, as shown in Figure 43(b). The direction of unit harvester placement was switched from vertical to horizontal. Compared with the previous design, this advanced design did double the power density from 8 W/m2 to 16.5 W/m2 with a small vertical displacement of 2.5 mm.

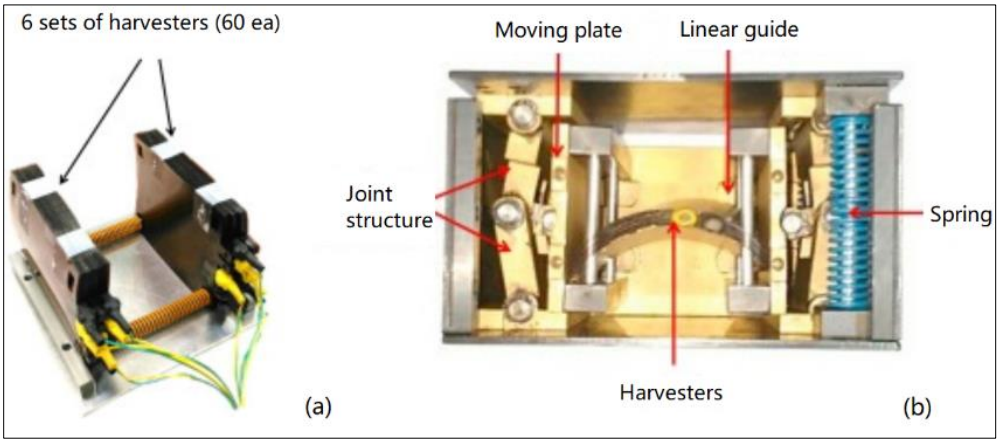

Figure 43. Flexible energy harvester design with harvesters (a) in vertical [114]; (b) in horizontal [113]

Speed bump is used as an ideal place for kinetic energy harvesting since the relatively large deformation is experiences. Song et al. (2019) [115] developed a piezoelectric harvester integrated with 40 piezoelectric generators inside for speed bump. The detailed design of this energy harvester was the same as the one proposed by Hwang et al. (2019) [111], as shown in Figure 44(a). The only difference is the size of entire module was

decreased from 50 cm × 20 cm to 30 cm × 20 cm. The set of experimental testing equipment are displayed in Figure 44 (b). As a result, when a medium-sized vehicle passed the device at 30 km/h, a maximum voltage output of 144 V and a maximum power output of 4.086 W were generated from this speed bump piezoelectric harvester. The power output from this device under nine vehicle passes was enough to charge a 10,000 μF capacitor to output 6 V electricity lasting 200 seconds. Such level of power output was enough to operate a cellphone.

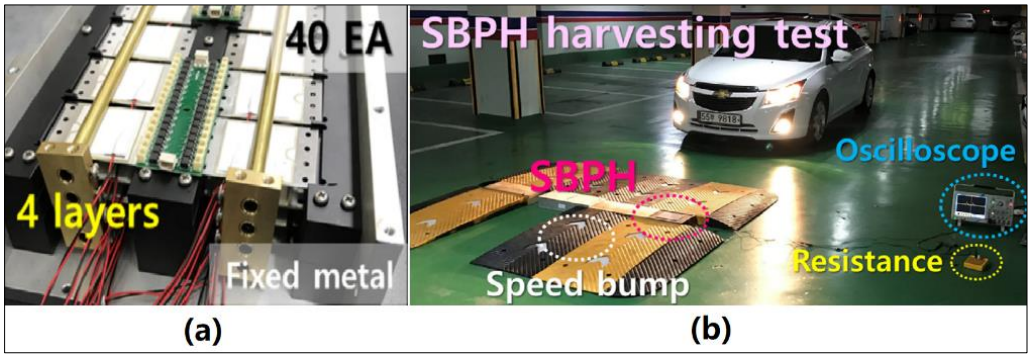

Figure 44. (a) Experimental setup for energy harvesting test of the SBPH; (b) Inner view of the SBPH [111]

Gholikhani et al. (2019) [116] built an electromagnetic speed bump for energy harvesting from passing vehicles. They placed springs inside the speed bump to create deformation under passing traffics. The vertical deformation was transferred to rotate around a horizontal axis via a rotating shaft and a rack. In the end, the rotating shaft triggered the generator for producing electricity. The detailed design of the electromagnetic speed bump is shown in Figure 45. As a result, under the deformation of around 2.95 mm, the electromagnetic speed bump produced 3mW power in average from each passing axle. The levelized cost of electricity from this design was $0.15 to $0.30 per kWh if the speed bump was installed on a road with 4000 average daily traffic.

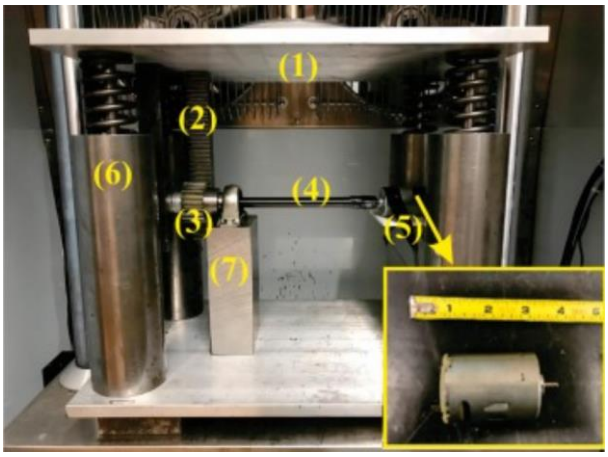

Figure 45. The electromagnetic speed bump (1) top plate, (2) rack, (3) pinion and clutch, (4) shaft, (5) generator, (6) support and spring for top plate, and (7) support [116]

Powering Wireless Sensors and ITS Devices at Ultra-Low Power

To better utilize the ability of power generation from piezoelectric elements, small piezoelectric energy harvesters were developed for supplying power to wireless sensors and devices used in roadway and intelligent transportation system (ITS) at ultra-low power (1 µW ~ 1 mW). Since the power needed by most sensors is low, the piezoelectric transducers used for this particular purpose are most likely designed as vibration-based structures (e.g., cantilevers) in small sizes. These small piezoelectric transducers are capable of converting ambient vibrations to electricity.

Cho et al. (2018) [117] built a battery-less wireless remote switch using piezoelectric cantilevers and a microcontroller as shown in Figure 46(a). The dimension of each piezoelectric cantilever was 3.5 cm × 10 cm. Once two piezoelectric cantilevers were vibrated by a pressing force of 5-8N, 140 µJ electricity was produced from these piezoelectric cantilevers. The electricity then powered a microcontroller which did transmit data packets through ZigBee Green Power communication. Those wireless transmitted data packets can be used to control smart LED bulbs or to connect with the wireless router for Internet of Things (IoT), as shown in Figure 46(b).

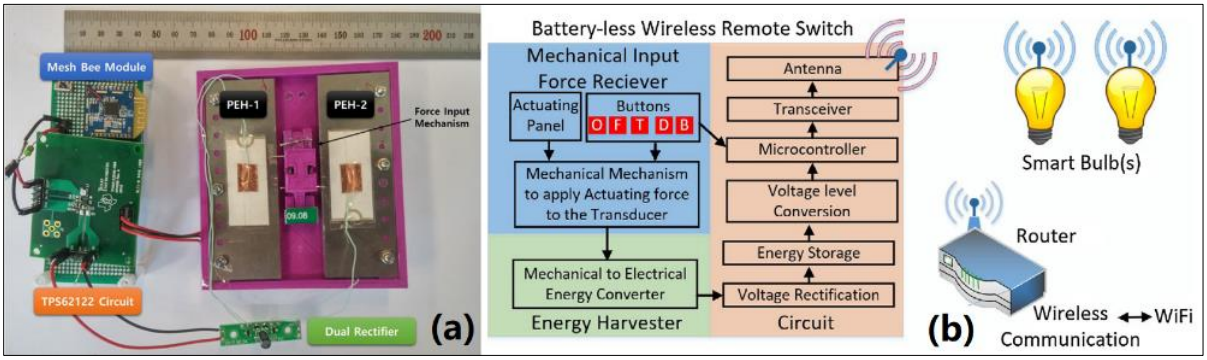

Figure 46. (a) wireless remote switch with two piezoelectric energy harvesters; (b) block diagram of the wireless remote switch

Trafford et al. (2019) [118] used piezoelectric cantilever beams in different sizes to generate electricity through roadside vibration. The lengths of these beams were from 0.89 inch to 1.89 inch, while the widths of these beams were from 0.44 inch to 0.65 inch. The resonances of these beams were from 33.4 Hz to 163 Hz. As results, under the vibration at a frequency range of 1-200 Hz at 1-g acceleration, these simple piezoelectric cantilevers produced 2.45-6.22 V open circuit voltage outputs and 63.6-289 µW maximum power outputs. That study demonstrates that the piezoelectric cantilevers under roadside vibration can produce a considerable amount of electricity to power low-power devices.

Radio-frequency identification (RFID) uses electromagnetic fields to automatically identify and track tags attached to objects that contain electronically stored information. RFID tags can be divided into two categories: one is passive without internal power source and another one is active with internal power source. The energy supplied to passive RFID tag is from the electromagnetic energy transmitted from a RFID reader,

which can be much lower than the energy from an internal power source to supply the active RFID. Due to the lower power supply, the read range of passive RFID tag is usually much shorter than that of active RFID tag under the same circumstance. Passive RFID tags are widely used in the transportation system by different ways, such as toll collection, traffic sign detection, and pedestrian detection, but within a short distance. On the other side, for active RFID tag, although it has a longer read range due to an internal power source, battery replacement cost of RFID limits its use in a large scale (such as in the roadway or bridge system). To overcome this shortcoming of active RFID, some researchers assemble an energy harvester with the active RFID tag to supply electricity to the tag.

Hande et al. (2010) [119] added a vibration-based energy harvesting (EH) system to an active RFID tag inside a high-value asset on roadway for monitoring purpose. The EH system contains an EH transducer, an EH power management, and an energy storage component, as shown in Figure 47. The EH transducer is made by a 0.38-mm cantilever structure attached with two macro-fiber composite (MFC) patches and a 10- mg tip mass. A 30-Hz resonant frequency was acquired. As a result, the EH system did produce more than 150 μW continuous power under a low excitation level of 0.07g peak. For the power requirement from the active RFID, it can be varied from 30-60 mW during full operation or 6-30 μW during the dormant or sleep mode. For most of the time in the field, a well-programmed active RFID was in sleep mode with low duty cycles. In average, operating an active tag required a level of 18-30 μW power, which was far less than the amount of supplied power from the EH system.

Figure 47. EH system with active RFID tags [119]

PIEZOELECTRIC CANTILEVER DESIGNS AND LABORATORY TESTS

Background and Motivation

When using energy harvesters in transportation infrastructure, one concern is the limited space available for placement of energy harvesters, without interrupting traffic flow or distracting drivers' attentions. One common way to fully utilize the available space on roadway for energy harvesting purpose is to embed compression-based energy harvesters under the roadway, which has been widely developed by previous studies [111, 114, 109, 120, and 121]. However, such embedment method can affect pavement structural integrity and long-term performance, and may cause extra energy loss from vehicles if any extra deformation is generated by those energy harvesters. Massive and frequent traffic loadings also can shorten the overall service life of compression-based energy harvesters, especially considering the brittleness of piezoelectric ceramics [122].

As compared to compression-based energy harvesters, vibration-based energy harvesters have several advantages. First of all, vibration-based energy harvester can be set on the roadside or under the bridge girder by occupying small attachment areas. Secondly, installation or maintenance for those energy harvesters will not interrupt traffic nor affect the existing pavement or bridge structures. Thirdly, without direct contact between vibration-based energy harvester and traffic loading, the service life of energy harvesters will not be affected by the additional stress from traffic loading. The compression-based energy harvesters rely on the compressive stresses instantly from passing vehicles, while the vibration-based energy harvesters inhibit the vibrations of the host structure. For vibration-based energy harvesters, flexible piezoelectric elements (e.g., PVDF film, macro-fiber-composite) can achieve high bending deformation to generate energy. Moreover, compared to the instant voltage output pulse generated from the compression-based energy harvester, the voltage output signal from vibration-based energy harvester oscillates with gradual attenuation over relatively longer time period, which can potentially contribute to greater energy in total. The power output of vibration-based energy harvester further depends on the vibration condition of host structure. In other words, the specific structure designs and material damping can directly affect the practical implementation of vibration-based energy harvesters in the field.

Laboratory experiments have been conducted to evaluate the performance of vibration-based energy harvesters. Wang et al. (2020) [123] used a Material Test System (MTS) to create harmonic loading functions on the energy harvester to test its power or voltage outputs under different frequencies and magnitudes. Since only compressive loads were applied via MTS, this testing method was limited for impact-induced vibrators which required direct and instant impact loading. Karimi et al. (2016) [98] built a vibrating system for testing energy harvesters. The customized signals to the shaker with the vibrating system, either simple or complex vibration scenario was simulated through the shaking system. This method was more suitable for cantilever-type energy harvesters. Zhang et al. (2018) [124] built a small-scale bridge model in the laboratory for evaluating the energy harvesters under moving loads. Complex vibration scenarios closing to the field

conditions were able to be simulated through this method, with counting the effects from host structure features and moving load characteristics.

However, vibration-based energy harvested cantilevers developed by the above previous studies in civil engineering field focused on the single degree-of-freedom (DOF) cantilevers, trying to match the specific resonant frequency of cantilever with one of the outstanding vibration frequencies encountered in the host structure for maximizing power output. Rather than only single vibration frequency involved, due to the nature of roadway or bridge structural characteristics, multiple vibration frequencies can simultaneously occur that affects energy harvesting performance of cantilever in different ways. The vibration frequencies are also highly related to the speeds of moving vehicles, which vary within different time periods. In this application case, the simple cantilever with only one resonant frequency has limited energy harvesting potential. Although the concept of dual-mass vibration energy harvester has been proposed with theoretical analysis ([125, 126]), laboratory demonstration with specific designs has not been conducted to evaluate the performance of 2-DOF as compared to 1-DOF system.

Multi-DOF Cantilever Designs

Figure 48 shows the schematics of vibration-based piezoelectric energy harvester for three different designs proposed in this study. Based on the same outline dimension, internal beams were created on the single-beam cantilever to create 2-DOF and 3D-DOF cantilevers, in addition to 1-DOF cantilever. With adding more internal beams and masses, more resonant frequencies were expected to be created with different vibration modes.

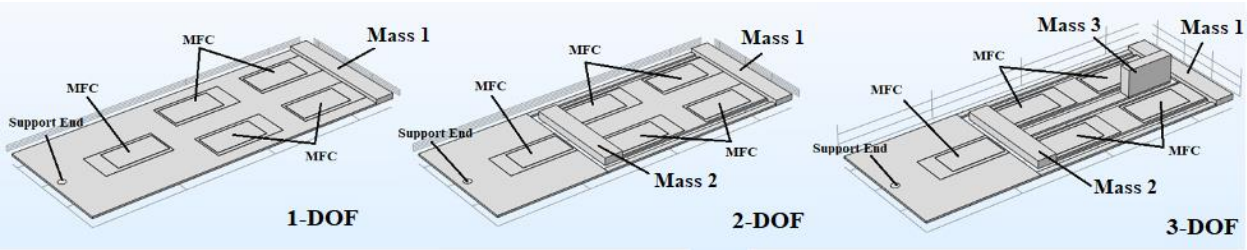

Figure 48. Schematics of piezoelectric cantilevers with different DOFs

The 1-DOF, 2-DOF, and 3-DOF cantilevers were fabricated via laser cutting on 1-mm thick aluminum plates. The outline dimensions of the cantilevers were kept at 170 × 70 × 1 mm^3 as the baseline, and further amplified by 1.1 and 1.2 scales to 187 × 77 × 1 mm^3 and 204 × 84 × 1 mm^3 for studying the size effect on energy harvesting performance. The support end of each cantilever was drilled in a hole for fixing the end on the top of the shaker with one accelerometer.

The masses were made by copper plates and attached on the ends of internal beams with different weights. The baseline of 10 g of mass 1, 21 g of mass 2, and 32 g of mass 3 were respectively set on the main beam, the secondary internal beam, and the third internal beam. For studying the mass effect on energy harvesting performance of the

cantilevers, given only mass 1 was consistently set on all cantilever designs, two different weights of mass 1 (20g and 30g) were further tried on the main beams of those cantilevers.

The piezoelectric components selected for energy harvesting purpose on the cantilevers are macro-fiber-composites (MFCs), that are flexible with high piezoelectric constants. The MFCs have a size of 28 × 14 mm^2 with a high piezoelectric constant (d_{31}) of -2.1×10^2 pC/N. Both electrodes on each MFC were connected with flexible 30-gauge copper wires by silver epoxy adhesive. On the interfaces between MFCs and cantilever beams, superglue made by cyanoacrylate was used to create strong bonding to reduce energy loss. For consistently testing energy harvesting performance at different vibration modes of cantilevers, three MFCs were attached throughout each baseline cantilever design. Those MFCs were numbered as MFC 1, MFC 2, and MFC 3 in an order of distance from beam support to tip end.

The cantilevers with specific design parameters are summarized in Table 13.

Table 13 - Detailed design parameters of three cantilevers

	1-DOF	2-DOF	3-DOF
Outline Dimension	170 × 70 × 1 mm^3 (scale 1.0)		
	187 × 77 × 1 mm^3 (scale 1.1)		
	204 × 84 × 1 mm^3 (scale 1.2)		
MFC Size	28 × 14 mm^2		
Piezoelectric Constant, d_{31}	-2.1E+02pC/N		
MFC tensile Modulus, E_m	30.336 GPa		
Beam tensile Modulus, E_b	70 GPa		
Mass Group	Mass 1: 10g, 20g, 30g	Mass 1: 10g, 20g, 30g Mass 2: 21g	Mass 1: 10g, 20g, 30g Mass 2: 21g Mass 3: 32g

Laboratory Test Program

Laboratory Equipment and Setup

The laboratory system used in this study was assembled by a permanent magnet shaker, LDS V201, an amplifier, LDS LPA100, an integrated electronics accelerometer, PCB 393B05, a data acquisition system, NI USB-4431, a laptop installed with Labview program, an oscilloscope, EDUX1002A, and an energy harvesting board, EH300. The entire laboratory setup is shown in Figure 49.

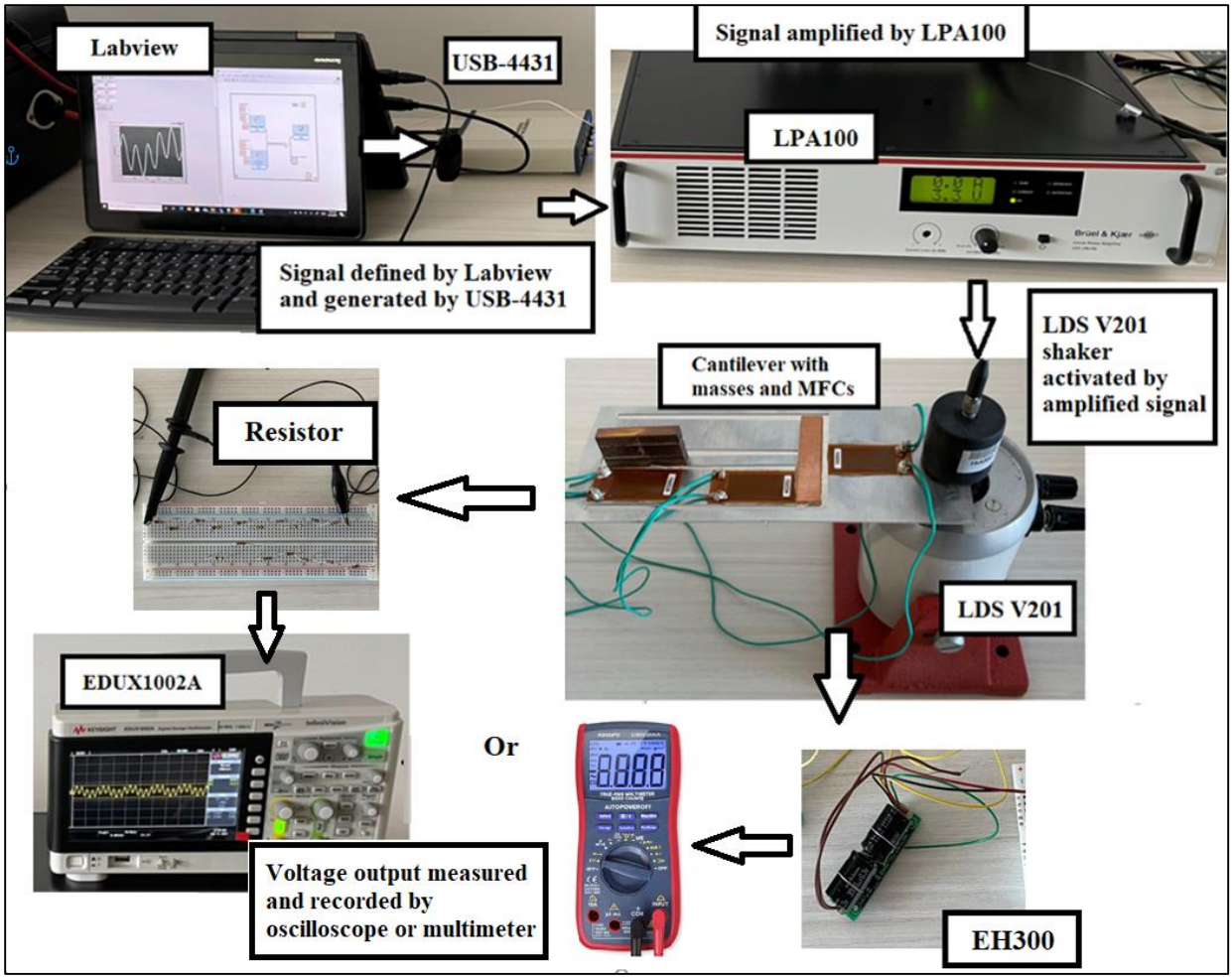

Figure 49. Energy harvesting system setup in the laboratory

The shaking system has the ability of creating well-controlled and complex acceleration signals for simulating different vibration scenarios. Through this shaking system, a specific vibration signal was first defined by Labview program and generated by USB-4431. The generated signal was then amplifiedfor activating the shaker. The acceleration signal was collected by the accelerometer. With adjusting the amplifier, the acceleration signal created by shaker can be adjusted to reach the desired amplitude on purpose. After the cantilever was fixed on the shaker and vibrated with an acceleration signal, the voltage output was measured and recorded by the oscilloscope with a sampling rate of 1 GSa/s. The system was able to generate multiple-frequency vibrations with any signal combinations for better simulating the real vibration conditions from civil structures. The energy harvesting board was used for evaluating the total energy charged from piezoelectric cantilevers. It was equipped with three major components, including an electrical power input conditioning circuit, a power storage capacitor, and a voltage trigger to conditionally release power under a minimum voltage output. Different from a regular capacitor on energy storage purpose, the energy harvesting board can efficiently store energy from irregularly low power sources in the field.

Laboratory Test and Evaluation

Two groups of laboratory tests were performed for comprehensively evaluating energy harvesting performance of different cantilever designs. The first group of tests measured voltage outputs under single or multiple vibration frequencies for two different purposes. On one hand, the single frequency vibration conditions aimed to capture the resonant frequencies of different cantilevers, acquire the maximum instantaneous power outputs in potential, and study the effects of design parameters on voltage outputs. On the other hand, the multiple frequency vibration conditions were to evaluate energy harvesting performance under more realistic scenarios similar to the field condition and evaluate the interactions between multiple resonant frequencies (from cantilever themselves) and vibration frequencies (from host structures) on the voltage outputs.

The second group of tests evaluated the charged capacitors on energy harvesting boards using different connection configurations with piezoelectric cantilevers. For quantifying the total energy stored in the capacitor, the increase of electric potential difference (in voltage) in the capacitor under certain vibration scenarios was recorded by a multi-meter. As results, the total charging time to reach certain electric potential difference within the capacitor and the total energy stored in the capacitor within certain charging time were recorded and calculated for comparison between different designs. Using different combinations of capacitors on power storage purpose, the optimized connection configuration of power storage units was explored for maximally storing the power generated.

The voltage output measurements combined with the given external resistance were further used to calculate the power outputs from MFCs. Since multiple-frequency vibrations were involved in the laboratory test, the calculation method of power output only based on peak voltage outputs and external resistances was not satisfied. The total power finally stored into the energy storage system is determined by the resistances of energy harvesting and storing components. Instead of measuring the peak instantaneous power outputs by the peak voltage outputs and external resistances, this study evaluated the total energy collected by energy harvesting board based on Equation 8.

$$E_c = C\frac{V_c^2}{2} \tag{8}$$

Where, E_c is the total energy stored in one capacitor; C is the total capacitance of capacitors set on EH300, which is given as 6.6 mF; V_c is the voltage accumulated per 10 minutes in the capacitor on EH300, which is measured by a multimeter.

Piezoelectric Cantilever under Single-Frequency Vibrations

Voltage Outputs from Different Cantilevers

The voltage outputs from cantilevers in 1, 2, and 3 DOFs with baseline designs (170 × 70 × 1 mm^3 outline size; and 10g of Mass 1, 21g of Mass 2, 32g of Mass 3) were first measured single-frequency sinuous vibrations within a frequency range between 1 to 25 Hz. An external resistance of 250 kΩ was connected with the MFC for evaluating its power output with the voltage output measurements.

Figure 50(a) shows the peak-to-peak voltage outputs from MFCs on the baseline case of 1-DOF cantilever design as the vibration frequency increased from 1 to 25 Hz. As can be seen, all those MFCs had a same resonant frequency of 16.5 Hz since they were attached on the same beam. As the MFCs were locating away from the support, their maximum voltage outputs were weakened from 38.2 V (from MFC1) to 6.3 V (from MFC3), due to the bending deformation decreased along the cantilever. This finding reflected that the area closer to the support shall be preferably selected to install MFCs for acquiring higher energy.

Compared to the voltage outputs from MFCs on 1-DOF cantilevers, one more voltage output peak from MFCs was observed on 2-DOF cantilevers, as shown in Figure 50(b), due to an extra vibration mode created. Moreover, the maximum voltage output did not occur on the MFC closest to the supporter (MFC1). Instead, one of the MFCs on the internal beam (MFC3) had maximum voltage output of 36 V at 12 Hz, which was 19.5 V higher than the maximum one from MFC1 at 11 Hz. These findings show that MFCs on different beams can separately contribute on energy harvesting under different vibrational modes, which means that more areas on the entire 2-DOF cantilever can potentially create peak power outputs under more vibration frequencies. However, similar to MFC2 and MFC3 against MFC1 on the 1-DOF cantilever, MFC2 had consistently lower voltage outputs than MFC3 on the 2-DOF cantilever since less bending deformation along the same beam they were located.

After two internal beams were created in 3-DOF cantilever, as shown in Figure 50(c), three peak voltage outputs, 17.3 V, 15.1 V, and 42.2 V were captured from MFC1, MFC2, MFC3 at three resonant frequencies, respectively at 7 Hz, 21.2 Hz, and 11.6 Hz. These peak voltages from MFCs at different resonant frequencies reflect that all MFCs can make their own contributions on energy harvesting with different vibration modes under certain vibration frequencies. It also displays that more areas on the 3-DOF cantilever can be utilized for efficiently energy harvesting by attaching MFCs under more vibration frequencies. Besides more potential area for energy harvesting purpose, the maximum voltage output of 42.2 V captured on 3-DOF cantilever was even higher than those on 1-DOF cantilever, indicating higher power output potential.

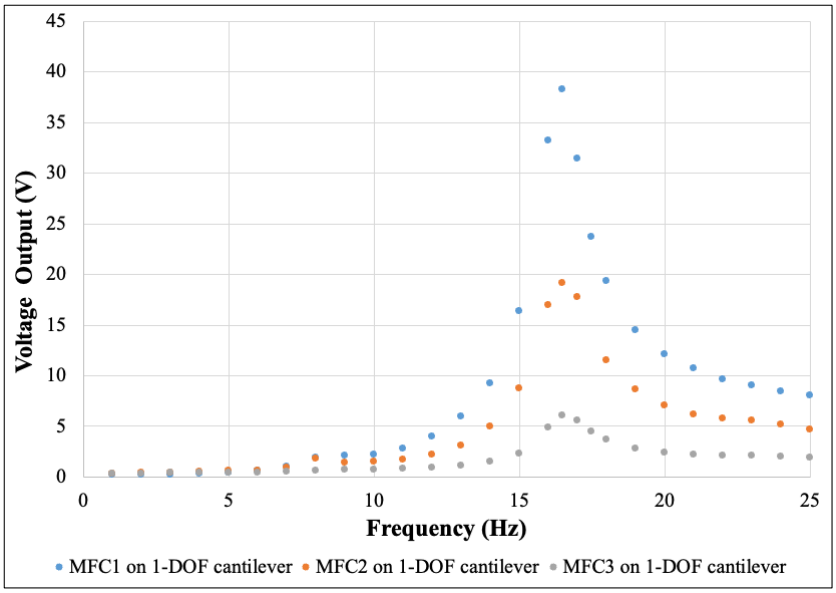
Voltage Output (V)
Frequency (Hz)
MFC1 on 1-DOF cantilever
MFC2 on 1-DOF cantilever
MFC3 on 1-DOF cantilever

(a)

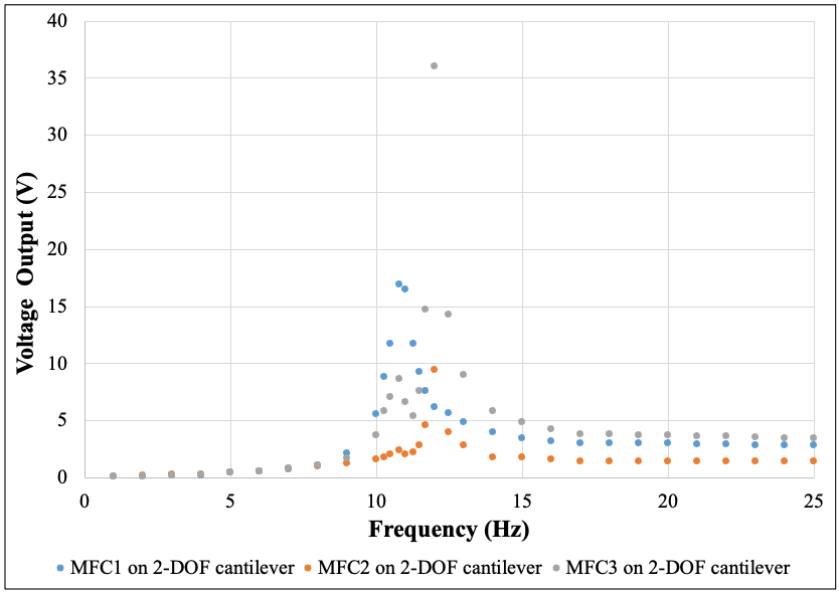
Voltage Output (V)
Frequency (Hz)
MFC1 on 2-DOF cantilever
MFC2 on 2-DOF cantilever
MFC3 on 2-DOF cantilever

(b)

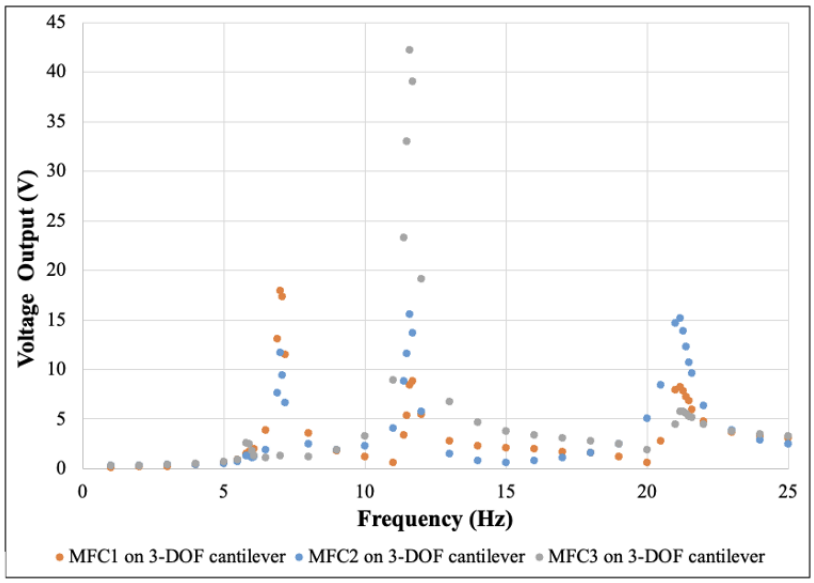

(c)

Figure 50. Voltage outputs from MFCs on cantilevers in a) 1-DOF; b) 2-DOF; c) 3-DOF

Effect of Mass Tips on Voltage Outputs

The mass tip on the main beam of cantilevers was varied from 10g, 20g, to 30g to investigate its effect on voltage outputs from cantilevers, as shown in Figure 51.

For 1-DOF cantilever, as can be seen from Figure 51(a), the voltage output was increased but the corresponding resonant frequency was dropped while the mass tip was increased. For 2-DOF cantilevers, as shown in Figure 51(b) and (c), with adding the tip mass on the main beam, the voltage output from MFC1 was gradually increased from 16.5 V to 19.3 V and the corresponding resonant frequency was shifted from 11 Hz to 7.5 Hz. However, the changing tip mass on the main beam did not significantly affect the voltage outputs from MFC3, which was attached on the inner beam. This finding reflects that the voltage output from MFC1 and MFC3 can be separately adjusted by only changing one mass tip on the beam.

For 3-DOF cantilevers, as shown in Figure 51(d), (e), and (f), with adding the mass tips on the main beam, the voltage outputs from MFC3 still remained the highest peak level (42 V) with the same resonant frequency (11.6 Hz). For MFC1, its maximum voltage output was slightly increased from 17.9 V to 18.3 V, while the corresponding resonant frequency was shifted from 7 Hz to 6 Hz. For MFC2, its maximum voltage output was significantly increased from 15.1 V to 22.7 V with the resonant frequency changing from 21.2 Hz to 17 Hz. These observation results reflect that changing the mass tip on the main beam can effectively adjust the voltage outputs from MFC2 (both voltage output and resonant frequency), partially adjust the voltage outputs from MFC1 (resonant frequency only), and ineffectively adjust the voltage outputs from MFC3.

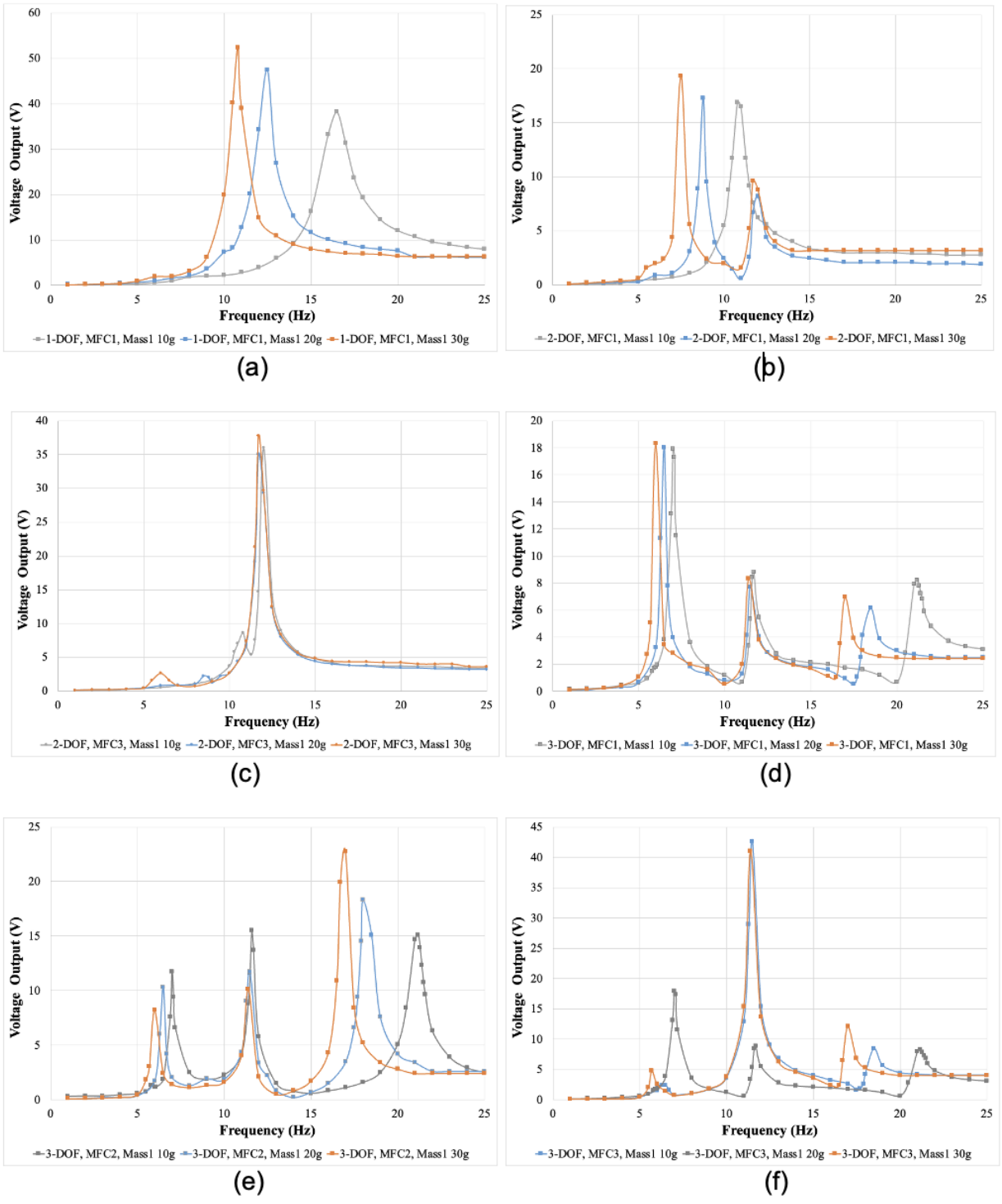

Figure 51. Voltage outputs from cantilevers attached by 10g, 20g, and 30g tip masses in: a) 1-DOF with MFC1; b) 2-DOF with MFC1; c) 2-DOF with MFC3; d) 3-DOF with MFC1; e) 3-DOF with MFC2; f) 3-DOF with MFC3

Effect of Cantilever Dimensions on Voltage Outputs

Besides mass tips, changing the dimensions of cantilever can also adjust the voltage outputs from MFCs. Given numerous geometric features of cantilevers can be changed, this study only proportionally adjusted the outline of cantilevers (width and length) by 1.1 and 1.2 scales to observe the effect of cantilever sizes on energy harvesting performance, as shown in Figure 52.

For 1-DOF cantilever, as can be seen from Figure 52(a), via increasing the overall cantilever size, the voltage output from MFC1 was gradually increased and the corresponding resonant frequency was lowered. For 2-DOF cantilevers, as shown in Figure 52(b) and (c), increasing the overall outline dimension consistently improved the voltage outputs while also dropped the corresponding resonant frequencies of both MFC1 and MFC3. Specifically, the peak voltage outputs from MFC1 and MFC3 were respectively increased from 16.5 V to 26.9 V and from 36 V to 47 V. The resonant frequencies from MFC1 and MFC3 respectively shifted from 10.8 Hz to 9 Hz and from 12.7 Hz to 9.7 Hz.

However, for 3-DOF cantilevers, the effects from the overall outline dimensions on the voltage outputs turned to be more complicate with unclear trends captured, as shown in Figure 52 (d), (e), and (f). The resonant frequencies of MFCs were consistently dropped as the overall dimensions were increased, while the peak voltages from MFCs showed unclear trends with dimension changes. Such unclear trend of peak voltage changes can be caused by complicated 3-DOF geometric features with three vibrational modes. This finding reflects challenges on controlling the performance of 3-DOF cantilevers through changing their outline dimensions.

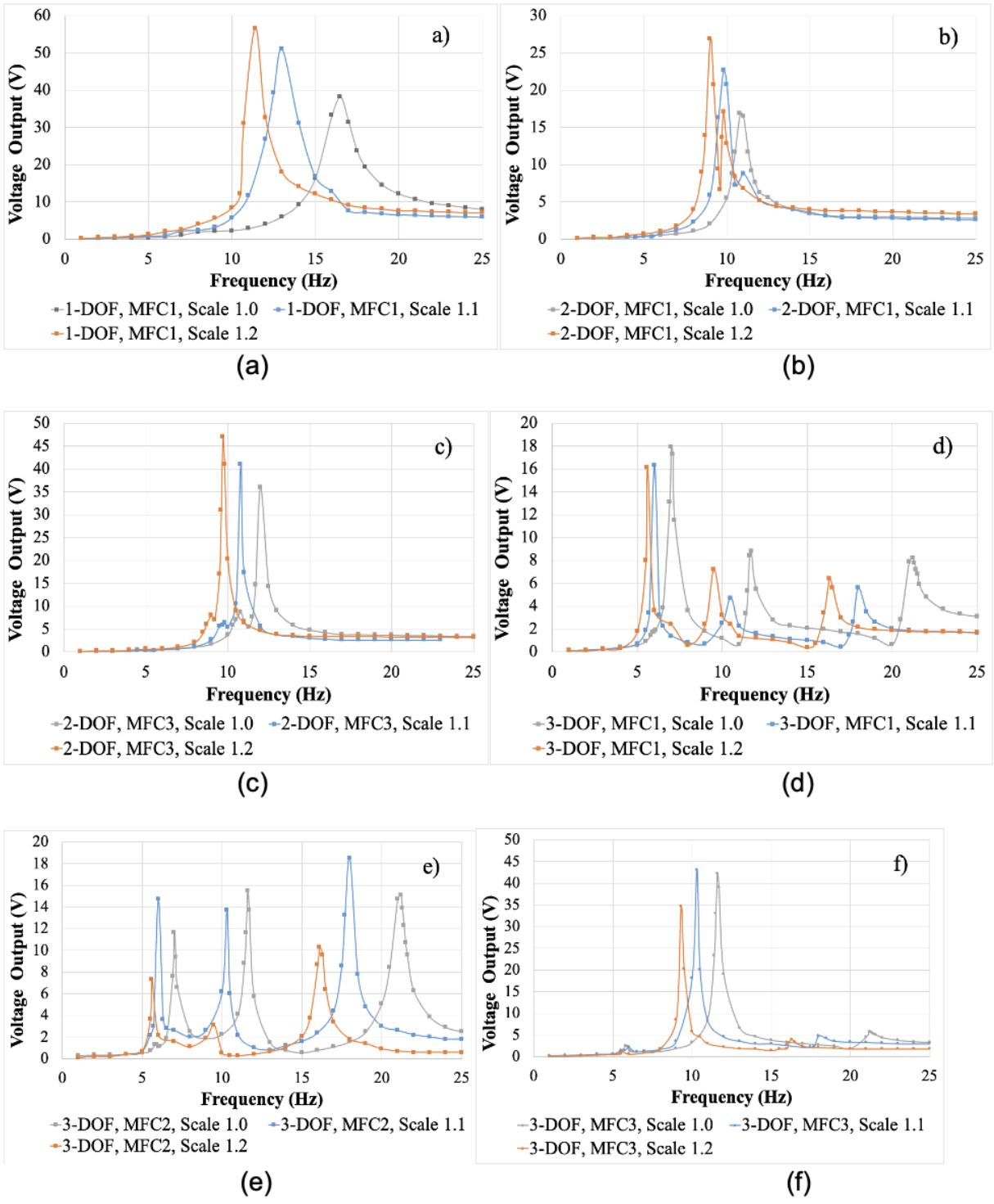

Figure 52. Voltage outputs from cantilevers scaled by 1.0, 1.1, 1.2 outline dimensions in: a) 1-DOF with MFC1; b) 2-DOF with MFC1; c) 2-DOF with MFC3; d) 3-DOF with MFC1; e) 3-DOF with MFC2; f) 3-DOF with MFC3

Piezoelectric Cantilever under Multiple-frequency Vibrations

Voltage Outputs under Two-Frequency Vibration Scenarios

For two-frequency vibration scenarios, this study first tested the performance of cantilevers when both vibration frequencies matched their resonant frequencies. The measured results of voltage outputs are shown in Figure 53. As can be seen, if the vibrational frequencies partially matched the resonant frequencies of 3-DOF cantilever (7 Hz and 11.6 Hz or 11.6 Hz and 21.2 Hz), the accumulated voltage outputs from MFC2 and MFC3 on 3-DOF cantilever in total were overall equal or higher than the ones from MFC1 and MFC3 on 2-DOF cantilever.

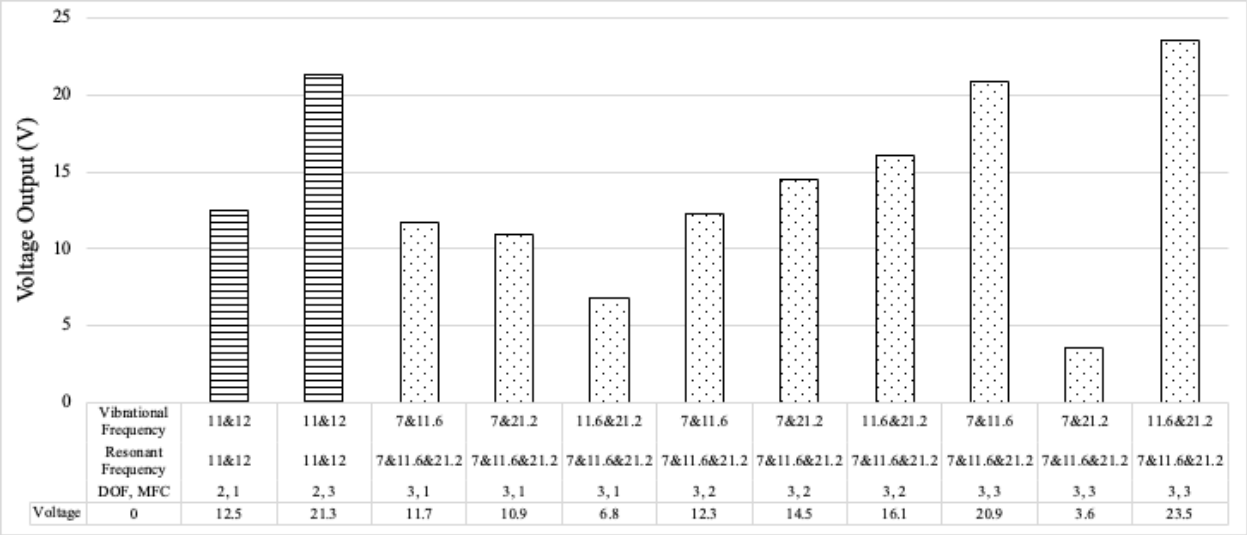

	Vibrational Frequency	11&12	11&12	7&11.6	7&21.2	11.6&21.2	7&11.6	7&21.2	11.6&21.2	7&11.6	7&21.2	11.6&21.2
	Resonant Frequency	11&12	11&12	7&11.6&21.2	7&11.6&21.2	7&11.6&21.2	7&11.6&21.2	7&11.6&21.2	7&11.6&21.2	7&11.6&21.2	7&11.6&21.2	7&11.6&21.2
	DOF, MFC	2, 1	2, 3	3, 1	3, 1	3, 1	3, 2	3, 2	3, 2	3, 3	3, 3	3, 3
Voltage	0	12.5	21.3	11.7	10.9	6.8	12.3	14.5	16.1	20.9	3.6	23.5

Figure 53. Voltage outputs from MFCs on different cantilevers under two-frequency vibrations without interference frequencies (5 Hz or 15 Hz)

The results were updated after one interference frequency (5 Hz or 15 Hz, which were not equal to cantilever's resonant frequency) replaced one of the vibration frequencies, as shown in Figure 54. The MFC3 on 3-DOF cantilever still remained above 20 V voltage output level, while the voltage outputs from both MFCs on 2-DOF cantilever were even lower than 15 V. For 1-DOF cantilever, if the interference frequency was close to its resonant frequency (15 Hz versus 16.5 Hz), it still remained high voltage output. However, if the interference frequency was significantly different from its resonant frequency (5 Hz versus 16.5 Hz), its voltage output was significantly dropped by more than 60% to 12.4 V. These results indicate that as compared to 1-DOF, 3-DOF cantilever may have more competitive performance if one of the vibration frequencies does not match the resonant frequencies of the cantilever.

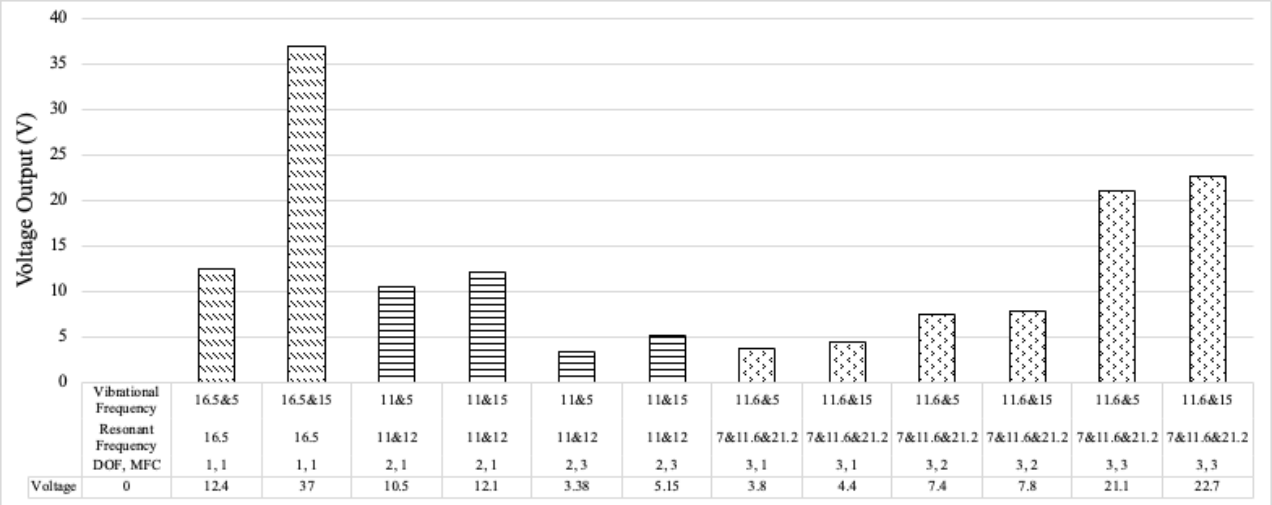

Figure 54. Voltage outputs from MFCs on different cantilevers under two-frequency vibrations with interference frequencies (5 Hz or 15 Hz)

Voltage outputs under Three-Frequency Vibration Scenarios

After adding one more vibration frequency to create three-frequency vibration scenarios, the measured voltage outputs are shown in Figure 55. For 1-DOF cantilever, if those three vibration frequencies were partially equal or close to its resonant frequency (16.5 Hz and 15 Hz versus 16.5 Hz), its voltage output dropped but still within a promising level (close to 20 V). However, if all three vibration frequencies did not match its resonant frequency, the voltage output from 1-DOF cantilever dropped to a low level of 5 V.

For 3-DOF cantilever, if three resonant frequencies all matched the three vibration frequencies, the overall voltage outputs of all MFCs remained at a level close to 10 V. Once adding interference frequencies to replace two vibration frequencies, the MFC3 on 3-DOF cantilever was still able to generate more than 10 V voltage output, which showed better performance on energy harvesting under complex vibration modes.

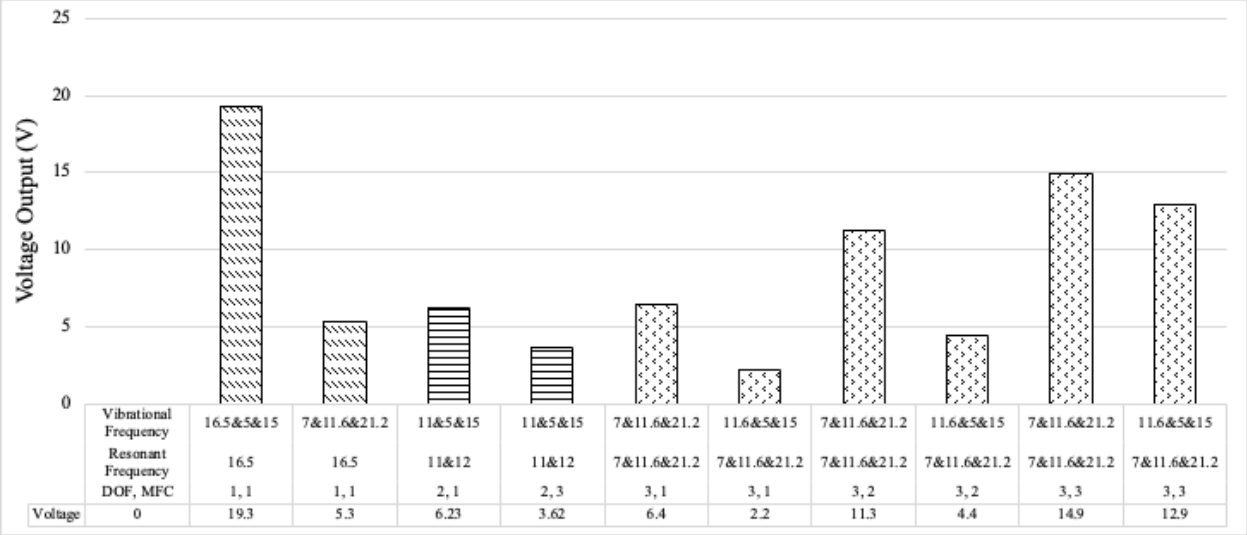

Vibrational Frequency	16.5&5&15	7&11.6&21.2	11&5&15	11&5&15	7&11.6&21.2	11.6&5&15	7&11.6&21.2	11.6&5&15	7&11.6&21.2	11.6&5&15
Resonant Frequency	16.5	16.5	11&12	11&12	7&11.6&21.2	7&11.6&21.2	7&11.6&21.2	7&11.6&21.2	7&11.6&21.2	7&11.6&21.2
DOF, MFC	1, 1	1, 1	2, 1	2, 3	3, 1	3, 1	3, 2	3, 2	3, 3	3, 3
Voltage 0	19.3	5.3	6.23	3.62	6.4	2.2	11.3	4.4	14.9	12.9

Figure 55. Voltage outputs from MFCs on different cantilevers under three-frequency vibrations

Voltage Outputs under Field-Matching Four-Frequency Vibration Scenarios

In addition to the assumed vibration scenarios, this study also tested the performance of cantilevers under a four-frequency vibration scenario that was collected from the bridge structure in the field (Camara and Ruiz, 2015). The four frequencies identified from acceleration measurements were 2 Hz, 3 Hz, 3.7 Hz, and 18.1 Hz, representing different bridge vibration modes. The particular vibration frequencies under each bridge structure were determined by the vibration modes involved within multiple spans (mainly multiple bending modes, torsional modes, and transversal vibrating modes), which can fall in a wide range from 1 Hz to 20 Hz in general.

The measured voltage outputs are shown in Figure 56. As can be seen, two highest voltage outputs over 10 V were generated by the MFC1 on 1-DOF cantilever in scale 1.0 and the MFC2 on 3-DOF cantilever in scale 1.1. Based on observation, both cantilevers had one resonant frequency close to 18.1 Hz. Especially for the 3-DOF cantilever in scale 1.1, one of its resonant frequencies exactly equaled to 18 Hz. Moreover, based on the finding from Figure 56, MFC2 shall be the one among all three MFCs to create the peak voltage output under the third vibration mode at the highest resonant frequency (18 Hz), which explained why the maximum voltage output occurred on MFC2 when the resonant frequency of 18 Hz matched one of the vibration frequencies.

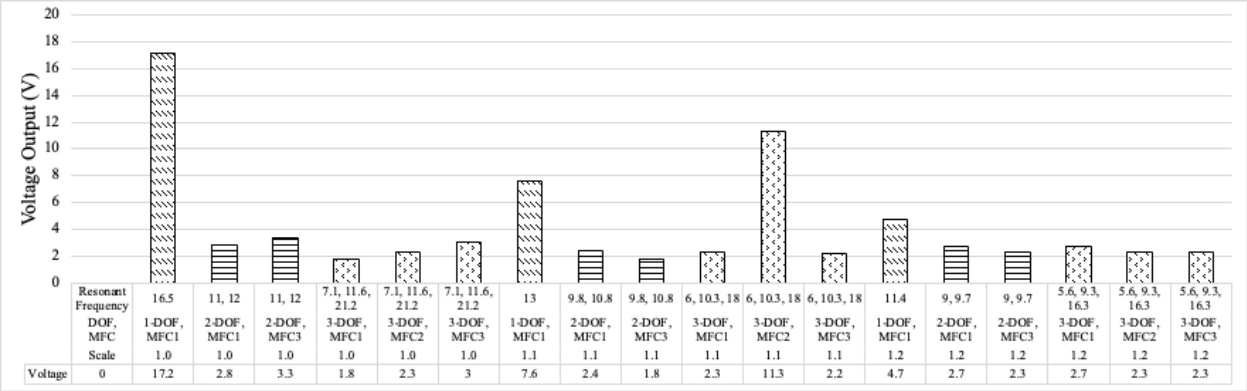

	Resonant Frequency	16.5	11, 12	11, 12	7.1, 11.6, 21.2	7.1, 11.6, 21.2	7.1, 11.6, 21.2	13	9.8, 10.8	9.8, 10.8	6, 10.3, 18	6, 10.3, 18	6, 10.3, 18	11.4	9, 9.7	9, 9.7	5.6, 9.3, 16.3	5.6, 9.3, 16.3	5.6, 9.3, 16.3
	DOF, MFC	1-DOF, MFC1	2-DOF, MFC1	2-DOF, MFC3	3-DOF, MFC1	3-DOF, MFC2	3-DOF, MFC3	1-DOF, MFC1	2-DOF, MFC1	2-DOF, MFC3	3-DOF, MFC1	3-DOF, MFC2	3-DOF, MFC3	1-DOF, MFC1	2-DOF, MFC1	2-DOF, MFC3	3-DOF, MFC1	3-DOF, MFC2	3-DOF, MFC3
	Scale	1.0	1.0	1.0	1.0	1.0	1.0	1.1	1.1	1.1	1.1	1.1	1.1	1.2	1.2	1.2	1.2	1.2	1.2
Voltage	0	17.2	2.8	3.3	1.8	2.3	3	7.6	2.4	1.8	2.3	11.3	2.2	4.7	2.7	2.3	2.7	2.3	2.3

Figure 56. Voltage outputs from MFCs on different cantilevers under four-frequency vibration

OPTIMIZATION OF DESIGN AND FULL-SCALE BRIDGE EVALUATION

Identification of Research Gaps

Energy harvesting on roadways or bridges using piezoelectric materials has been developed recently to provide in-situ power source for sensors, actuators, or wireless data transmission [127]. For piezoelectric energy harvesting on roadway, most relevant designs are compression-based [114, 109 and 128] and require structural integration with the existing pavement structures for the longevity of both pavement structures and energy harvesters. On the other side, for piezoelectric energy harvesting on bridges, most designs are vibration-based, consisting of cantilevers [97, 129 and 130]. The advantages from vibration-based energy harvesters over compression-based ones is that: 1) a longer service life is expected due to no direct traffic loading impact; 2) less impact on host structure without embedment needed; 3) less traffic control needed due to no installation directly on traffic lanes. Regarding the energy harvesting potential, compared to compression-based energy harvesters, vibration-based ones can still achieve promising voltage outputs via significant bending deformations from flexible piezoelectric patches on cantilever designs. Meanwhile, the voltage signal lasts much longer from vibration than that from instant compression, which allows the vibration-based energy harvester can generate more electrical energy than the compression-based one within a given time interval if their peak power outputs are close.

Previous studies have evaluated vibration-based energy harvesters using laboratory experiments, simulation models, and field tests. For laboratory experiments, harmonic direct loading was applied on the energy harvester under different loading frequencies and magnitudes, while such instant impacts did not generate the exact vibration of host structure [131]. A vibrating system was further built as a shaking system to better create the vibration scenarios in bridge structures, capable of creating single or complex vibrations in multiple setting frequencies [98]. To account for the effect of bridge structure and traffic on bridge vibration conditions, a steel beam-slab type bridge specimen in a span of 5 m was built and multiple single-beam cantilevers were attached on different locations of the bridge specimen. Cyclic loadings, rather than moving loads, were set on the bridge specimen to simulate the different traffic conditions (speed and weight) [132]. For more accurately simulating the bridge structure vibration under moving loads, a small-scale bridge model in the laboratory was further built by another study, with counting the factors from bridge structures and traffic moving loads [124].

Due to the efficiency of simulation models, multiple piezoelectric cantilever designs were tested under different boundary conditions set in finite element models (FEMs), including linear (unimorph) [96,*133*] and nonlinear energy harvester beam (e.g., multiple magnets involved) [134]. As one major output from FEMs, particular structure conditions (e.g., stress distribution, vibration mode) and charge distributions over the transducer were clearly captured. The boundary condition for activating the energy harvester was either directly from displacement inputs at a particular bridge structure [96] or indirectly from dynamic loads moving through a bridge structure [133]. As one example of a comprehensive FEM development, Song et al. (2019) [115] built an entire system of a double-span prestressed

concrete box girder bridge, attached with a unimorph energy harvester, under live loading of a moving train (composed of 20 cars) in the FEM [133]. Furthermore, Zhang et al. (2014) [102] built another similar comprehensive FEM of bridge, vehicle, and energy harvester system. The bridge selected in that study was a four concrete slab-on-girder bridge and the moving load was represented by either a single or a continuous flow of AASHTO HS20-44 trucks. Based on the FEM results, that study stated that the resonant frequency of single-beam cantilever needed to match the dominant vibration frequency of the bridge structure to generate the considerable amount of power at the level of 1 mW [102].

Field tests have also been conducted for piezoelectric cantilevers on the bridge. Peigney and Siegert (2013) [97] selected one prestressed concrete highway bridge for testing single-beam cantilevers. Instead of peak voltage outputs or instantaneous power outputs, the average power output used to charge one energy harvesting board (EH300) during a specific time interval was calculated. As a key result, an average power of 0.024 mW was charged into the EH300 within 210 seconds [97]. Rather than charging the power storage device, Tong et al. (2018) [100] built one unimorph, directly working as a wireless sensor based on its voltage signal generated under bridge vibrations and transmitted via a gateway system.

In general, the power outputs from current cantilever designs were found consistently at a level of 10 μW through laboratory tests to field tests [96, 98 and 99], which were further decided by particular vibration conditions (frequencies and accelerations) and entire electric circuit designs (external resistors, capacitors, and rectifiers). The power output level of 10 μW meets the power requirement from low-power electronic sensors (e.g., temperature sensor, strain gauge, MEMS) [95, 135]. The major challenge part of this energy harvesting application is that the power outputs from vibration-based energy harvesters are strongly affected by the host structural vibration scenarios, which may be uncertain with multiple vibration frequencies. To overcome this challenge for vibration-based energy harvesters, it has been demonstrated by theoretical analysis with some relevant laboratory tests that the multiple-degree-of-freedom (DOF) cantilever designs with wideband have potential to improve energy output under a multiple-frequency vibration source [136,*137, and 138*]. However, the relevant field tests have not been conducted to assess the power output of these new designs of multi-DOF cantilevers. In addition, no study has integrated laboratory measurement and simulation models to optimize the design of piezoelectric cantilevers to improve energy harvesting performance.

Optimization Approach for Vibration-Based Energy Harvesting

The proposed design optimization approach for vibration-based energy harvester on bridge applications in Figure 57. As can be seen, four major steps were involved, including measurement of bridge acceleration in the field and further processing, optimization of cantilever design relying on simulation models and regression models, assessment of optimized cantilever design in the laboratory prior to the field installation, and field installation with final adjustment if necessary.

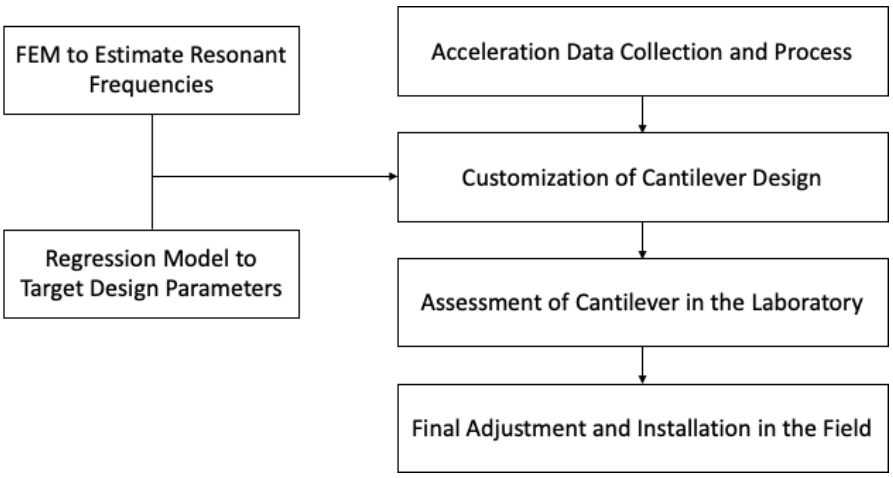

Figure 57. Proposed design procedure for vibration-based energy harvester on bridge

Acceleration Data Collection and Processing

Given that bridge vibration patterns are complex, with multiple and variable frequencies and accelerations, the first step of developing vibration-based energy harvester is to collect acceleration signals of the host structure in the field. Since the bridge superstructure consist of multiple components (e.g., decks, girders, cables, trusses), the installation locations potentially with high accelerations will be targeted based on historic acceleration records or engineering experiences. The acceleration signals in time domain will be measured and further processed through Fast Fourier Transform (FFT) to get the dominating acceleration frequencies with high acceleration peaks.

Customization and Optimization of Design Parameters

Once the particular frequencies and the corresponding accelerations from acceleration signals are obtained, the design parameters of the energy harvester will be further decided: the particular design categorized by the degree of freedom will be first selected by the number of dominating vibration frequencies from the locations on host structure; the detailed design parameters of the selected design (e.g., length, width, mass) will be then adjusted on the purpose of making its resonant frequencies to match the vibration frequencies of the host structure. The specific adjustment methods on the design parameters rely on the quantitative relationship between design parameters and resonant frequencies captured by simulation models or laboratory measurements.

Assessment of Optimized Design in the Laboratory

Considering that the resonant frequencies of each fabricated energy harvester may not exactly match the expectation due to multiple practical reasons, such as the exact weight of mass tip, the quality of fabrication, the material property of piezoelectric elements, and the unexpected damping occurred between interfaces of any components. To ensure the final design with desired resonant frequencies, the prototype should be evaluated in the laboratory to check its real resonant frequencies whether match the expected ones or not. If the resonant frequencies measured in the laboratory have more than 1-Hz difference than the expected ones, the customized cantilever need to be adjusted via modifying design parameters.

Final Installation and Adjustment

After the resonant frequencies of customized energy harvester are controlled with the specific design parameters, the prototype will be installed on the bridge. However, the installation method (magnetic attachment, screw or bolt, etc.) of energy harvester on host structure will affect its energy harvesting performance and survival life. The ideal resonant frequencies may be difficult to be reached because the effective length/width of vibration element may be changed due to space limitation. In this case, slight adjustment on the mass or the way of connection with host structure need be performed to maximize the energy output.

Piezoelectric Cantilever Design and Optimization

Multi-DOF Piezoelectric Cantilevers and Laboratory Measurements

The proposed vibration-based energy harvester in this study is the horizontal cantilever beam with the attached flexible piezoelectric transducers. Two energy harvester designs were selected in this study, including 2-DOF and 3-DOF cantilevers, as shown in Figure 58. By laser cutting techniques, internal beam(s) were created on one single beam. With adding one mass tip on each internal beam, more DOFs with different resonant frequencies were created. Multiple piezoelectric elements, macro-fiber-composites (MFCs), were attached on the cantilevers. As can be seen from Figure 58, MFC1, MFC2, and MFC3 were respectively defined as the one close to the hole (for fixing the cantilever), the one in the middle, and the one close to the mass tip on the main beam. Instead of soldering, low-temperature conductive epoxy adhesive was used to connect the wires with the electrodes on each MFC under room temperature to ensure good conductivity without damaging the MFC. Cyanoacrylate super glue was used to bond the MFCs and the cantilevers for minimizing energy loss from their interface.

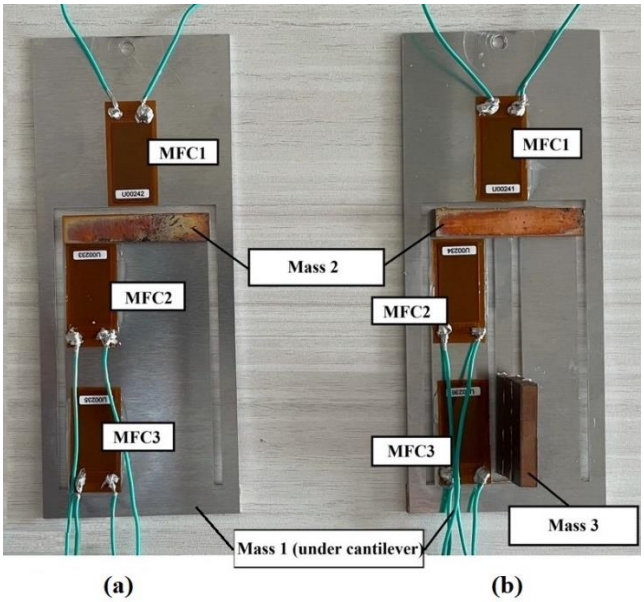

Figure 58. Cantilever designs involved in the BEAST test: (a) 2-DOF; (b) 3-DOF

On the purpose of comparing the performance of different cantilevers consistently, the same outline dimension in 170 × 70 × 1 mm^3 was used in both 2-DOF and 3-DOF cantilevers. Mass 1, Mass 2, and Mass 3 represented the mass tip on the main beam, the secondary internal beam (for both 2-DOF and 3-DOF cantilever), and the third internal beam (for 3-DOF cantilever only), respectively. An initial set of mass combination (Mass 1: 0 g, 6 g, and 10 g; Mass 2: 0 g, 21 g; Mass 3: 30 g) in total of six designs were used as the baseline for further comparison with optimized designs.

After piezoelectric cantilevers were fabricated, laboratory experiments were performed. The digital signal was created by a LabVIEW program and converted to an analog signal via a data acquisition system. The analog signal was then amplified by an amplifier to acquire sufficient voltage outputs to activate a permanent magnet shaker where the fixed end of cantilever was placed on. By adjusting the amplifier, vibration scenarios at certain acceleration levels (0.1 g to simulate bridge vibration in this study) were generated for actuating the cantilevers. The voltage outputs from different cantilevers under a wide range of vibration frequencies were collected and the resonant frequencies and the corresponding voltage outputs were determined.

Measurement of Acceleration and Voltage on Full-Scale Bridge

The bridge structural vibration with multiple frequencies similar to the field condition was simulated using the Bridge Evaluation and Accelerated Structural Testing System (BEAST) located on the campus of Rutgers University in New Jersey. The BEAST is capable of applying live loading from a tandem axle group (20~60 kips under up to 20 mph) on an 8-inch concrete deck, as shown in Figure 59(a). The entire composite concrete deck is 50 feet long by 28 feet wide, supported by four girders. In this study, dynamic loading of 60 kips was applied on two different locations on Girder 1 and Girder 2, as shown in Figure 59(b). Given the bridge vibration varied with traffic speeds, two moving speeds, 6 mph and 12 mph, were used in this study to obtain different vibration patterns.

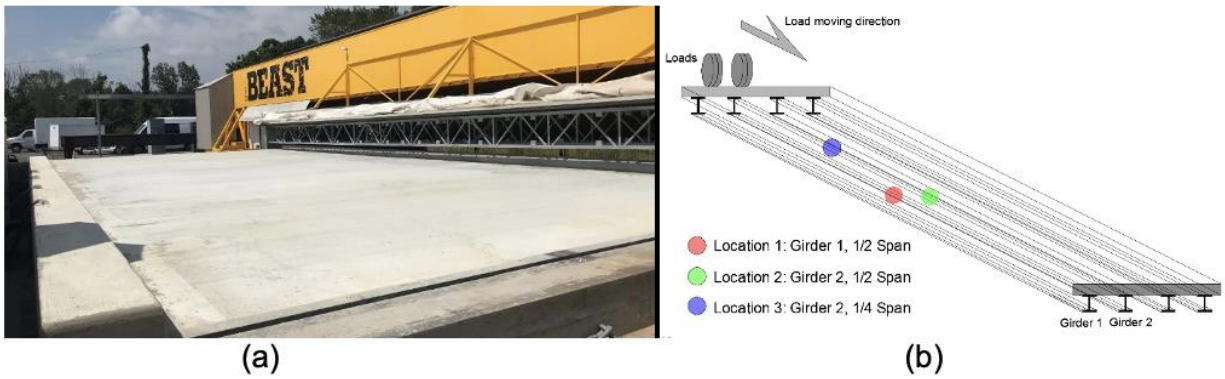

Figure 59. Live load applied in the BEAST (a) picture of one axle; (b) measurement locations

The acceleration of this full-scale bridge model was measured by the accelerometer attached on the girder, where was close to the cantilever installation location, as shown

in Figure 60(a). The type of accelerometer used was an Integrated Circuit-Piezoelectric accelerometer in PCB Model 393A03, which was capable of measuring accelerations in a range of ±5 g under a frequency from 0.5 to 2000 Hz. To ensure measurement flexibility and accuracy, strong magnetics were used to fix the accelerometer on the girder. The acceleration signals were continuously collected from the accelerometer and stored in local data acquisition system.

For the cantilever installation in the BEAST, as can be seen from Figure 60 (a) and (b), one end of the cantilever was also set on the girder fixed by a magnetic. To quantify the power output from the piezoelectric element on the cantilever, one external resistor was connected with the piezoelectric element by wires and one oscilloscope was used to measure and store the voltage output information across the external resistor, as shown in Figure 60 (c).

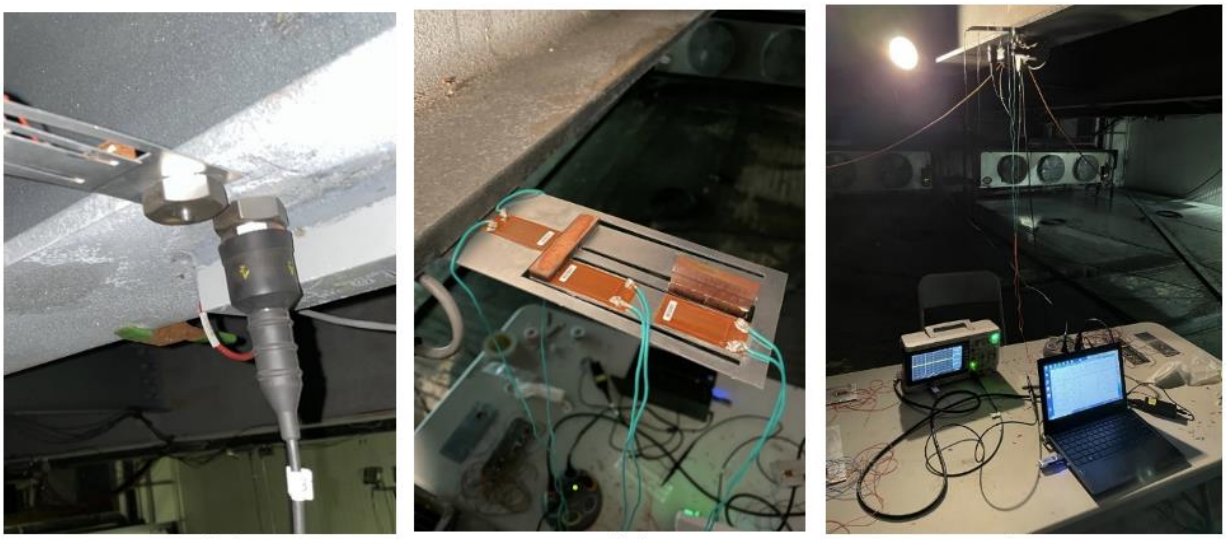

Figure 60. Field evaluation on BEAST: a) accelerometer setup on the girder; b) cantilever beam on the girder; c) voltage output measurement under the girder

Finite Element Modeling and Vibration Modes of Cantilevers

Ideally, laboratory experiments can be conducted on large amounts of cantilevers with different design parameters to measure resonant frequencies. However, this is labor and cost consuming for specimen fabrication and testing. Therefore, numerical modeling approach is proposed to predict the resonant frequency under frequency sweep simulation. The finite element models (FEMs) of multi-DOF cantilevers were develop and further verified by the corresponding laboratory tests.

The FEMs were built using COMSOL, a multi-physics simulation software. The model components include Solid Mechanics module for simulating the mechanical vibration, Electrostatics module for counting the charge generation from piezoelectric elements, and Electrical Circuit module for quantifying power output from piezoelectric elements. The tetrahedral and triangle meshes were the major two mesh shapes used in the FEMs,

while their mesh sizes were finer within the closer areas to the MFCs. Materials involved in the FEMs included 5052 aluminum (for beam), polyimide (for coating film on MFC), and MFC. The material properties of aluminum and polyimide were directly available in the material library provided by COMSOL, while the material properties of MFCs were searched out from manufacturer sheet (*23*) and previous studies (*24*).

Figure 61 displays the electric potentials (voltage outputs) from the MFCs on 2-DOF and 3-DOF cantilevers under different vibration modes. As can be seen, two vibration modes are captured on 2-DOF cantilever: the first one bends the entire beam in the same direction, while the second one only bends the internal beam. The voltage outputs from MFC1 and MFC3 on 2-DOF cantilever also respectively reach to the maximum under vibration mode 1 and 2. For the 3-DOF cantilever, one more vibration mode 3 is captured: only the secondary internal beam is bended while the main beam and the third internal beam are almost kept static. The voltage outputs from MFC1, MFC3, and MFC2 on the 3-DOF cantilever reach to the maximum under vibration mode 1, 2, and 3 in turns.

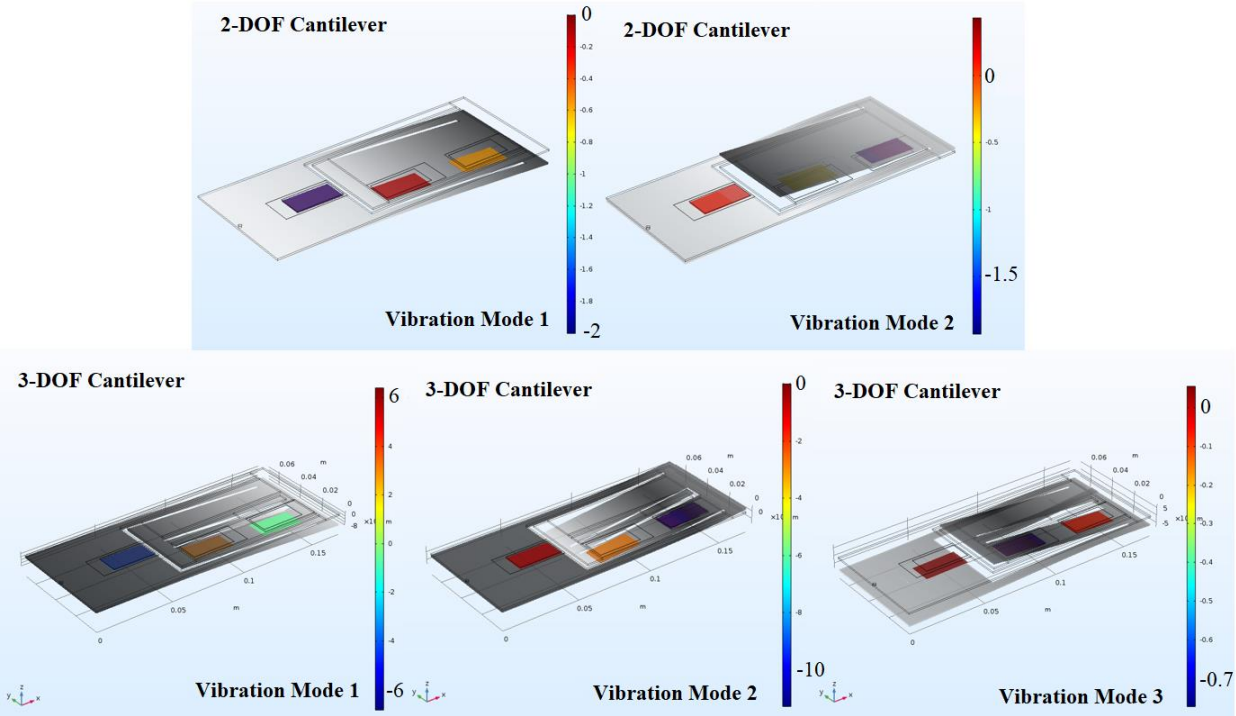

Figure 61. FEM outputs of 2-DOF and 3-DOF cantilevers: vibration modes (voltage outputs in colors)

On verification purpose, the resonant frequencies of specific 2-DOF (Mass 1: 10g; Mass 2: 21g) and 3-DOF (Mass 1: 10g; Mass 2: 21g; Mass 3: 30g) cantilever designs obtained from finite element models were compared to the ones obtained from laboratory tests. As results, the consistent voltage outputs from the macro-fiber-composites were captured by laboratory tests and FEMs, as shown in Figure 62.

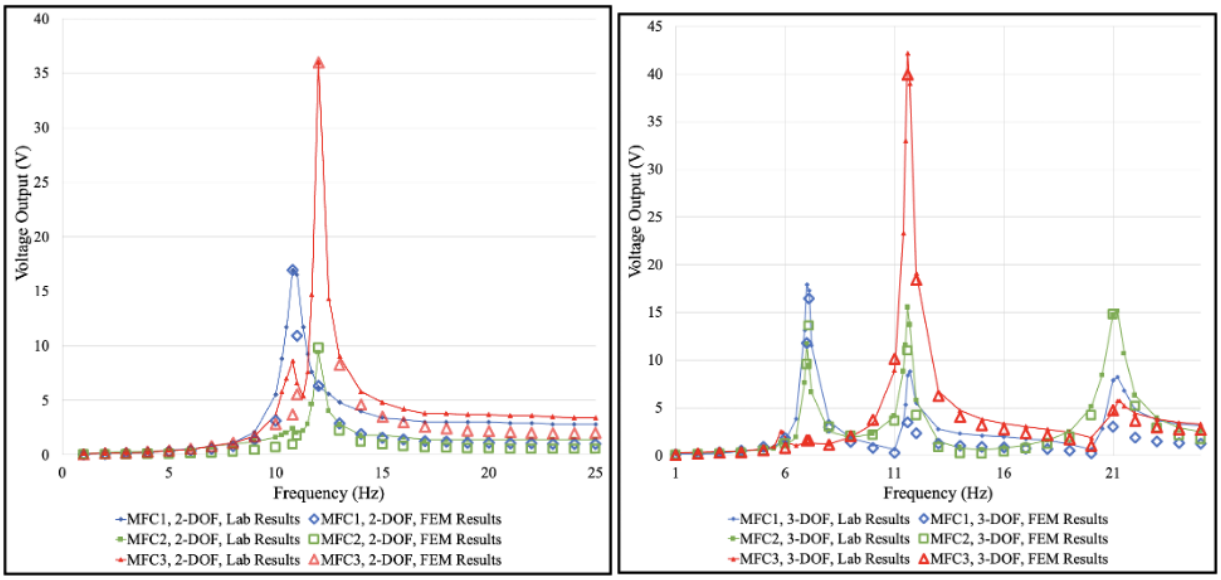

Figure 62. Laboratory versus FEM Results of 2-DOF; and (2) 3-DOF Cantilevers

Relationship between Resonant Frequency and Mass Combinations

After the FEM results were verified with laboratory tests, a variety of cases can be run to obtain the database of resonant frequencies with different design parameter. Although the geometry of cantilever (length, width, thickness) can be changed, it is more convenient to adjust the attached masses on the cantilevers. Thus, FEM cases were run to develop the regression models between resonant frequencies and mass combinations, as shown in Equations 9 to 13.

- 2-DOF cantilever:

$$Y_{2,1} = 14.6240 - 0.4863X_{2,1} + 0.0127X_{2,1}^2 - 0.0001X_{2,1}^3,\ R^2 = 0.9996 \quad (9)$$

$$Y_{2,2} = 22.722 - 0.9712X_{2,2} + 0.0303X_{2,2}^2 - 0.0004X_{2,2}^3,\ R^2 = 0.9953 \quad (10)$$

- 3-DOF cantilever:

$$Y_{3,1} = 10.6888 - 0.08358X_{3,1} - 0.0765X_{3,2},\ R^2 = 0.8885 \quad (11)$$

$$Y_{3,2} = 20.629 - 0.7171X_{3,2} + 0.0187X_{3,2}^2 - 0.0002X_{3,2}^3,\ R^2 = 0.9999 \quad (12)$$

$$Y_{3,3} = 33.560 + 0.0480X_{3,1} - 0.1436X_{3,2} - 0.0177X_{3,1} \times X_{3,2},\ R^2 = 0.8372 \quad (13)$$

Where, $Y_{2,1}$, $Y_{2,2}$, $Y_{3,1}$, $Y_{3,2}$, and $Y_{3,3}$ respectively represent resonant frequency of 2-DOF cantilever in vibration mode 1, 2-DOF cantilever in vibration mode 2, 3-DOF cantilever in vibration mode 1, 3-DOF cantilever in vibration mode 2, and 3-DOF cantilever in vibration mode 3; $X_{2,1}$, $X_{2,2}$, $X_{3,1}$, $X_{3,2}$, $X_{3,3}$ respectively represent mass 1 on 2-DOF cantilever, mass 2 on 2-DOF cantilever, mass 1 on 3-DOF cantilever, mass 2 on 3-DOF cantilever, and mass 3 on 3-DOF cantilever.

It is clear to see that each resonant frequency of 2-DOF cantilever can be well controlled by an individual mass tip. The resonant frequency of vibration mode 1 can be solely controlled by mass tip 1, while the resonant frequency of vibration mode 2 can be only

controlled by mass tip 2. However, for 3-DOF cantilever, the two resonant frequencies need be simultaneously controlled by multiple mass tips. The resonant frequency of vibration mode 1 is controlled by mass tip 1 and mass tip 3, while the resonant frequency of vibration mode 3 is controlled by mass tip 1 and mass tip 3 plus their interactions. For the resonant frequency of vibration mode 2 on 3-DOF cantilever, it is only controlled by mass tip 2 instead. Such complicated relationships between mass tips and resonant frequencies of 3-DOF cantilever are mainly contributed by the design feature of 3-DOF cantilever. Relative to the fix end, mass tip 1 and mass tip 3 are on the same side of the beams which can bend the main beam and the third internal beam in the same direction, while mass tip 2 is on the opposite side of the beam which can bend the secondary internal beam independently under different vibration modes.

As the results shown in Figure 63, for 2-DOF cantilever designs, the resonant frequencies in vibration mode 1 and mode 2 can be both estimated by the given mass tips at a high confidence level. However, the predicted resonant frequency of vibration mode 1 could be more confident than that of vibration mode 2, as comparing the scatter points at lowest and highest resonant frequencies.

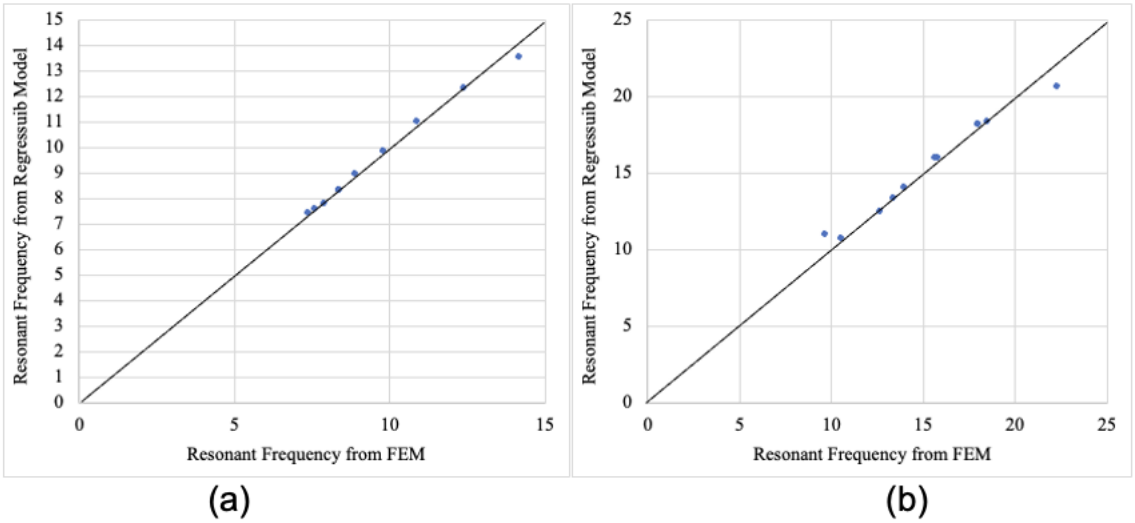

Figure 63. Regression model versus FEM outputs of resonant frequencies on 2-DOF cantilevers: a) mode 1; and b) mode 2

For 3-DOF cantilever designs, as shown in Figure 64, the resonant frequency in vibration mode 2 can be confidently predicted by the mass tip 2, and the resonant frequency in vibration mode 1 still remains an acceptable goodness of fit with two mass tips. However, predicting the resonant frequency in vibration mode 3 by two-mass combination are challenging with a weaker Goodness of Fit, *despite* the scatter points away from the diagonal line are within controlled deviations. These figures illustrate that, more the number of beams having the mass tips in the same direction (relative to the fix end), more difficult the resonant frequency can be controlled by relevant mass tips, due to more tip masses involved in the specific beam vibration.

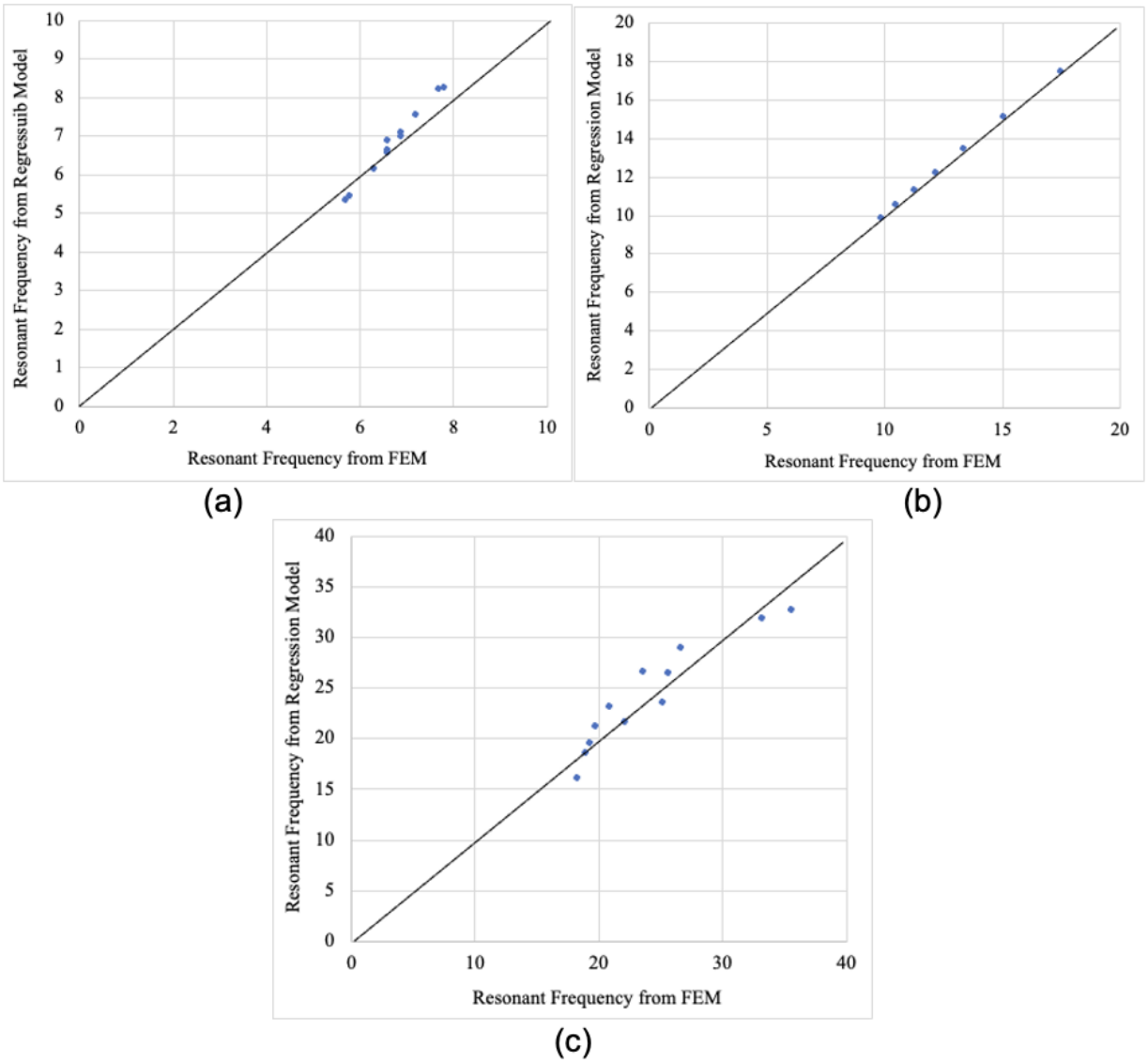

Figure 64. Regression model versus FEM outputs of resonant frequencies in 3-DOF cantilevers: a) mode 1; b) mode 2; c) mode 3

Bridge Vibration Frequencies from Measured Accelerations

After collecting the acceleration signals in the BEAST, the vibration frequencies of acceleration signals were captured via Fast Fourier Transform (FFT), as shown in Figure 65. The detailed resonant frequencies of acceleration signals at different locations under different speeds are summarized in Table 14. As can be seen through Table 14, three significant acceleration peaks were consistently observed from girder 1, while two significant acceleration peaks were observed from girder 2. Among those vibration frequencies, as the loading speed was changed from 6 mph to 12 mph, the frequency of one vibration mode was shifted from 18 Hz to 16.5 Hz for girder 2 and from 18 Hz to 13.6 Hz for girder 1. The vibration frequency of 16 Hz also was a common one observed regardless the measurement location or the loading speed.

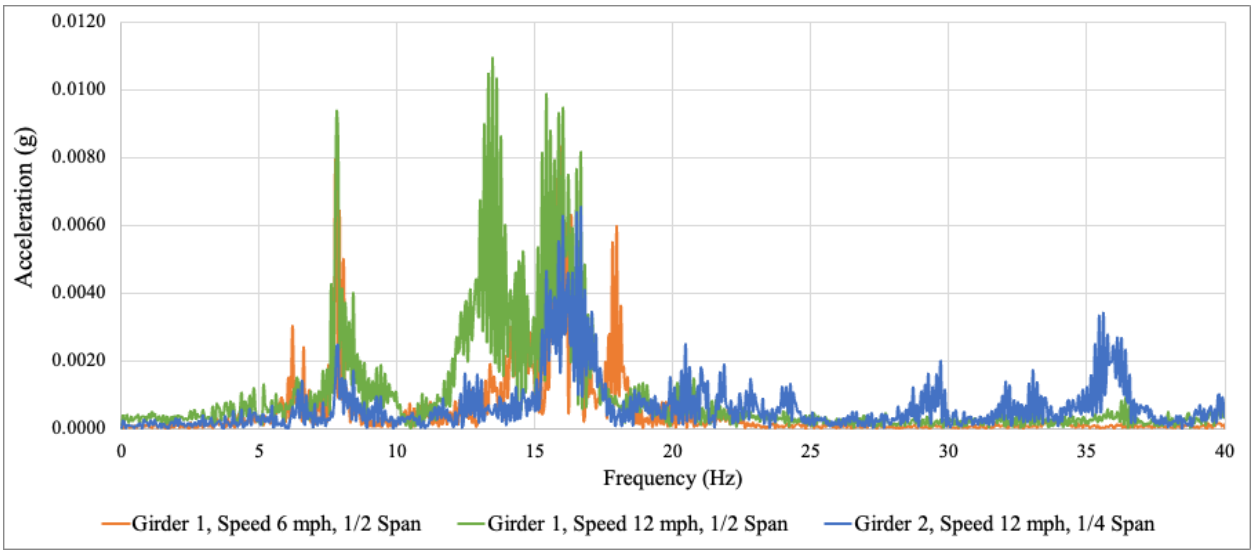

Figure 65. FFT examples of Acceleration Signals from Different Girders, Spans, and Speeds

Table 14 - Vibration Frequencies Measured in BEAST

Main Vibration Frequencies (Hz)			
	Girder 1, 1/2 Span	Girder 2, 1/2 Span	Girder 2, 1/4 Span
Speed 12 mph	7.8, 13.6, 16.0	16.0, 16.5	16.0, 16.5
Speed 6 mph	7.8, 16.0, 18.0	16.0, 18.0	16.0, 18.0

Optimized Designs for Matching Resonant Frequencies

After the dominant vibration frequencies were found, the optimized designs for 2-DOF and 3-DOF cantilevers can be obtained by adjusting the mass combinations to match their resonant frequencies with the vibration frequencies from the BEAST. Given the dominant vibration frequencies varied at different locations and loading speeds as shown in Table 1, the targeted resonant frequencies were selected to be 7.8 Hz and 16 Hz for 2-DOF cantilevers, and 7.8 Hz, 13.6 Hz, and 18 Hz for 3-DOF cantilevers in this study.

Based on regression models shown through Equation 9 to Equation 13, the optimized mass combinations were determined. For 2-DOF cantilever, the mass 1 on the main beam was set to 29 g and the mass 2 on the secondary beam was set to 10 g; for 3-DOF, the mass 1, 2, and 3 from the main beam to the most inner beam were subsequently set to 10 g, 14 g, and 25 g. The optimized 2-DOF cantilever was expected to have two resonant frequencies of 7.9 Hz and 15.7 Hz, while the optimized 3-DOF cantilever was expected to have three resonant frequencies of 7.7 Hz, 13.8 Hz, and 22.1 Hz (as much as closer to 18 Hz).

To verify the accuracy of resonant frequencies predicted from the regression model, the resonant frequencies of two optimized cantilevers were measured in the laboratory. As

shown in Figure 66, the resonant frequencies measured in the laboratory were close to those estimated from regression models. This confirmed the reliability of simulation models and regression models developed in this study to control the resonant frequencies for matching the desired values on optimization purpose.

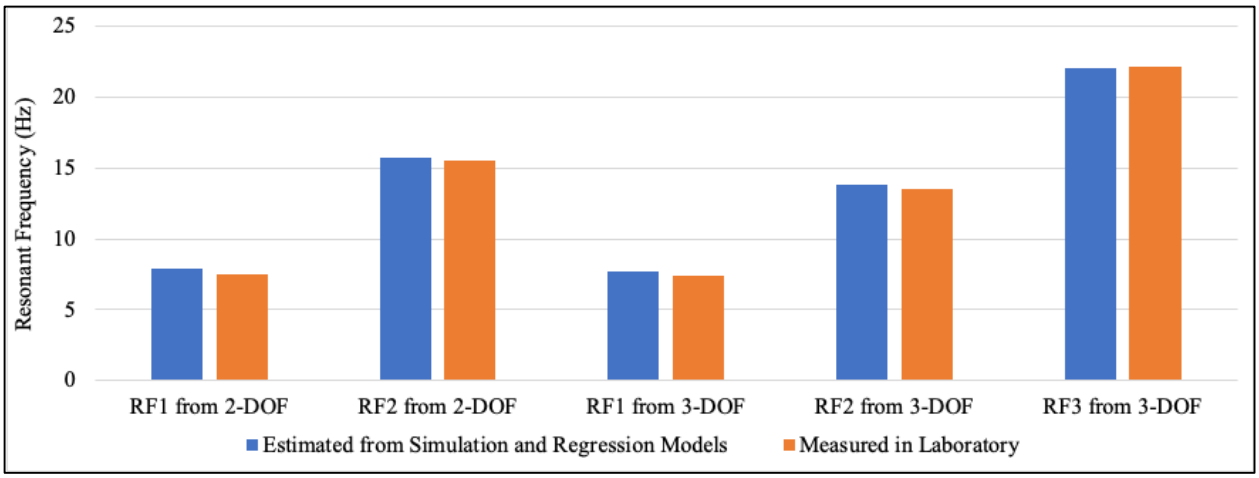

Figure 66. Resonant frequencies (RFs) of optimized cantilever designs: estimation from simulation and regression models vs. measurements in the laboratory

Power Outputs from Optimized Cantilever Designs

With confirmed resonant frequencies, the optimized 2-DOF and 3-DOF cantilever designs were set on all three locations of two girders in the BEAST. For comparison purpose, the initial designs of 2-DOF and 3-DOF cantilevers without matching frequencies were also tested at the same conditions. Their voltage outputs from MFCs crossing the external resistors were captured under each loading pulse. The total energy generated over each loading pulse was calculated to assess energy harvesting performance of different cantilever designs, as shown in Equation 14.

$$E_r = \int_{t_0}^{t_0+T} \frac{{V_{out}}^2}{R_{external}} dt \quad (14)$$

Where, t_0 is the starting time point; T is the time duration of one loading pulse; $R_{external}$ is the external resistor connected with the MFC; V_{out} is the recorded voltage output signal from an oscilloscope; and dt is the time sampling interval set in the oscilloscope.

The comparisons of energy outputs between initial and optimized designs of 2-DOF and 3-DOF cantilevers are shown in Figure 67 and Figure 68. It is clear to see that, after the cantilever designs were adjusted by using the optimized mass combinations, the energy outputs from 2-DOF and 3-DOF cantilevers were improved in general, while the maximum energy outputs from both cantilever designs were significantly improved by even more than 200% times. These outstanding energy output improvements demonstrate the feasibility of the design optimization strategy proposed in this study.

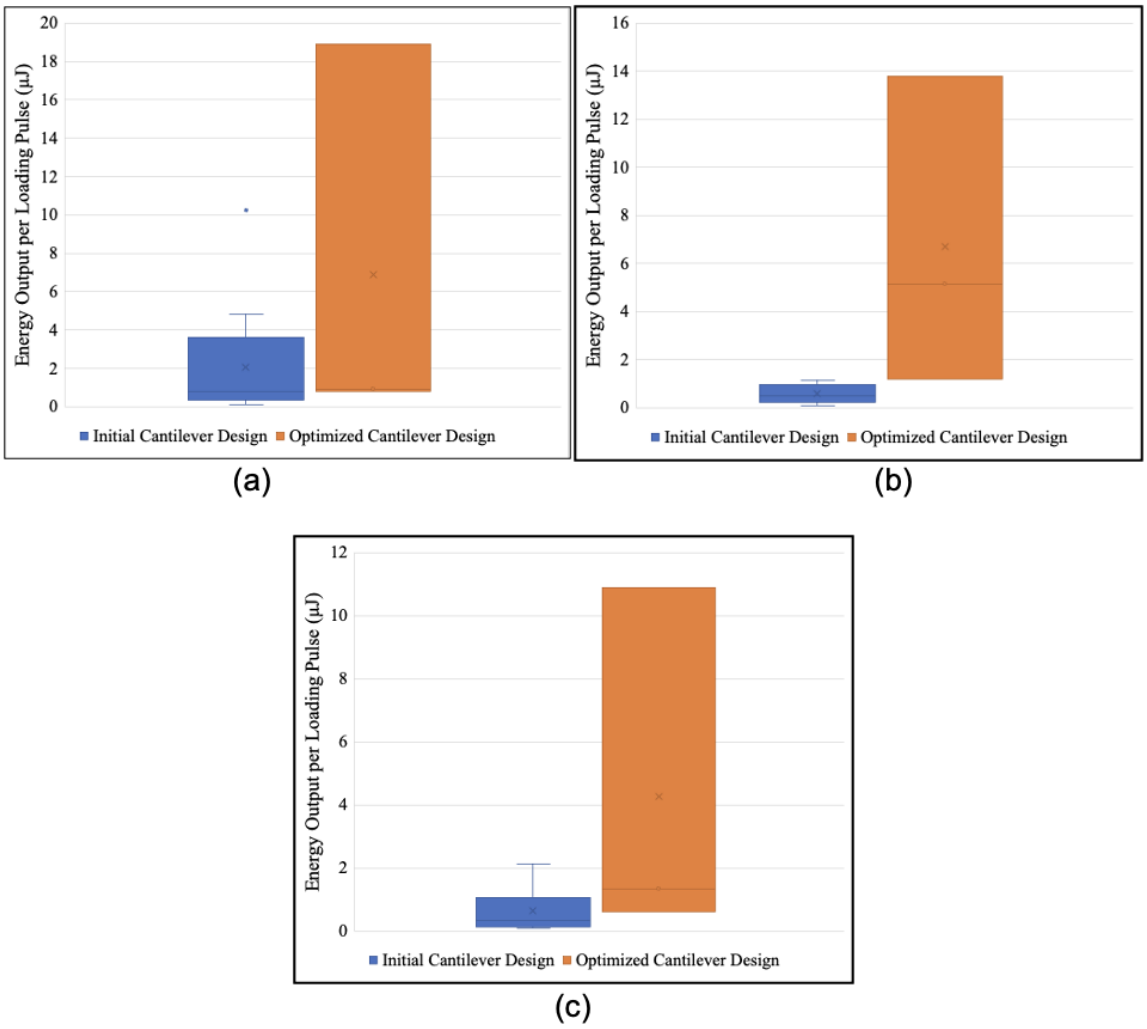

Figure 67. Energy output comparison between initial and optimized designs of 2-DOF cantilevers at: (a) ½ span of girder 1; (b) ½ span of girder 2; (c) ¼ span of girder 2

In details, as shown in Figure 67, the 2-DOF cantilever showed more consistently improved energy harvesting performance over three locations, due to its resonant frequencies partially matching the vibration frequencies over all three locations. For 3-DOF cantilever, Figure 68 shows that it generated significantly higher energy outputs at Girder 1 as expected, due to all three resonant frequencies matched the structural vibration frequencies as much as possible.

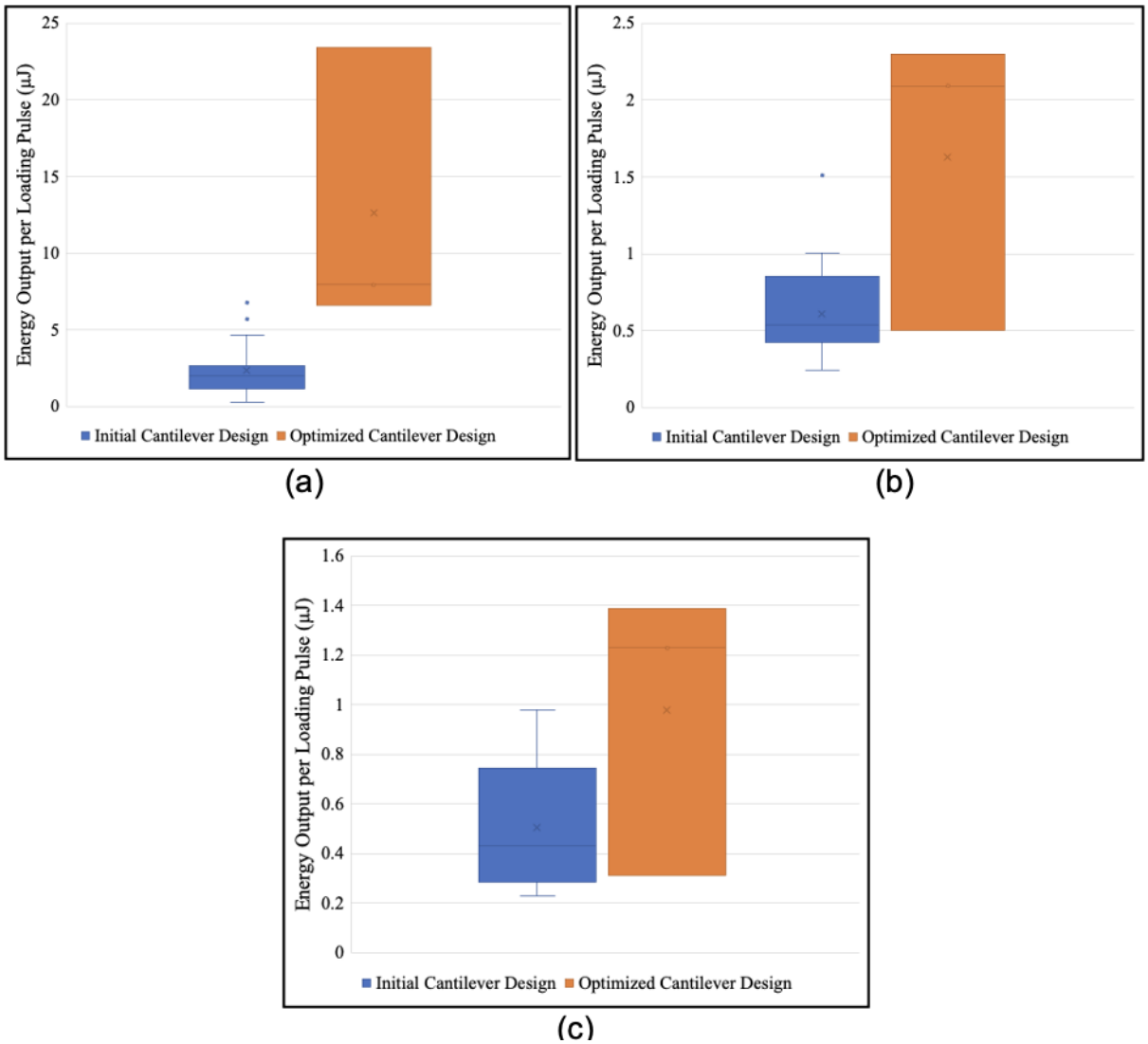

Figure 68. Energy output comparison between initial and optimized designs of 3-DOF cantilevers at: (a) ½ span of girder 1; (b) ½ span of girder 2; (c) ¼ span of girder 2

Given the complex traffic conditions in the field scenario, this study also evaluates the reliability of energy harvesting performance from optimized cantilevers under different loading speeds. As comparing the results from Figure 69(a) and (b**)**, 2-DOF cantilever showed more stable energy harvesting performance than 3-DOF cantilever under two different loading speeds. For 3-DOF cantilever, its energy harvesting performance (especially at girder 1) was significantly higher at 12 mph speed than that at 6 mph speed. However, the consistency of energy harvesting performance from 3-DOF at different locations was not as good as the one from 2-DOF. This indicates that the multiple-DOF cantilever designs need to particularly fit the vibration scenario of the selected installation location for maximizing their energy harvesting potential. Otherwise, its energy harvesting performance could be significantly weakened.

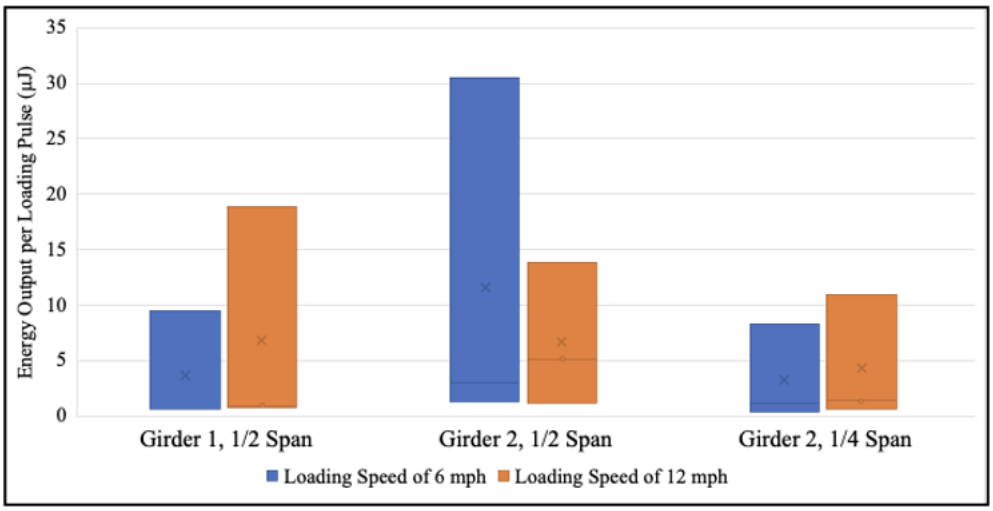

(a)

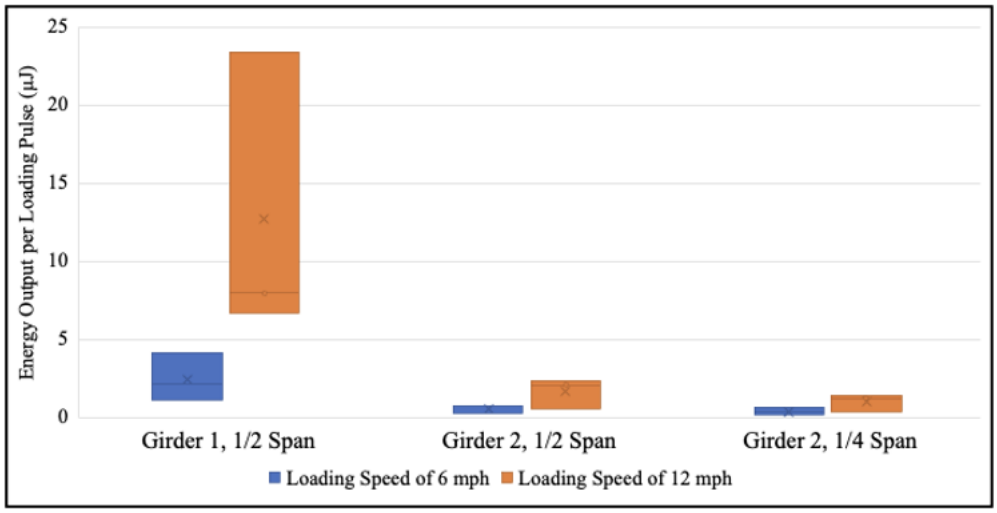

(b)

Figure 69. Energy outputs under different loading conditions: (a) 2-DOF; (b) 3-DOF cantilevers

CONCLUSIONS AND RECOMMENDATIONS

Conclusions on Energy Harvesting on Roadways and Bridges

In summary, the preferred energy harvesting technology for roadway and bridge applications may vary depending on the working principle and application purpose. The following major findings are concluded from the preliminary comparison of different technologies for roadway applications:

- Although photovoltaic system is most powerful in terms of the amount of energy output, they are best suitable for roadside applications. Challenges still exist when it is applied to roadways regarding vehicle operation and skid resistance. In addition, the initial construction cost of the prototype is expensive, although the returning benefits could be high in long term.

- Geothermal energy harvesting is perceived to be at advanced stage in the development process but is geologically and geographically limited. From safety and economic aspects, using geothermal energy piping system in critical areas such as airport apron and bridge, would be more beneficial. However, the cost of building geothermal pumps could be high.

- The solar collectors require embedment of many pipes in asphalt pavements and the energy output depends on pipe size, layout design, fluid type, and flow rate. The energy harvesting process, at the same time, has additional benefits of lowering pavement temperature and mitigating urban heat island effect.

- The energy output for thermoelectric energy is relatively low and the cost is high, although the installation process can be more flexible and easier. The future of harvesting thermoelectric from pavement is promising with system efficiency improvement by structure design and material properties.

- Different energy harvester designs made of piezoelectric material can be used for stress-based or vibration-based energy harvesting in roadways. The generated energy output is usually small for individual piezoelectric transducer under one vehicle pass, but can be significant for multiple sensor arrays under repeated traffic loading. It also brings the additional function of traffic data monitoring as sensor applications.

- Electromagnetic systems are based on structure vibrations and thus have specific application fields, such as structure health monitoring system of bridge or speed bump on roadway. However, they cannot be used for large areas of roadways due to small vibrations under traffic loading.

- Wind energy is considered the fastest growing clean energy source. In highways, the passing of vehicle traffic brings the opportunity of wind energy harvesting in highway medians. This turbine can be also a barrier preventing the interruption of high intensity

light coming from the vehicles on opposite directions. However, there are very few studies that focused on highway wind turbine.

- Among all vibrational energy harvesting devices, the electrostatic systems have advantages of both compatibilities with microelectromechanical systems (MEMS). There are many advantages of using electrostatic energy harvesters such as high voltage, low cost, high coupling coefficient, and size reduction increase capacitance. However, the electrostatic energy harvesting is more appropriate for small-scale energy harvesters such as sensor systems.

Conclusions on Solar Energy Harvesting on Roadways

The following conclusions can be concluded from the analysis of solar energy harvesting on ROW and noise barriers of roadway.

- The technical and economic feasibility of solar array in the ROW was presented and proved. The analysis results showed that the project is feasible for single owned, or third part owned. For the third part owned with power purchase agreement, the challenge is to agree on the electricity price to benefit both transportation agency and private company. The profitability is the highest when the system is owned by the agency itself. However, the initial investment, operation, and maintenance is responsibility of the agency. The solar energy potential at ROW of NJ roadway is estimated to be 4,271 GWh per year.

- In the project level analysis of PVNB, the design configuration with the shingles built-on has the highest energy output; while the energy outputs of top-mounted tilted and top-mounted bifacial configurations vary depending on barrier orientation. The simplified regression models provide a quick way to estimate total energy output for each design configuration considering different orientations of noise barriers. For the state-level estimation of PVNB in New Jersey, the shingles built-on design can produce energy output of 56,164 MWh per year.

- PVNB implementation can result in economic, environmental, and social benefits. The proposed decision-making framework for site selection includes factors that impact these three categories to increase economic return, reduce environmental impacts, and improve public welfare. The framework can be used to recommend the appropriate list of noise barriers for PVNB, which can then be further analyzed with life-cycle assessment and life-cycle cost analysis. Agencies can implement PVNB projects through direct ownership or third-party ownership as business models.

Conclusions on Piezoelectric Energy Harvesting on Bridges

The following conclusions can be concluded from the analysis of piezoelectric energy harvesting from bridge vibrations.

- The multi-DOF cantilever designs allow more space in the cantilever to be utilized for producing energy under different vibration modes. The resonant frequencies of different cantilevers were adjustable by changing outside dimensions and mass combinations. Under multiple frequency vibration scenarios, 3-DOF cantilever showed the higher possibility of matching resonant frequencies with vibration frequencies in a wide range. On the contrary, the 1-DOF cantilever has high voltage output when the single resonant frequency is matched but it dropped dramatically if the vibration frequency changes.

- The proposed optimization approach can be used for designing multi-DOF piezoelectric cantilevers to maximize power output. The power output improvement achieved by the proposed approach was demonstrated on a full-scale bridge testing facility. The design optimization is fulfilled through multiple-DOF cantilever designs, finite element model simulations, and optimization model developments.

- Multiple-DOF cantilever designs can generate considerable energy outputs after proper geometric design optimizations to match resonant frequencies with vibrational frequencies of host structure. Under one loading pass, the optimized 2-DOF and 3-DOF cantilevers was capable of generating 30.5 μJ and 23.4 μJ electrical energy, respectively, which were twice higher than those from the baseline cantilever designs.

Recommendations for Future Research

Solar energy harvesting showing great potential to generate renewable energy using roadway assets in ROW, noise barriers, rest areas, building, etc.The state-level analysis of solar energy potential in ROW and noise walls is based on rough estimation and future studies need consider the influences of slope, solar obstruction, terrain, and vegetation. Future implementation of PVNB should consider the quantified economic, environmental benefits for site selection and configuration design in the project planning phase to increase system performance and efficiency. The impact of PVNB on glare and traffic safety should be also studied for the selected sites before implementation.

The energy harvesting performance of piezoelectric cantilevers relies on the matching between resonant frequencies and external vibration frequencies. The proposed multi-DOF cantilevers and optimization approach is more compatible to a variety of vibration features from bridges under different external conditions. Future study should be conducted to further optimize the design of vibration energy harvesting system based on different bridge structures. The specific installation methods and the integration methods with sensors or power storage devices need be further studied.

REFERENCES

1. The White House (2021). President Biden Sets 2030 Greenhouse Gas Pollution Reduction Target Aimed at Creating Good-Paying Union Jobs and Securing U.S. Leadership on Clean Energy Technologies. Retrieved from: https://www.whitehouse.gov/briefing-room/statements-releases/2021/04/22/fact-sheet-president-biden-sets-2030-greenhouse-gas-pollution-reduction-target-aimed-at-creating-good-paying-union-jobs-and-securing-u-s-leadership-on-clean-energy-technologies/
2. Conference of European Directors of Roads CEDR (2017) State of the art in managing road traffic noise: noise barriers. Technical Report 2017-02 ISBN: 979-10-93321-27-1
3. Carder D. R. and Barker, K. J. (2006) Trials of renewable energy generation in highways: Feasibility study. Published Project Report PPR178 TRL Limited
4. Poe, C., Plovnick, A., Hodges, T., Hastings, A. and Dresley, S. (2017). Highway Renewable Energy: Photovoltaic Noise Barriers. U.S. Department of Transportation.
5. Wakulat RJ (2016). Photovoltaics (PV). Salem Press.
6. Chu, Y., Meisen, P. (2011) Review and Comparison of Different Solar Energy Technologies. Global Energy Network Institute.
7. Chiarelli A, Al-Mohammedawi A, Dawson AR, García A. (2017) Construction and configuration of convection-powered asphalt solar collectors for the reduction of urban temperatures. International Journal of Thermal Sciences. 2017, 112, 242-51.
8. Uchida, K-i., Adachi, H., Kikkawa, T., Kirihara, A., Ishida, M., Yorozu, S., (2016) Thermoelectric generation based on spin Seebeck effects.
9. Madvar, M. D., Ahmadi, F., Shirmohammadi, R., & Aslani, A. (2019). Forecasting of wind energy technology domains based on the technology life cycle approach. Energy Reports, 5, 1236–1248.
10. Kumar, R., Raahemifar, K., & Fung, A. S. (2018). A critical review of vertical axis wind turbines for urban applications. Renewable and Sustainable Energy Reviews, 89, 281-291
11. Pavlov, G.K., Olesen, B.W., (2012) Thermal energy storage - a review of concepts and systems for heating and cooling applications in buildings: Part 1 - Seasonal storage in the ground. HVAC&R Research. 18, 515-38.
12. Uchino, K. (2009) Ferroelectric Devices 2nd Edition, CRC press.
13. Saha, C.R. (2011) Modelling theory and applications of the electromagnetic vibrational generator. Sustainable Energy Harvesting Technologies-Past, Present and Future: InTech.
14. Jung, H-J., Park, J., Kim, I-H. (2012) Investigation of applicability of electromagnetic energy harvesting system to inclined stay cable under wind load. IEEE Transactions on Magnetics. 48, 3478-81.
15. Naruse, Y., Matsubara, N., Mabuchi, K., Izumi, M., Suzuki, S. (2009) Electrostatic micro power generation from low-frequency vibration such as human motion. Journal of Micromechanics and Microengineering. 19, 094002
16. Poe, C., Plovnick, A., Hodges, T., Hastings, A. and Dresley, S. (2017). Highway Renewable Energy: Photovoltaic Noise Barriers. U.S. Department of Transportation.
17. Innovia Technology Limited (2017). Demonstrating Solar Noise Barriers on The Ray.

18. Hyder, F., Sudhakar, K. and Mamat, R. (2018). Solar PV tree design: A review. Renewable and Sustainable Energy Reviews, 82, pp.1079-1096.
19. Renugadevi, V. (2017). An Approach to Solar Power Tree. In: International Conference on Electrical, Instrumentation and Communication Engineering (ICEICE2017).
20. Gupta, S. and Gupta, M. (2015). The Benefits and Applications of Solar Tree with Natural Beauty of Trees. SSRG International Journal of Electrical and Electronics Engineering, 2348(8379), pp.29 - 34.
21. Cmeri.res.in. (2019). Solar Artifact | Central Mechanical Engineering Research Institute. [online] Available at: https://www.cmeri.res.in/technology/solar-artifact
22. Solar Power Trees: Spotlight Solar Products (2019) [online]. Available at: https://spotlightsolar.com/products
23. F.S. Power (2019). Solar power Europe. *Sol. Ind. Reports,* pp. 1 – 32.
24. Liu, G. (2014) Sustainable feasibility of solar photovoltaic powered street lighting systems, International Journal of Electrical Power & Energy Systems, Volume 56, Pages 168-174, ISSN 0142-0615.
25. Reinders, A.H.M.E., Pramusito, A. Sudradjat, V.A.P. van Dijk, R. Mulyadi, W.C. Turkenburg. (1999) Sukatani revisited: on the performance of nine-year-old solar home systems and street lighting systems in Indonesia, Renewable and Sustainable Energy Reviews, Volume 3, Issue 1, Pages 1-47, ISSN 1364-0321.
26. Dezfooli, A., Nejad, F., Zakeri, H. and Kazemifard, S. (2017). Solar pavement: A new emerging technology. Solar Energy, 149, pp.272-284.
27. Matrawy, K and Farkas, I. Comparison study for three types of solar collectors for water heating. Energy Convers Manage 1997. 38: 861-869.
28. Rooij, R. (2017). "Dutch Solar Bike Path SolaRoad Successful & Expanding. Retrieved from https://cleantechnica.com/2017/03/12/dutch-solar-bike-path-solaroad-successful-expanding/
29. "Solar Bike Path Opens This Week in The Netherlands". (2014) Retrieved from https://www.npr.org/sections/thetwo-way/2014/11/10/363023227/solar-bike-path-opens-this-week-in-the-netherlands
30. Milberg, E. (2017). World's First Composite Solar Panel Road Opens in France. Retrieved from http://compositesmanufacturingmagazine.com/2017/01/composite-solar-panel-road-in-france/
31. Todd, F. (2019) "What is China's solar highway? Profiling the 1km energy-producing road in Shandong. Retrieved from https://www.nsenergybusiness.com/features/china-solar-highway-energy/
32. Oregon Department of Transportation (2011). Solar Highway Program: From Concept to Reality.
33. Yu, X., Puppala, A. and Zhang, N. (2017). Use of Geothermal Energy for Deicing Approach Pavement Slabs and Bridge Decks, Phase 1: Final Report. University of Texas at Arlington.
34. Geothermal Heating and Cooling Technologies. (n.d.) Retrieved from https://www.epa.gov/rhc/geothermal-heating-and-cooling-technologies
35. Eugster, W. (2007). Road and Bridge Heating Using Geothermal Energy. Overview and Examples. Proceedings European Geothermal Congress 2007 Unterhaching, Germany, 30 May-1 June 2007.

36. Morita, K., Tago, M. (2005). Snow-Melting on Sidewalks with Ground-Coupled Heat Pumps in a Heavy Snowfall City. Proceedings World Geothermal Congress 2005 Antalya, Turkey, 24-29 April 2005.
37. “Geothermal heat keeps road clear of snow”. (2016) Retrieved from https://www.smart2zero.com/news/geothermal-heat-keeps-road-clear-snow
38. Minsk, D. (1999). "Heated bridge technology: report on ISTEA Sec. 6005 program."Washington, DC 20590, internal-pdf://4282711904/Heated Bridge Technolog - a reprot by FHWA.pdf
39. Grasman, S., Long, S., Qin, R., Rolufs, A., Thomas, M. and Lin Y. (2011). Alternative Energy Resources for the Missouri Department of Transportation. Report Number OR11-010.
40. Champagnie, B., Altenor, G. and Simonis, A. (2013). Highway Wind Turbines. B.S. Thesis of Florida International University.
41. “Advantages and Challenges of Wind Energy”, (n.d.) Retrieved from https://www.energy.gov/eere/wind/advantages-and-challenges-wind-energy
42. Khalil, W., Arslan, M., Imaad Ayub, M. and Usman, M. (2011). Load & Stress Analysis of Horizontal Axis Wind Turbine and Comparison between Fiberglass & Carbon Fiber Blades. B.S. Thesis. University of Engineering and Technology Lahore.
43. Schubel, P. and Crossley, R. (2012). Wind Turbine Blade Design. Energies 2012, 5(9), 3425-3449; https://doi.org/10.3390/en5093425
44. Kheirabadi, A. and Nagamune, R. (2019). A quantitative review of wind farm control with the objective of wind farm power maximization. Journal of Wind Engineering and Industrial Aerodynamics, 192, pp.45-73.
45. Mabrouk, I., Hami, A., Walha, L., Zghal, B. and Haddar, M. (2017). Dynamic vibrations in wind energy systems: Application to vertical axis wind turbine. Mechanical Systems and Signal Processing, 85, pp.396-414
46. Stout, C., Islam, S., White, A., Arnott, S., Kollovozi, E., Shaw, M., Droubi, G., Sinha, Y. and Bird, B. (2017). Efficiency Improvement of Vertical Axis Wind Turbines with an Upstream Deflector. Energy Procedia, 118, pp.141-148.
47. Pope, K., Dincer, I. and Naterer G.F. (2010). Energy and exergy efficiency comparison of horizontal and vertical axis wind turbines. Renewable Energy, 35 (9), pp.2102-2113
48. “Wind turbine uses air generated by passing trucks to power roadside devices” (n.d.) Retrieved from https://www.worldhighways.com/sections/environment/news/wind-turbine-uses-air-generated-by-passing-trucks-to-power-roadside-devices/
49. NREL (2014). PVWatts Version 5 Manual. Technical Report. NREL/TP-6A20-6264.
50. Perez, R.; Stewart, R.; Seals, R.; Guertin, T. (1988). The Development and Verification of the Perez Diffuse Radiation Model. Technical Report; Sandia National Labs: Albuquerque, NM, USA, 1 October 1988.
51. Michalsky, J. J. (1988) The Astronomical Almanac's algorithm for approximate solar position (1950–2050), Solar Energy, Volume 40, Issue 3, Pages 227-235, ISSN 0038-092X.
52. PVWatts (n.d.). https://pvwatts.nrel.gov
53. Greentech Renewables (n.d.) Determining Module Inter Row Spacing. Retrieved from: https://www.greentechrenewables.com/article/determining-module-inter-row-spacing

54. University of Oregon Solar Radiation Monitoring Laboratory (n.d.) http://solardat.uoregon.edu
55. HelioScope (n.d.) http://helioscope.com
56. Hirsch, A. (2018). Free Energy Solar Highway Program. New Mexico Department of Transportation. Report ID No. NM17ENV-03.
57. “Net Metering and Interconnection”, (n.d.) Retrieved from https://www.njcleanenergy.com/renewable-energy/programs/net-metering-and-interconnection
58. Bayraktar, M., Zhu, Y., and Mahmoud, N. (2013). Opportunities on the state highway system to generate revenue or offset expenditures for the state of Florida. Florida Department of Transportation.
59. System Advisory Model (SAM) NREL (n.d.) https://sam.nrel.gov
60. Urban-Brookings Tax Policy Center (n.d.) https://www.urban.org/policy-centers/urban-brookings-tax-policy-center
61. NJ Treasury Division of Taxation (n.d.) https://www.nj.gov/treasury/taxation/corp_over.shtml
62. The White House – Office of Management and Budget (n.d.) https://www.whitehouse.gov/omb/information-for-agencies/circulars/
63. U.S. Department of Labor - Bureau of Labor Statistics (2020) https://www.bls.gov/regions/mid-atlantic/news-release/2020/pdf/consumerpriceindex_northeast_20201210.pdf
64. NC Clean Energy Technology Center (n.d.) Solar Energy Sales Tax Exemption. https://programs.dsireusa.org/system/program/detail/219
65. Solar Energy Industries Association (n.d.) Solar Investment Tax Credit (ITC) https://www.seia.org/initiatives/solar-investment-tax-credit-itc
66. New Jersey’s Clean Energy Program (n.d.) https://njcleanenergy.com
67. NJSREC (n.d.) https://njsrec.com
68. NREL (2014). PVWatts Version 5 Manual. Technical Report. NREL/TP-6A20-6264.
69. Perez M. J. R, Fthenakis, V., Kim, C. H. and Pereira, A. O. (2012) Façade-integrated photovoltaics: a life cycle and performance assessment case study. Prog Photovolt: Res Appl 2012;20(8):975–90.
70. Perez, R.; Stewart, R.; Seals, R.; Guertin, T. (1988). The Development and Verification of the Perez Diffuse Radiation Model. Technical Report; Sandia National Labs: Albuquerque, NM, USA, 1 October 1988.
71. National Renewable Energy Laboratory (NREL). (n.d.) Solar Resource Data, Tools, and Maps. Retrieved from: https://www.nrel.gov/gis/assets/images/solar-annual-ghi-2018-usa-scale-01.jpg
72. Oregon Department of Transportation (2016). Solar Highway Program: From Concept to Reality. A guidebook for Departments of Transportation to Develop Solar Photovoltaic Systems in the Highways Right-of-Way.
73. Hirsch, A. (2018) Free Energy Solar Highway Program. New Mexico Department of Transportation. Report ID No. NM17ENV-03.
74. Stevens, K. A., Michaud, G. and Jenkins, D. (2020) Impact Analysis of Power Purchase Agreements (PPAs) in Florida. Retrieved from: https://www.solarunitedneighbors.org/wp-content/uploads/2020/10/Impact-Analysis-of-Power-Purchase-Agreements-in-Florida.pdf

75. Schirone, L., Bellucci, P. and Grasselli, U. (2003). Quality issues for photovoltaic-sound barriers. Clinical Nutrition Supplements. 89. 2459 - 2462 Vol.3. 10.1109/WCPEC.2003.1305089.
76. “Solar Energy Can Be a Health Hazard” (n.d.) Retrieved from http://www.eiwellspring.org/solaremfhazard.pdf
77. “Radiation Resource Outside the EPA” (n.d.) retrieved from https://www.epa.gov/radiation/radiation-resources-outside-epa
78. U.S. Energy Information Administration (2009). Household Energy Use in New Jersey. Retrieved from: https://www.eia.gov/consumption/residential/reports/2009/state_briefs/pdf/nj.pdf
79. Kimber, A., Mitchell, L., Nogradi, S. and Wenger, H. (2006) The Effect of Soiling on Large Grid-Connected Photovoltaic Systems in California and the Southwest Region of the United States, IEEE 4th World Conference on Photovoltaic Energy Conference, 2006, pp. 2391-2395, doi: 10.1109/WCPEC.2006.279690.
80. Goetzberger, A., Kleiss, G., Catello, S., Hille, G., Reise, C., Wiemken, E., van Dijk, V., Betcke, J., Pearsall, N., Hynes, K., Gaiddon, B., Nordmann, T., and Froelich, A. (1999) Evaluation of the potential of PV noise barrier technology for electricity production and market share: Final Report Volume 1. European Union PVNB POT. Freiburg, Germany.
81. Vallati, A., de Lieto Vollaro, R., Tallini, A. and Cedola, L. (2015) Photovoltaics Noise Barrier: Acoustic and Energetic Study, Energy Procedia, Volume 82, 2015, Pages 716-723, ISSN 1876-6102, https://doi.org/10.1016/j.egypro.2015.11.797.
82. Zhang, J., Lu, Y., Lu, Z., Liu, C., Sun, G. and Li, Z. (2015). A new smart traffic monitoring method using embedded cement-based piezoelectric sensors. Smart Materials and Structures, 24(2), p.025023.
83. Levenberg, E. (2014). Estimating vehicle speed with embedded inertial sensors. Transportation Research Part C: Emerging Technologies, 46, pp.300-308.
84. Hostettler, R., Birk, W. and Nordenvaad, M.L. (2015). Joint vehicle trajectory and model parameter estimation using road side sensors. IEEE Sensors Journal, 15(9), pp.5075-5086.
85. Reguieg, S.K., Ghemari, Z., Benslimane, T. and Saad, S. (2019). Modeling and enhancement of piezoelectric accelerometer relative sensitivity. Sensing and Imaging, 20(1), p.1.
86. Ye, Z., Wang, L., Xu, W., Gao, Z. and Yan, G. (2017). Monitoring traffic information with a developed acceleration sensing node. Sensors, 17(12), p.2817.
87. Ye, Z., Xiong, H.C. and Wang, L.B. (2019). Collecting comprehensive traffic information using pavementvibration monitoring data, Computer-Aided Civil and Infrastructure Engineering, 2019, 1-16
88. Ji, X., Hou, Y., Chen, Y. and Zhen, Y. (2019). Attenuation of acoustic wave excited by piezoelectric aggregate in asphalt pavement and its application to monitor concealed cracks. Construction and Building Materials, 216, pp.58-67.
89. Lin, M., Qing, X., Kumar, A. and Beard, S.J. (2001). Smart layer and smart suitcase for structural health monitoring applications. In Smart structures and materials 2001: industrial and commercial applications of smart structures technologies (Vol. 4332, pp. 98-106). International Society for Optics and Photonics.

90. Lynch, J.P. (2005). Design of a wireless active sensing unit for localized structural health monitoring. Structural Control and Health Monitoring: The Official Journal of the International Association for Structural Control and Monitoring and of the European Association for the Control of Structures, 12(3-4), pp.405-423.
91. Karaiskos, G., Deraemaeker, A., Aggelis, D.G. and Van Hemelrijck, D. (2015). Monitoring of concrete structures using the ultrasonic pulse velocity method. Smart Materials and Structures, 24(11), p.113001.
92. Lajnef, N., Chatti, K., Chakrabartty, S., Rhimi, M. and Sarkar, P. (2013). Smart pavement monitoring system (No. FHWA-HRT-12-072). United States. Federal Highway Administration.
93. Alavi, A.H., Hasni, H., Lajnef, N. and Chatti, K. (2016). Continuous health monitoring of pavement systems using smart sensing technology. Construction and Building Materials, 114, pp.719-736.
94. Sazonov, E., Janoyan, K. and Jha, R. (2004). Wireless intelligent sensor network for autonomous structural health monitoring. In Smart Structures and Materials 2004: Smart Sensor Technology and Measurement Systems (Vol. 5384, pp. 305-314). International Society for Optics and Photonics.
95. Sazonov, E., Li, H., Curry, D. and Pillay, P. (2009). Self-powered sensors for monitoring of highway bridges. IEEE Sensors Journal, 9(11), pp.1422-1429.
96. Ali, S.F., Friswell, M.I. and Adhikari, S. (2011). Analysis of energy harvesters for highway bridges. Journal of Intelligent Material Systems and Structures, 22(16), pp.1929-1938.
97. Peigney, M. and Siegert, D. (2013). Piezoelectric energy harvesting from traffic-induced bridge vibrations. Smart Materials and Structures, 22(9), p.095019.
98. Karimi, M., Karimi, A.H., Tikani, R. and Ziaei-Rad, S. (2016). Experimental and theoretical investigations on piezoelectric-based energy harvesting from bridge vibrations under travelling vehicles. International Journal of Mechanical Sciences, 119, pp.1-11.
99. Cahill, P., Jaksic, V., Keane, J., O'Sullivan, A., Mathewson, A., Ali, S.F. and Pakrashi, V. (2016). Effect of road surface, vehicle, and device characteristics on energy harvesting from bridge–vehicle interactions. Computer-Aided Civil and Infrastructure Engineering, 31(12), pp.921-935.
100. Tong, X., Song, S., Wang, L. and Yang, H. (2018). A preliminary research on wireless cantilever beam vibration sensor in bridge health monitoring. Frontiers of Structural and Civil Engineering, 12(2), pp.207-214.
101. Hu, X., Wang, B. and Ji, H. (2013). A wireless sensor network-based structural health monitoring system for highway bridges. Computer-Aided Civil and Infrastructure Engineering, 28(3), pp.193-209.
102. Zhang, Y., Cai, S.C. and Deng, L. (2014). Piezoelectric-based energy harvesting in bridge systems. Journal of intelligent material systems and structures, 25(12), pp.1414-1428.
103. Wang, L., Todaria, P., Pandey, A., O'Connor, J., Chernow, B. and Zuo, L. (2016). An electromagnetic speed bump energy harvester and its interactions with vehicles. IEEE/ASME Transactions on Mechatronics, 21(4), pp.1985-1994.
104. Xiong, H. (2014). Piezoelectric energy harvesting for public roadways. PHD Other-Dissertation, Civil Engineering, Virginia Polytechnic Institute and State University.

105. Wang, C., Wang, S., Li, Q.J., Wang, X., Gao, Z. and Zhang, L. (2018). Fabrication and performance of a power generation device based on stacked piezoelectric energy-harvesting units for pavements. Energy conversion and management, 163, pp.196-207.
106. Roshani, H., Dessouky, S., Montoya, A. and Papagiannakis, A.T. (2016). Energy harvesting from asphalt pavement roadways vehicle-induced stresses: A feasibility study. Applied Energy, 182, pp.210-218.
107. Guo, L. and Lu, Q. (2017). Modeling a new energy harvesting pavement system with experimental verification. Applied energy, 208, pp.1071-1082.
108. Zhao, H., Yu, J. and Ling, J. (2010). Finite element analysis of cymbal piezoelectric transducers for harvesting energy from asphalt pavement. Journal of the Ceramic Society of Japan, 118(1382), pp.909-915.
109. Jasim, A., Yesner, G., Wang, H., Safari, A., Maher, A. and Basily, B. (2018). Laboratory testing and numerical simulation of piezoelectric energy harvester for roadway applications. Applied energy, 224, pp.438-447.
110. Liu, X. and Wang, J. (2019). Performance Exploration of A Radially Layered Cymbal Piezoelectric Energy Harvester under Road Traffic Induced Low Frequency Vibration. In IOP Conference Series: Materials Science and Engineering (Vol. 542, No. 1, p. 012075). IOP Publishing.
111. Hwang, W., Kim, K.B., Cho, J.Y., Yang, C.H., Kim, J.H., Song, G.J., Song, Y., Jeon, D.H., Ahn, J.H., Do Hong, S. and Kim, J. (2019). Watts-level road-compatible piezoelectric energy harvester for a self-powered temperature monitoring system on an actual roadway. Applied energy, 243, pp.313-320.
112. Cho, J.Y., Kim, K.B., Hwang, W.S., Yang, C.H., Ahn, J.H., Do Hong, S., Jeon, D.H., Song, G.J., Ryu, C.H., Woo, S.B. and Kim, J. (2019). A multifunctional road-compatible piezoelectric energy harvester for autonomous driver-assist LED indicators with a self-monitoring system. Applied energy, 242, pp.294-301.
113. Shin, Y.H., Jung, I., Noh, M.S., Kim, J.H., Choi, J.Y., Kim, S. and Kang, C.Y. (2018). Piezoelectric polymer-based roadway energy harvesting via displacement amplification module. Applied energy, 216, pp.741-750.
114. Jung, I., Shin, Y.H., Kim, S., Choi, J.Y. and Kang, C.Y. (2017). Flexible piezoelectric polymer-based energy harvesting system for roadway applications. Applied Energy, 197, pp.222-229.
115. Song, G.J., Kim, K.B., Cho, J.Y., Woo, M.S., Ahn, J.H., Eom, J.H., Ko, S.M., Yang, C.H., Do Hong, S., Jeong, S.Y. and Hwang, W.S. (2019). Performance of a speed bump piezoelectric energy harvester for an automatic cellphone charging system. Applied Energy, 247, pp.221-227.
116. Gholikhani, M., Nasouri, R., Tahami, S.A., Legette, S., Dessouky, S. and Montoya, A. (2019). Harvesting kinetic energy from roadway pavement through an electromagnetic speed bump. Applied Energy, 250, pp.503-511.
117. Cho, J.Y., Kim, K.B., Jabbar, H., Woo, J.S., Ahn, J.H., Hwang, W.S., Jeong, S.Y., Cheong, H., Yoo, H.H. and Sung, T.H. (2018). Design of optimized cantilever form of a piezoelectric energy harvesting system for a wireless remote switch. Sensors and Actuators A: Physical, 280, pp.340-349.
118. Trafford, R., Russo, D., Clark, C., Shin, S. and Schmalzel, J.L. (2019). Characterization of Piezoelectric Cantilever Beams for use in Roadside Vibration

Energy Harvesting. In 2019 IEEE Sensors Applications Symposium (SAS) (pp. 1-6). IEEE.
119. Hande, A., Bridgelall, R., Zoghi, B. (2010) “Vibration Energy Harvesting for Disaster Asset Monitoring Using Active RFID Tags,” *Proc. of the IEEE*, 98(9), pp. 620-628, September.
120. Guo, L.K., Wang, H., Soares, L., Lu, Q., and Brito, L. (2021) Multi-Physics Modeling of Piezoelectric Pavement System for Energy Harvesting under Traffic Loading, *International Journal of Pavement Engineering*, Published online
121. Wang, C. H., Wang, S., Gao, Z. and Song, Z. (2021). Effect evaluation of road piezoelectric micro-energy collection-storage system based on laboratory and on-site tests. *Applied Energy*, *287*, p.116581.
122. Jasim, A., Wang, H., Yesner, G., Safari, A., and Szary, P. (2019). Performance Analysis of Piezoelectric Energy Harvesting in Pavement: Laboratory Testing and Field Simulation, *Transportation Research Record*, Vol. 2673, No. 3, pp. 115-124
123. Wang, S., Wang, C., Gao, Z. and Cao, H. (2020). Design and performance of a cantilever piezoelectric power generation device for real-time road safety warnings. *Applied Energy*, *276*, p.115512.
124. Zhang, Z., H. Xiang, Z. Shi, and J. Zhan. (2018) Experimental Investigation on Piezoelectric Energy Harvesting from Vehicle-Bridge Coupling Vibration. *Energy Conversion and Management*. 163:169-179.
125. Tang, X. and Zuo, L. (2011). Enhanced vibration energy harvesting using dual-mass systems. *Journal of Sound and Vibration*, *330*(21), pp.5199-5209.
126. Tang, L. and Yang, Y. (2012). A multiple-degree-of-freedom piezoelectric energy harvesting model. *Journal of Intelligent Material Systems and Structures*, *23*(14), pp.1631-1647.
127. Wang, H., A. Jasim, and X. Chen. (2018) Energy Harvesting Technologies in Roadway and Bridge for Different Applications–A Comprehensive Review. *Applied Energy*. 212:1083-1094.
128. Wang, C., S. Wang, Z. Gao, and Z. Song. (2021) Effect Evaluation of Road Piezoelectric Micro-Energy Collection-Storage System Based on Laboratory and On-Site Tests. *Applied Energy*. 287:116581.
129. Camara, A. and A. M. Ruiz-Teran. (2015) Multi-mode Traffic-induced Vibrations in Composite Ladder-Deck Bridges under Heavy Moving Vehicles. *Journal of Sound and Vibration*. *355*:264-283.
130. Li, M. and X. Jing. (2019) Novel Tunable Broadband Piezoelectric Harvesters for Ultralow-Frequency Bridge Vibration Energy Harvesting. *Applied Energy*. *255*: 113829.
131. Wang, S., C. Wang, Z. Gao, and H. Cao. (2020) Design and Performance of a Cantilever Piezoelectric Power Generation Device for Real-Time Road Safety Warnings. *Applied Energy*. 276:115512.
132. Kim, S. H., Ahn, J. H., Chung, H. M., and Kang, H. W. (2011) Analysis of Piezoelectric Effects on Various Loading Conditions for Energy Harvesting in a Bridge System. *Sensors and Actuators A: Physical*, 2011. 167:468-483.
133. Song, Y. (2019) Finite-element Implementation of Piezoelectric Energy Harvesting System from Vibrations of Railway Bridge. *Journal of Energy Engineering*. 145:04018076.

134. Upadrashta, D. and Yang, Y. (2015) Finite Element Modeling of Nonlinear Piezoelectric Energy Harvesters with Magnetic Interaction. *Smart Materials and Structures*, 2015. 24:045042.
135. Gaglione, A., Rodenas-Herraiz, D., Jia, Y., Nawaz, S., Arroyo, E., Mascolo, C., Soga, K. and Seshia, A.A. (2018) Energy Neutral Operation of Vibration Energy-Harvesting Sensor Networks for Bridge Applications. International Conference on Embedded Wireless Systems and Networks, Madrid, Spain.
136. Xue, H., Hu, Y., and Wang, Q.M. (2008). Broadband Piezoelectric Energy Harvesting Devices Using Multiple Bimorphs with Different Operating Frequencies. *IEEE transactions on ultrasonics, ferroelectrics, and frequency control*. 55:2104-2108.
137. Qi, S., Shuttleworth, R., Oyadiji, S.O., and Wright, J. (2010) Design of a Multiresonant Beam for Broadband Piezoelectric Energy Harvesting. *Smart Materials and Structures*. 19:094009.
138. Liu, H., Tay, C. J., Quan, C., Kobayashi, T. and Lee, C. (2011). Piezoelectric MEMS Energy Harvester for Low-Frequency Vibrations with Wideband Operation Range and Steadily Increased Output Power. *Journal of Microelectromechanical systems*. 20:1131-1142.